

METHODS OF IN-SITU MONITORING OF SUSPENSION POLYMERISATION FOR PROCESS UNDERSTANDING AND OPTIMISATION

A thesis submitted to the University of Strathclyde for the degree
of:

Doctor of Philosophy
in the Faculty of Science

2019

Barry Thomas Robertson

Department of Pure and Applied Chemistry



**METHODS OF IN-SITU MONITORING OF SUSPENSION POLYMERISATION FOR
PROCESS UNDERSTANDING AND OPTIMISATION / by Barry Robertson – Glasgow –
University of Strathclyde - 2019**

Supervisors:

Dr. Alison Nordon

Professor Suresh Thennadil

This work was performed at the Centre for Process Analytical Technology (CPACT), Department of Pure and Applied Chemistry, University of Strathclyde and was funded by the European Commission's Framework 7 programme through the OPTICO consortium. The contents of the publication reflect only the author's view.



Declaration of Author's Rights

This thesis is the result of the author's original research. It has been composed by the author and has not been previously submitted for examination which has led to the award of a degree.

The copyright of this thesis belongs to the author under the terms of the United Kingdom Copyright Acts as qualified by University of Strathclyde Regulation 3.50. Due acknowledgement must always be made of the use of any material contained in, or derived from, this thesis.

Barry Robertson

January 2019

For my family

Acknowledgements

The process of completing this PhD has without doubt been one of the toughest challenges I have ever faced. It is often said that we should push ourselves to test the boundaries of what we are capable, but almost never are we told what to do when we come up against them. At times – many times – on this journey, these limits have seemed insurmountable, and feelings of self-doubt and anxiety have been increasingly familiar. It is only through the help, guidance and complete selflessness of a few key people that have helped me reach this stage and for that, I will be eternally grateful.

Firstly, to my family: I honestly cannot think of a day where I was made to feel like there was anything I couldn't achieve. Encouragement to do my best and achieve my goals – no matter how high – has always been there. The support I've received at every stage of my life has made every achievement possible, and I am grateful every day for their unwavering kindness and generosity.

To my wife, Hannah: This process has been as much a trial for you as it has for me in recent years, and I haven't always made it easy. But your willingness to be by my side encouraging and supporting me has left me in awe, truly. I will make it my life's mission to make it all worthwhile and let you know just how much this has meant to me (and feel free to make it as difficult for me as you like!).

Finally, to my supervisor Alison: Words can't possibly express how grateful I am to you for getting me this far. Through the lab days to the excruciating write-up period, the words, "support" and, "encouragement" don't do the help you've given me justice. There is no doubt in my mind that my professional and home lives (never mind the thesis!) wouldn't be in anywhere near as good a shape as they're in without you. No amount of Lego in the world can make up for that, but I'll try.

Furthermore, to all that I've met and worked with over the PhD years, every one of you has impacted my life for the better and it should go without saying that I will be forever grateful – but I'll say it anyway. Dr. Gledson Emidio Jose – my partner in crime through those long lab sessions. They shouldn't have been anywhere near as enjoyable as they were. Suresh Thennadil, for having our back during all of those, "lively" project meetings around Europe. To Professor David Littlejohn, Dr. Christine Davidson, Trevor Whittley, Dr. Piotr Gromski, Dr. Gang Yi, Dr. Zeng-Ping Chen, Meghan Sanders, Gillian Rundell, everyone at CPACT (and all of those I no doubt have regretfully forgotten to mention – sorry): thank you so much.

Abstract

Increasing Environmental and Health and Safety regulations mean that the demands for cost-effective, accurate and information-rich methods of process analysis are increasing exponentially. This project aimed to evaluate the use of technologies – Raman and Acoustic Emission Spectroscopies – coupled with a variety of multivariate analysis tools to provide a framework for the optimisation of polystyrene suspension polymerisation, allowing industrial partners to monitor the reaction progression, determine particle size information and unreacted monomer concentration. Spectral data collected during a series of lab-scale polymerisation reactions and basic model mixtures was used to determine the effectiveness of each method – including the use of a variety of probe configurations for Raman analysis. The data was treated with established pre-treatment methods (Savitzky-Golay filtering, SNV transformation and EMSC) and a novel method (OPLECM) to enhance the performance of mathematical models and investigate the effectiveness of the methods for this application.

The results indicate that Raman and Acoustic Emission spectroscopies can provide monomer concentration and particle size information for this reaction, respectively. Offline Raman data is shown to be approximately 33% less variable than current offline HPLC methods, and in-situ analysis showing qualitatively similar results to offline gravimetric determination of residual monomer. Furthermore, the potential benefit of increasing laser diameter is shown. The pre-treatment of this data prior to modelling shows Savitzky-Golay derivatisation to provide the least improvement (11.4% RMSEp); with SNV, EMSC and OPLECM performing similarly (4.1, 3.8 and 4.1% respectively). Models built with EMSC and OPLECM pre-treatment provide best results overall, with just 4 and 3 latent variables, respectively. Finally, Acoustic Emission spectroscopy provided data which showed good correlation to offline sieving analysis, indicating a strong potential for its use in PSD determination during this reaction.

LIST OF ABBREVIATIONS

AES – acoustic emission spectroscopy

DBPO – dibenzoyl peroxide

EMSC – extended multiplicative scatter correction

EPS – expanded polystyrene

FBRM – Focussed beam reflectance measurement

HPLC – High performance liquid chromatography

IO – Immersion optic

IR – infra-red

LOD – Limit of detection

LV(s) – latent variable(s)

MIR – mid infra-red

MSC – Multiplicative scatter correction

MVA – multivariate analysis

NCO – Non-contact optic

NIR – near infra-red

OPLEC – optimal path length estimation and correction

OPLECM – modified optimal path length estimation and correction

pBq – *para*-Benzoquinone

PhAT[®] – Pharmaceutical area testing

PLS – partial least squares

PSD – particle size distribution

PVM – particle video microscopy

RM – residual monomer

RMSE_{cv} – Root mean-square error of cross validation

RMSE_p – Root mean-square error of prediction

RS – Raman spectroscopy

RSD – Relative standard deviation

SD – Standard deviation

SDBS – Sodium dodecylbenzenesulfonate

SG – Savitzky-Golay

SGFD – Savitzky-Golay first derivatisation

SNV – standard normal variate

TCP – Tricalcium phosphate

THF – Tetrahydrofuran

UV-VIS – Ultraviolet-visible

WAI – Wide area illumination

List of Figures

Figure 1.1 – Molecular structures of (a) DBPO and (b) SDBS.

Figure 1.2 – Schematic of suspension polymerisation. (a) Oil-soluble initiator, I , dissolves into monomer droplets which, in turn, diffuse into micelles formed by surfactant molecules; (b) monomer-initiator droplets are dispersed throughout medium in micelles; (c) bead swelling as polymer is produced.

Figure 1.3 – Radical polymerisation of styrene scheme where $R = \text{DBPO}$.

Figure 2.1 – An electromagnetic wave separated into electric and magnetic components showing the direction of propagation and wavelength.

Figure 2.2 – Regions of the electromagnetic spectrum emphasising the visible light region.

Figure 2.3 – Simple diatomic molecule where nuclei are represented by m_1 and m_2 held together by a 'spring'.

Figure 2.4 – Potential energy curve for a harmonic oscillator as a function of Δr .

Figure 2.5 - Potential energy curve for an anharmonic oscillator as a function of Δr (black) compared to that for a harmonic oscillator (dotted).

Figure 2.6 – Rayleigh scattering vs. (a) Stokes Raman scattering and (b) anti-Stokes Raman scattering.

Figure 2.7 - General schematic for a concentric unfiltered fibre bundle or "n-around-1" probe and the filtered probe.

Figure 2.8 – Left: Schematic of spot sizes on a tablet (yellow circle) achieved from using different lasers; Right: Schematic of the Raman PhAT probe showing the wider illumination area and long working distance.

Figure 2.9 - Schematic of a cross-section through a typical optical fibre.

Figure 2.10 – Schematic for Pulse-echo (a) and Pitch-catch (b) methods of active acoustic monitoring techniques showing sound waves emitting from transducers (black boxes) and travelling through the system before collection. Adapted and modified from Bellamy, L. J.

Figure 2.11 – Schematic for passive acoustic emission showing waves propagating from an internal acoustic event (e.g. a polystyrene bead striking the vessel wall) within the process vessel. Adapted and modified from Bellamy, L. J.

Figure 2.12 – General schematic of a HPLC system showing the sample path from injection, through the column, to detection.

Figure 2.13 - General schematic of (a) a sample passing through an HPLC column and separating analytes (red, blue and green circles) and (b) the resulting chromatogram as the separated analytes pass through the UV detector.

Figure 2.14 – Schematic representation of PCA.

Figure 2.15 – Schematic representation of PLS modelling.

Figure 2.16 – Reactor set-up showing a) Radley's stirrer/motor control unit, b) immersion temperature probe, c) Kaiser immersion optic Raman probe and d) jacketed 1L Radley's reaction vessel.

Figure 3.1 – Waters 2690 HPLC system.

Figure 3.2 – Shimadzu SPD-6A variable wavelength UV detector.

Figure 3.3 - Particle size distributions of EPS bead batches 1 (cyan), 2 (blue), 3 (red) and 4. Data provided by industrial partners.

Figure 3.4 - Offline EPS bead analysis set-up showing: a) shuttered sample housing unit, b) Kaiser NCO Raman MR probe head and c) glass vial containing EPS beads.

Figure 3.5 – Schematic of small area probe sample depth study set-up showing sample tube with increasing sample depth going from (a) to (b).

Figure 3.6 – Schematic of wide area probe sample depth study set-up showing (a) glass vial with no lid and x mm of EPS beads, (b) sulphur disc placed between bottom of the vial and (c) a foil jacket, (d) the 203 mm collimated beam housing sitting above (e) the jacket and sample vial and (f) the completed system ready for spectral acquisition.

Figure 3.7 – The 600 – 1800 cm^{-1} region of the average ($n = 51$) MIR spectrum of pure styrene using an ABB MB3000 FTIR spectrometer (Clair Scientific, Northampton, UK) coupled with polycrystalline silver halide optical fibres. Measurements were made with a resolution of 16 cm^{-1} and subtracting an air background.

Figure 3.8 – Average ($n = 51$) MIR spectra of pure styrene (red), 50% styrene (green) and 10% styrene (blue) mixtures. All spectra shown have a resolution of 16 cm^{-1} and a subtracted air background.

Figure 3.9 – Average ($n = 5$, 1.5 s exposure) Raman spectrum (785 nm, 100-3240 cm^{-1}) of neat styrene in a glass vial using an NCO MR probe head in a shuttered housing.

Figure 3.10 – Average ($n = 5$, 2 s exposure) Raman spectrum (785 nm, 100-3240 cm^{-1}) of polystyrene beads in a glass vial using an NCO MR probe head in a shuttered housing.

Figure 3.11 – Average ($n = 5$, 2 s exposure) Raman spectrum (785 nm, 100-3240 cm^{-1}) of crystalline DBPO in a glass vial using an NCO MR probe head in a shuttered housing.

Figure 3.12 – Average ($n = 5$, 1 s exposure) Raman spectrum (785 nm, 100-3240 cm^{-1}) of crystalline TCP in a glass vial using an NCO MR probe head in a shuttered housing.

Figure 3.13 – A 3D representation of the 1548-1680 cm⁻¹ region of the Raman spectra (785 nm laser) taken hourly throughout a reaction using an immersion optic probe head. Each spectrum was an average of 10 acquisitions of 12 s each.

Figure 3.14 – Average Raman spectra of styrene (n=10, blue) and its first derivative (red) using an NCO Raman probe (785 nm, 20 s exposure per acquisition). Derivatisation was carried out using the Savitzky-Golay function on Matlab using a 31-point window. Spectra obtained with an NCO MR Raman probe.

Figure 3.15 – Average Raman spectra (n=5, 20 s per acquisition) of styrene (red) and polystyrene beads (purple) indicating the styrene peak at 1631 cm⁻¹. Spectra were acquired using an NCO through a glass vial.

Figure 3.16 - Derivative offline Raman spectra of batch 3 polystyrene beads as received (blue), successfully impregnated (green) and one week after the experiment (red). Spectra are averaged from 10 accumulations of 10 s exposure each.

Figure 3.17 – Screenshot of a typical HPLC trace from a 40 ppm standard solution analysed using a Waters 2690 with a Shimadzu SPD-6A variable wavelength UV detector and Chromeleon software.

Figure 3.18 – Calibration curve for a series of styrene/THF mixtures after HPLC analysis. The linearity of the 1630 cm⁻¹ peak area from 0 to 80% v/v styrene is shown by the R² value.

Figure 3.19 - Residual styrene content of batch 3 polystyrene beads measured via HPLC plotted against that measured via offline Raman spectroscopy followed by first-order derivatisation.

Figure 3.20 - Second order derivatisation of offline Raman spectrum of EPS beads as received from BASF (black), with additional styrene added (blue) and one week after addition of styrene (red).

Figure 3.21 - Second order peak magnitude at 1630 cm^{-1} from offline Raman spectrum of different bead batches with differing RM content as determined via HPLC.

Figure 3.22 – Correlation between residual monomer measurements made via HPLC and offline Raman spectroscopy of small EPS beads (0.827 mm mean diameter, Raman spectra averaged from 5 acquisitions, 20 s exposure per acquisition). Error bars indicate one standard deviation.

Figure 3.23 - Correlation between residual monomer estimations made via HPLC and offline Raman spectroscopy of medium EPS beads (1.003 mm mean diameter, Raman spectra averaged from 5 acquisitions, 20 s exposure per acquisition). Error bars indicate one standard deviation.

Figure 3.24 - Correlation between residual monomer estimations made via HPLC and offline Raman spectroscopy of large EPS beads (1.334 mm mean diameter, Raman spectra averaged from 5 acquisitions, 20 s exposure per acquisition). Error bars indicate one standard deviation.

Figure 3.25 – Correlation between residual monomer estimations made via HPLC and offline Raman spectroscopy of all EPS bead size fractions. The area circled indicates the Raman response for all bead sizes with a similar residual monomer level as determined by HPLC.

Figure 3.26 - Overlay of derivatised Raman spectra of sulphur disc (blue) with polystyrene beads (black) in $100\text{-}550\text{ cm}^{-1}$ region.

Figure 3.27 – Sulphur peak (468 cm^{-1}) intensity changing with increasing depth of large (1 mm) diameter polystyrene beads using an NCO MR Raman probe with a $100\text{ }\mu\text{m}$ spot diameter.

Figure 3.28 - Overlay of derivatised sulphur (black) and polystyrene (blue) spectra taken using an NCO MR Raman probe indicating a polystyrene peak at 997 cm^{-1} .

Figure 3.29 - Changing polystyrene peak height with increasing sample depth using NCO MR Raman probe and large (1 mm) polystyrene beads.

Figure 3.30 – Sulphur peak (468 cm⁻¹) intensity changing with increasing depth of large (1 mm) diameter polystyrene beads using a PhAT Raman probe with a 6 mm spot diameter.

Figure 3.31 – Changing polystyrene peak height with increasing sample depth using a PhAT Raman probe and large (1 mm) polystyrene beads.

Figure 3.32 - Derivative peak of sulphur standard diminishing as the depth of sample between the standard and the laser increases. A non-contact MR Raman probe and 0.8 mm diameter beads were used.

Figure 3.33 - Changing polystyrene peak height with increasing sample depth using a NCO MR Raman probe and small (0.8 mm) polystyrene beads.

Figure 3.34 - Diminishing sulphur peak intensity as the depth of 0.8 mm diameter beads between the standard and the non-contact PhAT Raman probe laser was increased.

Figure 3.35 – Changing polystyrene peak height with increasing sample depth using a Raman PhAT probe and small (0.8 mm) polystyrene beads.

Figure 4.1. – Weights and volumes of reaction components and sample components of the sample taken at $t = 15$ minutes. Values were used to calculate the % conversion at this timepoint.

Figure 0.2 – Schematic of data processing method used to perform PCA on spectral data.

Figure 0.3 – Changing Raman spectrum as a reaction progresses from 0 – 6 hours. Spectra were collected using an IO probe head submerged in

reaction media in a 1 L Radley's reaction vessel. Each spectrum shown is an average of 10 acquisitions, 20 s per acquisition.

Figure 0.4 - Changing peak height at 1630 cm^{-1} ('styrene peak') as a reaction progresses. Measurements were taken using an IO probe head over 7 hours at 15 minute intervals. Each measurement was an average of 10 acquisitions, 15 s per acquisition.

Figure 4.5 – EMSC treated Raman intensity of C=C peak height as the reaction progresses (blue points) using an IO probe head. Each spectrum was an average of 10 acquisitions, at 15 s exposure per acquisition. Red points indicate samples taken for HPLC analysis.

Figure 4.6 – Raman intensity of the C=C peak (red) vs. HPLC residual monomer content (blue) of samples taken towards the end of a suspension polymerisation reaction.

Figure 4.7 - Conversion estimates made by gravimetric analysis using Method A (squares) and Method B (triangles) with the standard deviation over 3 measurements (error bars).

Figure 4.8 - Gravimetric analysis results from 10 different suspension polymerisation reactions and their standard deviation from the average conversion estimate at each timepoint using gravimetric method B.

Figure 4.9 - Principal component 1 scores as a suspension polymerisation reaction progresses with (a) no preprocessing and (b) MSC preprocessing.

Figure 4.10 - Principal component 1 scores for all 10 suspension polymerisation reactions with MSC preprocessing. Points A and B indicate the point of surfactant addition and the average endpoint, respectively.

Figure 4.11 - Loadings plots for the first 3 PCs from PCA of all 10 sets of reaction data.

Figure 4.12 - Scores for the first three PCs for all 10 reactions. Blue shaded area indicates the experimental plane in which most of the data lies.

Figure 4.13 – PLS validation plots showing the conversion measured via Gravimetry vs. the conversion estimated from validation Raman treated with (a) no preprocessing; (b) SGFD; (c) SNV; (d) EMSC and (e) OPLEC.

Figure 4.14 – (a) The correlation coefficient (R^2) and (b) RMSEP for predictive models built using different values of OPLEC Component, J, and different numbers of LVs used in the dual calibration step of OPLEC. High values (red) for R^2 and low values (blue) for RMSEP indicate optimum settings.

Figure 4.15 – Plot of r vs. $\min_p f(p)$ obtained from OPLECm.

Figure 5.1 - Average AES power spectrum in the 0-300 kHz range for 800-1000 μm beads in a 250 mL vessel at concentrations from 5 - 60% w/v. Highlighted areas denote spectral frequency regions used to calculate the area of each peak – A (0-72 kHz), B (72-117 kHz) and C (119-138 kHz). Red arrow indicates the increasing acoustic signal corresponding to increasing bead concentration.

Figure 5.2 – Areas of three peaks in the acoustic emission spectrum (A blue, B orange, C grey) of 800-1000 μm EPS beads in a 250 mL vessel as the bead concentration increases from 5 – 60 % w/v.

Figure 5.3 – Areas of three peaks in the acoustic emission spectrum (A blue, B orange, C grey) of 500-630 μm EPS beads in a 250 mL vessel as the bead concentration increases from 5 – 60 % w/v. Slight loss of acoustic signal seen after 55% concentration.

Figure 5.4 – The changing area of peak A - 0-72 kHz - as the bead concentration increases for 4 different bead size ranges. Error bars denote \pm one standard deviation ($n=3$).

Figure 5.5 – Changing acoustic frequency in the 0-200 kHz region at a fixed bead concentration of 30% w/v with different bead size fractions in a 250 mL vessel.

Figure 5.6 – Average AES in the 0-200 kHz range for 800-1000 μm beads in a 1 L vessel at concentrations from 5 - 50% w/v.

Figure 5.7 – Average AES signals obtained from 800-1000 μm EPS beads at a concentration of 50% w/v in a 250 mL vessel (blue) and a 1000 mL vessel (red).

Figure 5.8 – Changing peak height for peaks A - C with increasing concentration for small (left), medium (middle) and large (right) bead ranges in a 1 L vessel.

Figure 5.9 – The area of peak C as a percentage of the entire spectrum excluding the audible region, as the bead concentration changed from 0-60% w/v in a 250 mL vessel with agitation.

Figure 5.10 – The area of peak C as a percentage of the entire spectrum excluding the audible region, as the bead concentration changed from 0-50% w/v in a 1000 mL vessel with agitation.

Figure 5.11 – Loadings (top) and scores (bottom) plots from PCA of model mixture data in a 250 mL vessel. Arrows in the scores plot indicate the order of each data cluster (red = 500-630 μm , green = 800-1000 μm , blue = 1000-1250 μm and cyan = 1250-1400 μm) with increasing bead concentration.

Figure 5.12 – Loadings (top) and scores (bottom) plots from PCA of model mixture data in a 1000 mL vessel. Arrows in the scores plot indicate the order of each data cluster (red = 500-630 μm , green = 800-1000 μm and blue = 1000-1250 μm) with increasing bead concentration.

Figure 5.13 – Selected AES data collected throughout suspension polymerisation reaction 1. The 0-72 kHz region is highlighted and its area plotted against time (inset). This was performed in a 1 L Radlleys reaction vessel with a stirrer rate of 300 rpm.

Figure 5.14 – The area of peak C as a percentage of the entire spectrum excluding the audible region, throughout each suspension polymerisation reaction.

Figure 5.15 – The area of peak C as a percentage of the entire spectrum excluding the audible region, from 5 hours after each reaction had started until completion.

Figure 5.16 - Bead sieving analysis of the beads produced by reaction 1. Each fraction is shown as a percentage of the total weight of beads produced.

Figure 5.17 - The area of peak C as a percentage of the entire spectrum excluding the audible region, as the concentration of 500-630 um beads increased in a 1000 mL reactor vessel with agitation at 300 rpm.

List of Tables

Table 1.1 - Generalised Free-Radical Polymerisation Reaction Scheme showing (a) initiation by free radical I^\bullet , (b) propagation of free radicals through interaction with monomer M and polymer R, (c) termination via combination and (d) termination via disproportionation.

Table 1.2 - A summary table of relevant analytical techniques and their advantages and disadvantages in the monitoring of polymerisation.

Table 3.1 – Categorisation of provided EPS beads by mean particle diameter and corresponding RM content as determined by HPLC at BASF.

Table 3.2 – Analytical data of 4 different polystyrene bead batches as provided by industrial partners. Shown is the particle size determined by sieving and the residual monomer content determined by HPLC.

Table 3.3 – Experimental conditions for polystyrene bead impregnation method development performed in a 250 mL Radleys jacketed reaction vessel. Impeller speed was kept at 400 rpm in each experiment.

Table 3.4 – HoloGRAMS settings for non-contact Raman analysis of dry impregnated EPS beads.

Table 3.5 - MIR band assignments for the spectrum of pure styrene

Table 3.6 – Standard curve data for quantifying styrene in ppm from the area under the curve in the HPLC response.

Table 3.7 – Residual monomer content of polystyrene beads provided by BASF showing (left) the known monomer content as provided by BASF via

HPLC and (right) the monomer content calculated by Strathclyde following implementation of the HPLC method.

Table 3.8 - Residual styrene contents of batch 3 polystyrene beads from HPLC (left) and Raman spectroscopy (right).

Table 3.9 – Varying second order Raman peak magnitudes from different EPS bead samples with corresponding RM levels determined via HPLC.

Table 3.10 – Detection limits resulting from immersion, PhAT and non-contact Raman probes with EPS beads.

Table 4.3 - Reaction conditions of 10 suspension polymerisation reactions. All reactions performed in a 1 L Radley's reaction vessel.

Table 4.1 - Raman band assignments for the suspension polymerisation reaction matrix.

Table 4.2 - %RSD from four samples taken in the final hour of three reactions and analysed via HPLC and *in-situ* Raman.

Table 4.3 – Predictive performance and number of latent variables used in PLS models built using different preprocessing methods. Predictive performance based on a concentration range of 6 – 85% conversion.

Table 5.1 – Conditions for model mixture experiments in a 250 mL vessel.

Table 5.3 - Initiator and stabiliser weights used in reactions monitored with AES. Stirrer speed was kept at 300 rpm for all reactions.

Table of Contents

METHODS OF IN-SITU MONITORING OF SUSPENSION POLYMERISATION FOR PROCESS UNDERSTANDING AND OPTIMISATION.....	i
1. Introduction	1
1.1. The Polymerisation Process	2
1.2. Suspension Polymerisation of Styrene ^{6, 7}	3
1.3. Advantages of PAT Implementation.....	5
1.4. Implementation of PAT for Polymerisation	7
1.4.1. Process Temperature Sensors.....	8
1.4.2. Process Flow and Pressure Sensors	9
1.4.3. Chemical Data Sensors.....	11
1.4.4. Ultraviolet Spectroscopy.....	13
1.4.5. Raman Spectroscopy.....	14
1.4.6. Mid-Infrared Spectroscopy	15
1.4.7. Near Infrared Spectroscopy	17
1.4.8. Acoustic Emission Spectroscopy	18
1.5. Project Aims.....	23
2. Theory and Instrumentation	26
2.1. Raman Spectroscopy.....	27
2.1.1. Vibrational Spectroscopy Theory.....	27
2.1.3. Raman MR Probes.....	37
2.1.4. Raman PhAT Probes	40
2.1.5. Optical Fibres	41
2.2. Acoustic Emission Spectroscopy	42
2.2.1. Active.....	43

2.2.2. Passive	44
2.3. High Performance Liquid Chromatography ^{93, 94}	48
2.4. Multivariate Data Analysis ^{95, 96}	50
2.4.1. Principal Component Analysis.....	51
2.4.2. Partial Least Squares	52
2.5. Spectral Preprocessing ¹⁰⁸	53
2.5.1. Savitzky-Golay Derivatisation.....	54
2.5.2. (Extended) Multiplicative Scatter Correction and Standard Normal Variate Transformation	55
2.5.3. (Modified) Optimal Path-Length Optimisation and Correction.....	57
2.6. Raman Instrumentation	59
2.7. Reactor Equipment	60
3. Quantification and Monitoring of Residual Styrene Within Polystyrene Beads	62
3.1. Introduction.....	62
3.2. Instrumentation and Materials	63
3.2.1. HPLC	63
3.2.2. EPS Beads	64
3.3. Experimental	64
3.3.1. Polystyrene Bead Impregnation.....	65
3.3.2. EPS Bead Impregnation Verification via High Performance Liquid Chromatography	67
3.3.3. EPS Bead Impregnation Verification via Offline Raman	69
3.6.4. Effect of EPS Bead Size on Raman Spectroscopic Measurements.....	70
3.6.5. Wide Area Illumination Study	70

3.6.6.	Detection Limits of Styrene in EPS Beads via Raman MR and PhAT Probes	73
3.6.	Results and Discussion	73
3.6.5.	Detection of Styrene via MIR Spectroscopy	73
3.6.6.	Detection of Styrene via Raman Spectroscopy	77
3.7.3.	Detection of Styrene in EPS beads via Raman Spectroscopy	82
3.7.4.	Effect of EPS Bead Size on Raman Spectroscopic Measurements	93
3.7.5.	Wide Area Probe and Information Depth Study	97
3.7.6.	Detection Limits of Styrene in EPS Beads via Raman MR and PhAT Probes	108
3.9.	Conclusions and Further Work	110
4.	In-Situ Polymerisation Monitoring via Raman Spectroscopy and Spectral Data Preprocessing Investigation	112
4.1.	Introduction	112
4.2.	Instrumentation and Materials	113
4.3.	Experimental	113
4.3.1.	Suspension Polymerisation Reactions	113
4.3.2.	Reaction Monitoring via Raman Spectroscopy	115
4.3.3.	Reaction Monitoring via Offline Gravimetry	115
4.3.4.	Multivariate Analysis –PCA and PLS Modelling	120
4.3.5.	OPLEC Parameter Optimisation	122
4.4.	Results and Discussion	123
4.4.1.	Reaction Monitoring via Raman Spectroscopy	123
4.4.2.	Reaction Monitoring via HPLC	126
4.4.3.	Reaction Monitoring via Gravimetric Analysis	130

4.4.4. Multivariate Analysis – PCA and PLS Modelling.....	132
4.4.4. OPLEC Optimisation	140
4.5. Conclusions and Further Work.....	144
5. Monitoring of Suspension Polymerisation via Passive Acoustic Emission Spectroscopy.....	146
5.1. Introduction.....	146
5.2. Equipment and Materials	147
5.3. Experimental Procedures	147
5.3.1. Model Mixtures.....	147
5.3.1.1. Effect of EPS Bead Concentration	148
5.3.1.2. Effect of EPS Bead Size	148
5.3.1.3. Effect of Vessel Size.....	148
5.3.2. Suspension Polymerisation Reactions	149
5.4. Results and Discussion	149
5.4.1. Effect of EPS Bead Concentration and Size in Model Mixtures	149
5.4.2. Effects of Vessel Size and Dimensions	154
5.4.3. Relative Peak Area	158
5.4.4. Determination of Size and Concentration by PCA	161
5.4.5. Suspension Polymerisation Reactions	164
5.5. Conclusions and Further Work.....	168
6. Project Conclusions and Further Work	170
7. References.....	176

1. Introduction

Polystyrene is one of the most widely used plastic materials today due to its many applications, including packaging, appliances, construction, automobiles, electronics, furniture, toys, CD casings and luggage. The thermoplastic is low-cost, easily-formed through heat fabrication, highly efficient in thermal and electrical insulation and can come in rigid or foamed forms,¹ making it a highly-versatile and useful polymer. The foamed form, known as expanded polystyrene (EPS), is a closed-cell foam and is formed by introducing spherical polystyrene beads to a foaming agent – usually pentane. It is lightweight yet tough and so is particularly useful for the production of reliable packaging and cost-efficient construction materials.²

Styropor® – a form of EPS – was invented by BASF, a chemical company based in Ludwigshafen, Germany, in 1951. Founded in 1865, the company began plastics manufacture in 1929 with the synthesis of styrene and quickly moved onto developing polymer synthesis. A process known as suspension polymerisation is used to produce solid polystyrene beads which are then foamed with pentane, creating Styropor®. With the market value of EPS expected to rise to (U.S.) \$15bn by the year 2020,³ optimisation of its manufacture is of great interest to industry. To maximise the efficiency of the suspension polymerisation process and, thus, ensure a high-quality polymer product, the ability to monitor and control the process on-line has become a much-studied area. The implementation of these process analytical technologies (PAT) is of great benefit and interest to many chemical industries including pharmaceuticals, petrochemicals, bioprocesses and polymers. However, suspension polymerisation is a multi-phase system involving several organic and inorganic additives, which can lead to difficulties when attempting to retrieve real-time information.

1.1. The Polymerisation Process

Polymerisation is a widely studied and important chemical reaction, the products of which have a major impact on our daily lives due to their immense versatility. Polymers can be found in widely varied applications such as packaging, films, electronics, automotives, clothing, prosthetics and drug delivery supports⁴ to name but a few. The variety of the products of polymerisation is mirrored in the number of available methodologies for the reaction, one of the most commonly used being free-radical polymerisation. In general, free radical polymerisation can be described by the scheme in Table 1.1.⁵

Table 1.1 - Generalised Free-Radical Polymerisation Reaction Scheme showing (a) initiation by free radical I•, (b) propagation of free radicals through interaction with monomer M and polymer R, (c) termination via combination and (d) termination via disproportionation.

Reaction Step	General Scheme
(a) Initiation	$I-I \rightarrow 2 I\bullet$
(b) Propagation	$I\bullet + M \rightarrow R_1\bullet$
	$R_i\bullet + M \rightarrow R_{(i+1)}\bullet$
(c) Termination 1	$R_i\bullet + R_j\bullet \rightarrow R_{(i+j)}$
(d) Termination 2	$R_i\bullet + R_j\bullet \rightarrow R_i + R_j$

This is a chain reaction whereby the build-up of monomer 'building blocks' into a polymer chain occurs via a polymeric radical, $R_i\bullet$. In step (a), the initiator decomposes into two units of the radical species $I\bullet$. This radical then comes in contact with a molecule of monomer, M , and adds to its vinyl bond, forming an entirely new radical species, $R_1\bullet$ (b part 1). This radical species continues to propagate and grow by adding to the vinyl bonds of present monomer units, Step (b part 2), until the reaction is stopped either through combination, Step (c), or disproportionation, Step (d).

This general scheme holds true for polymer products whether they are manufactured in a homogeneous (e.g. bulk polymerisation) or heterogeneous (e.g. suspension polymerisation) manner. Heterogeneous polymerisation reactions often provide further challenges to monitoring systems due to their multi-phase nature and the presence of additives – e.g. surfactants and stabilisers – which can interfere with spectroscopic measurements.

1.2. Suspension Polymerisation of Styrene^{6,7}

Suspension polymerisation involves small monomer droplets dispersed in medium (Figure 1.2) – usually water – using a micelle-forming surfactant, which for this reaction is sodium dodecylbenzenesulfonate (SDBS, Figure 1.1). The surfactant is dissolved in water, forming a solution of micelles which, under agitation, allows the monomer of interest to be dispersed throughout the medium by partitioning into the micelles as opposed to forming a separate distinct layer. The initiator in suspension polymerisation reactions – in this case, dibenzoyl peroxide (DBPO, Figure 1.1a) – is soluble in the monomer phase. Furthermore, an inorganic salt – tricalcium phosphate (TCP) – is often used to stabilize the micelle suspension and prevent coalescence of monomer droplets and coagulation once the polymerisation process begins. Each of these droplets can be treated as a miniature batch reactor suspended in water and, as such, it is assumed that all reactants are evenly distributed to allow polymerisation. Furthermore, if all monomer droplets are considered individual batch reactors, it follows that some unreacted monomer is left dispersed throughout the polymer bead product. This presents safety considerations for BASF in the handling and release of these beads as products due to the toxicity of styrene.

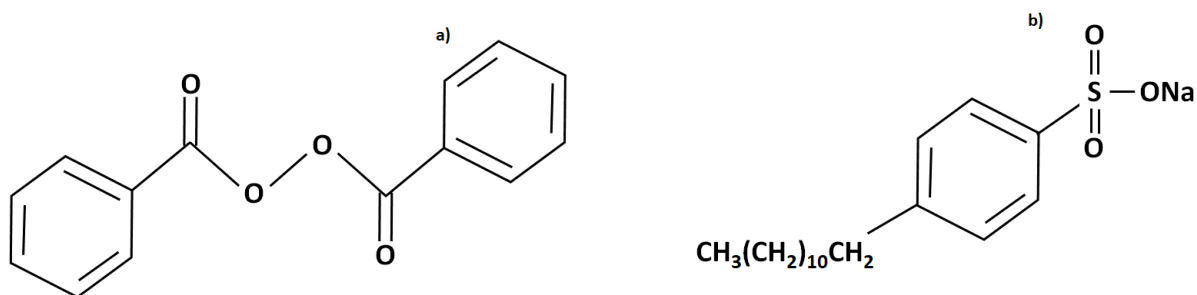


Figure 1.1 – Molecular structures of (a) dibenzoyl peroxide (DBPO) and (b) sodium dodecyl benzene sulfonate (SDBS).

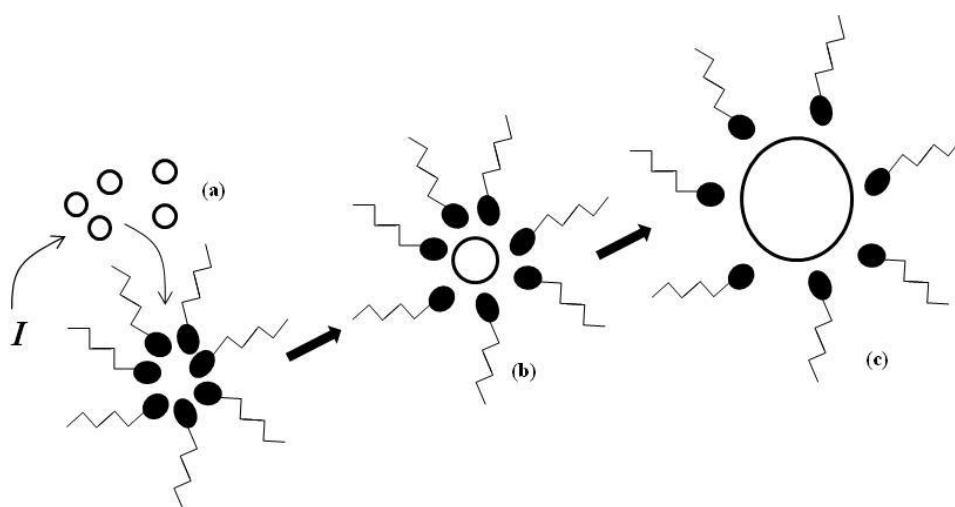


Figure 1.2 – Schematic of suspension polymerisation. (a) Oil-soluble initiator, *I*, dissolves into monomer droplets which, in turn, diffuse into micelles formed by surfactant molecules; (b) monomer-initiator droplets are dispersed throughout medium in micelles; (c) bead swelling as polymer is produced.

Once the reaction begins in each droplet, the surrounding water acts as an extremely effective heat transfer agent, allowing the reaction to proceed safely. Factors such as surfactant choice, stirrer rate and monomer-water ratio can affect the size of the monomer droplets at the outset of the reaction (Figure 1.2) which, in turn, influences the size of the reaction product beads.

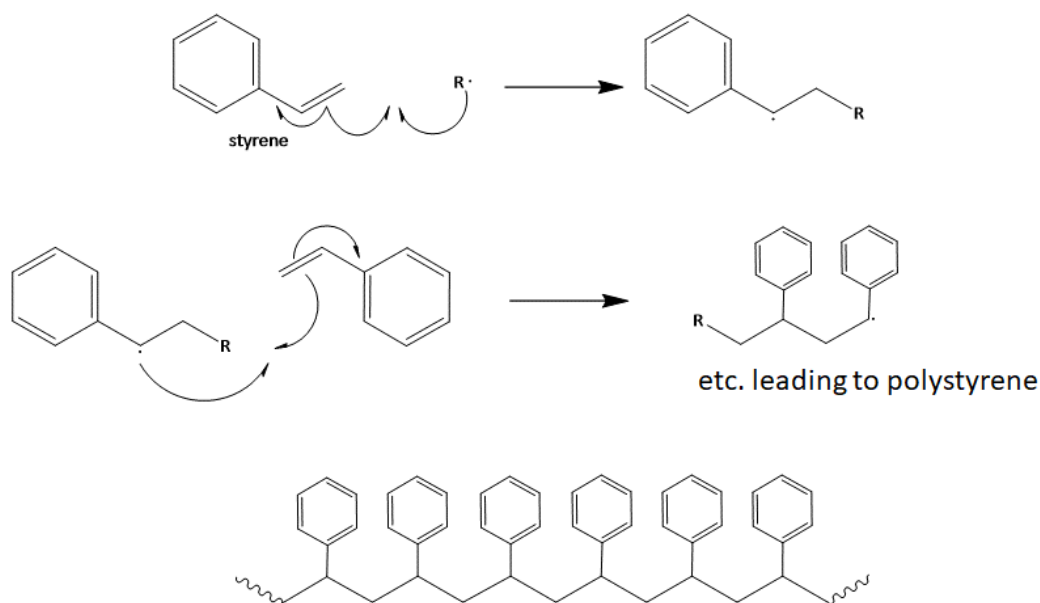


Figure 1.3 – Radical polymerisation of styrene scheme where R = DBPO.

Suspension polymerisation is very similar to emulsion polymerisation, therefore the issues encountered in implementing measures for monitoring and control of it are also similar. In emulsion polymerisation, the initiator is instead water-soluble and so results in much smaller polymer particles forming. The polymerisation begins in the monomer-swollen micelles which convert into latex particles although the precise mechanism for this is not fully understood.

1.3. Advantages of PAT Implementation

The implementation of PAT – sensors for the monitoring and control of chemical processes – has become one of the foremost areas of research and development (R&D) for industry for several reasons. Offline or at-line analytical methods can be costly, time-consuming and are not always able to provide real-time information. This can lead to product loss, batch-to-batch variability and over-running reactions at the expense of time and money. The inability to reliably monitor and control industrial chemical processes can also result in non-conformance with legislative

responsibilities – environmental, product/process safety, etc. – hindering product development and innovation.

Gathering real-time information from complex chemical processes allows the process to be run in a safe manner, avoiding hazardous situations such as runaway reactions which is of particular concern in the case of exothermic reactions such as the suspension polymerisation of styrene. Processes which consistently or repeatedly fail can be indicative of faulty equipment as well as improper chemical usage. By monitoring reactions which continue to fail in real-time, the factors contributing to the failure can be pinpointed which might highlight the maintenance and repair status of the reactor or other equipment, minimising the occurrence of batch-to-batch variation. Safety concerns are further alleviated by online process monitoring because the need for extractive sampling is minimised. By exploiting in-situ sensors, the need for physically taking samples from a reactor for off-line testing can be minimised, increasing the safety level of the production floor.

Bearing in mind the continuously available information on a reaction allows the optimisation of processes, for example those which involve feed systems⁸, thus minimising wastage and production costs by controlling feed-rates and energy consumption. Costs are also lowered by reducing the need for mid- and post-production quality control (QC) testing, saving time and manpower. This control is not only financially beneficial, but also provides key fundamental knowledge and understanding of the process being monitored. A 2012 ICHEMA trend report by Kessler *et. al.* found this to be the leading benefit of PAT from a poll of pharmaceutical companies.⁹

1.4. Implementation of PAT for Polymerisation

The implementation of PAT in some form in the chemical industry has been a continuously growing process since the early 1930s¹⁰ but has only come to the forefront of research and development since 2004 when the Food and Drug Administration (FDA) published guidelines¹¹ and current good manufacturing practices (cGMPs) which recognised PAT's true importance and set the industry on a dedicated path of innovation and discovery. These guidelines emphasised the need within industry for *real-time* quality assurance and incorporating risk-based quality management *into* the manufacturing process. By utilising state-of-the-art scientific instruments, powerful data-processing tools and innovative thinking, a greater understanding of chemical processes and the ability to exploit the various interdependent processes and chemical factors are gained, allowing quality to be built into a product via rigorous real-time quality monitoring and process understanding. Consequently, minimal product testing will be required, allowing for real-time release and minimising batch rejection.

Whilst industry guidelines initially focussed on pharmaceutical development and manufacture,¹¹ it was the intention that PAT could be used to the benefit of several chemical industries and scientific disciplines. This thesis aims to highlight how polymerisation science has benefitted from developments in PAT in recent years. Through examination of the various types of process and analytical information available and the techniques by which this information can be monitored and interpreted, an understanding of some of the benefits and limitations of PAT regarding monitoring of polymerisation reactions can be gained.

Polymerisation reactions, particularly heterophase systems such as suspension polymerisation, lend added difficulties to PAT implementation. As the reaction proceeds, liquid droplets gradually transform into solid particles of varying size, meaning that monitoring of the kinetics of the changing composition, as well as colloidal parameter variations, is required to fully describe the reaction's progress.

Furthermore, these reactions progress through stages where very viscous and sticky materials are formed, which could result in residual build-up on sensors in direct contact with the reaction medium *i.e.* spectroscopic probes or be too viscous to flow through sensor slits, travel lines or columns, as is often seen with online gas chromatography (GC).

Despite these difficulties, there have been various successful implementations of PAT throughout the polymer industry with many more on the horizon. Industrial-scale reactors for polymerisation reactions can range from 30 m³ to over 100 m³ and these large sizes influence the implementation of PAT. For instance, the exothermic nature of the reactions combined with the immense scale can lead to pronounced heat flux within the reactor. This makes temperature change a very easy parameter to monitor in real-time which can give fruitful information on the reaction kinetics. Temperature sensors – along with pressure, flow and power consumption sensors – have been successfully implemented in the polymer industry through combining the physical data they provide with chemical and mathematical modelling. These are known as ‘soft sensors’, whereby the inference of product properties that are difficult to measure (e.g. the rheology of the system) can be made from system properties which are easy to measure (e.g. reactor pressure).¹² These sensors can provide this information at the end or even during a process run, streamlining bottlenecks in the process (*i.e.* minimising end product quality testing) and shortening cycle times.

1.4.1. Process Temperature Sensors

Temperature of the processes are routinely monitored throughout the polymer industry. It is vital to be able to monitor the temperature of polymerisation reactions in real-time as they are exothermic and by monitoring the changes in temperature as the reaction proceeds it is possible to infer the reaction kinetics at any given time. This information can be obtained either through contact or non-contact equipment;

the choice of which depends on the accuracy and sensitivity that are required along with the temperature range involved in the process and the hostility of the environment to be monitored. However, it has been shown that, unsurprisingly, non-contact methods using infrared (IR) and fibre-optic technology are being used in preference to thermocouples and other contact temperature probes throughout the industry.¹³ Fibre-optic thermometers offer high degrees of accuracy and generate results very quickly but can be expensive and data can be challenging to interpret at high temperatures. IR sensors have proved very reliable in the polymer industry¹⁴ and have even been combined with attenuated total reflectance (ATR) Fourier-transform IR (FTIR) and optical pyrometry (OP)¹⁵ to yield superior results. OP is considered to be the most accurate in non-contact temperature monitoring technology for systems operating at very high temperatures.

1.4.2. Process Flow and Pressure Sensors

Rheology is defined as “the study of the deformation and flow of matter”¹⁶ and it is important to obtain information about the flow of a system because it pertains to how much material is being transported through the reaction vessel. Furthermore, polymerisation reactions, by their very nature, undergo extreme and often sudden changes in viscosity, thus, being able to monitor the flow of a reaction can give a lot of information about its progress. Information on the flow of a material has been classically obtained through measuring differences in: mass; velocity; positive displacement or differential pressure.¹⁷ However, the more recent developments in this area involve thermal, ultrasonic, Coriolis¹⁸ and electromagnetic sensors as well as multivariable transmitters, electric time-domain reflectometry (E-TDR) and process tomography (PT). ETDR involves sending a picosecond rise-time voltage step wave in a transmission line before detecting reflected voltages, which result from impedance discontinuities within the line, as a function of wave propagation time. In flow measurements, impedance discontinuities are created by the infiltrating resins. E-TDR has been widely applied to liquid composite modelling (LCM)¹⁹ and has the

capability to provide hundreds of sensing elements with a single probe, allowing the detection of multiple flow fronts.²⁰

Process tomography is a non-invasive imaging technique which has allowed the monitoring of wet and dry particulate processes²¹ with the potential for use in suspension and emulsion polymerisations (e.g. of styrene). However, despite the advantages of PT systems being simple and robust with a high imaging rate, there are several key operating considerations preventing them from being used more widespread in industry²². Before implementation of a PT system, the following must be addressed: High temperatures and pressures require careful planning and innovative thinking before these sensors can be incorporated into a process; sensor fouling is always an issue; electrical safety must be up to industry standard; finally, an imaging technique provides little in the way of automated control of a system, therefore a computational method of converting the images into numbers which can be processed is key.

A study which compared the performance of Coriolis, electromagnetic and ultrasonic sensors²³ found Coriolis sensors to be the most accurate for the analysis of non-Newtonian fluids like polymer solutions. These sensors use vibrating tubes with known vibratory profiles under no-flow conditions which twist when flowing material is introduced through them. This twist causes a phase shift in the sine wave produced by the vibration of the tube(s) which is recorded by the Coriolis detector.¹⁸ Ultrasonic sensors were found to be significantly inaccurate under the same conditions due to its sensitivity to changes in the flow velocity profile. The main advantage of a Coriolis sensor is that they are unaffected by temperature or viscosity changes. Finally, multivariable transmitters have become available which can measure differential pressure, process pressure and temperature with a single transmitter, allowing the flow of the system to be calculated in real-time, monitored and controlled.

The pressure of a system – be it differential, gauge or absolute pressure – is easily and routinely measured for polymerisation reactions. Many types of pressure sensing apparatus exist but recently fibre-optic technology has provided novel and innovative pressure sensing techniques for use in the type of harsh environment commonly encountered in polymerisation processes.²⁴ The high degree of research and development in this area has led to sensors which are low-cost, simpler to manufacture and able to withstand high temperature and pressure environments.²⁵

The development of ‘soft sensor’ approaches has been invaluable to the polymer industry and the chemical industry as a whole. By computational means, easily measurable reactor variables such as pressure, reactor temperature and even the current at which the agitator in the reactor is working²⁶ can provide a wealth of information about the reaction (rheology, monomer conversion, weight average molecular weight, etc) as it progresses *i.e.* in real-time. This, in turn, allows real-time control over the reaction which is hugely beneficial both monetarily and intellectually as they improve process efficiency whilst providing insight into the chemistry of the reactions.

1.4.3. Chemical Data Sensors

For greater control over polymerisation processes, more in-depth information about the chemistry of the reaction itself (as opposed to reactor variable information) is required. In-line and on-line sensors for monitoring polymerisation reactions have developed immensely in the past decade to overcome many challenges. There have been many innovative techniques developed as well as novel applications of existing techniques and, again, soft sensors provide the key to interpreting the data which these techniques provide.

There are many techniques which utilise soft sensor technology to infer chemical information during polymerisation processes. For the purposes of this report, spectroscopic techniques will be the primary focus, however it is worth mentioning briefly some of the other important techniques and their usefulness in this field:

1) Conductometry can be used for processes where there is an established relationship between ion concentration and conductivity.¹⁶ This technique has been applied to polymerisation reactions by Santos et al.²⁷ to monitor ionic surfactant coverage during emulsion polymerisation of styrene.

2) Gas Chromatography (GC) has been used on many occasions to quantify the unreacted monomer in a reaction i.e. polymer molecular weight averages and molecular weight distributions²⁸. However, the sampling times can run too high for any hope of automated process control.

3) Ion mobility spectrometry (IMS) is similar to GC although it involves the ionisation of the gas phase using ultraviolet (UV) light. It has shown great potential as a low-cost, precise, reliable and fast way of determining monomer concentrations in emulsion polymerisation, even at small concentrations.²⁹

4) Calorimetry is a well-established and reliable technique which has found new life in online reaction monitoring through developments in soft sensors. Calorimetry lends itself well to monitoring polymerisation reactions due to their exothermic nature. Calorimetric methods have been employed in the recent past to monitor and control polymerisations³⁰ as well as predicting polymer latex properties for emulsion polymerisations.³¹ Despite its usefulness, however, the technique remains flawed as its output is univariate. Multi-monomer reactions present problems in that conversion rates for individual monomers cannot be obtained without coupling

calorimetry with another – usually spectroscopic – technique such as Raman or IR spectroscopy.³²

There are many spectroscopic methods which have proved themselves invaluable assets in monitoring and control of polymerisation processes. Raman spectroscopy (RS) and Mid-Infrared (MIR) spectroscopy were used in this investigation but other techniques such as Near-IR (NIR) and UV-Visible (UV-Vis) have also been used.

1.4.4. Ultraviolet Spectroscopy

Ultraviolet spectroscopy is a well-known technique that has been successfully applied in the monitoring of polymerisation reactions. A study by Gossen and MacGregor³³ showed UV-Vis spectroscopy to be useful for predicting the weight fraction for different polymers in a styrene/methyl methacrylate copolymerisation although a sample conditioning loop was required to dilute the sample beforehand. More recently, Celis and Garcia³⁴ used UV-Vis spectroscopy to monitor the droplet size distribution as a function of the temperature and oil phase concentration, however a dilution step was required to condition the sample before presenting it to the detector. Other groups have successfully applied UV-Vis spectroscopy to the automatic, continuous, on-line monitoring of polymerisation reactions (ACOMP) – a technique pioneered by Reed^{35, 36} which involves the continuous and automatic dilution of small sample streams from the reactor. Using this technique with UV-Vis spectroscopy, the solution copolymerisation of methyl methacrylate (MMA) and styrene was monitored, and the real-time co-monomer concentrations and incorporation rates were obtained.

Chai *et. al*³⁷ used ATR-UV spectroscopy to monitor the conversion in the miniemulsion polymerisation of MMA with the aid of a partial least squares (PLS) calibration model. This feasibility study showed a very good agreement between off-

line gravimetric measurements and on-line ATR-UV measurements. However, the adoption of UV spectroscopy for the monitoring of polymerisation reactions has not been as widespread due to the low number of vinyl polymers exhibiting UV absorption.³⁸

1.4.5. Raman Spectroscopy

Raman Spectroscopy has been used for off-line characterisation of polymerisation products for some time. However, Santos *et al.*³⁹ demonstrated the potential for RS to be used non-invasively for monitoring the suspension polymerisation process of styrene in real-time. Using a Fourier transform Raman spectrometer with a 1064 nm laser, on-line measurements, each spectrum produced was an average of 32 scans to produce fast results comparable to the reaction dynamics, were compared to off-line measurements, each spectrum this time being an average of 256 scans, improving the signal-to-noise ratio (S/N). The small number of scans taken on-line led to a poor S/N; therefore, a smoothing spline filter was applied online to provide a smooth representation of the noisy measured data without being affected by any random changes. By applying this, the Raman data showed very good agreement with off-line gravimetric analysis and the conversion could be accurately estimated.

Furthermore, there was evidence that variations in the heterogeneity of the reaction medium affected the Raman signal, showing potential for RS in the determination and monitoring of particle size. To assess this, principal component analysis (PCA) was used and the results were also compared to off-line measurements – again, using an average of 256 scans with the Raman spectrometer. The results of on-line and off-line analysis suggested that smaller particle sizes give rise to larger Raman scattering, particularly in the region under 600 cm⁻¹.

In addition to this, Jiang et al.⁴⁰ were able to infer kinetic information on the solution polymerisation of methyl methacrylate (MMA) by using a non-invasive 785 nm Raman microscope. They monitored the reaction by taking a 20 second scan every 75 seconds over a 3-hour time interval, performing several of these and changing different parameters each time (initial monomer concentration; initiator concentration and temperature). As before, a smoothing filter was used to aid interpretation of noisy data but here a novel multivariate chemometric technique, band-target entropy minimisation (BTEM), allowed the elucidation of pure component spectra from the reaction mixture. This data was used to infer the conversion of monomer which, in turn, was used to calculate key kinetic data i.e. reaction orders with respect to monomer and initiator concentrations (1.41 and 0.55 respectively); a monomer consumption rate equation and the activation energy for the polymerisation (121 kJ mol⁻¹).

However, several obstacles are presented by the use of RS in polymerisation monitoring. Component materials in such reactions (e.g. monomers, surfactants, stabilisers) can cause fluorescence which interferes with the Raman signal. This is often overcome by using higher excitation wavelengths (e.g. 785 nm or 1064 nm) however this in turn can cause issues as it causes a decrease in the Raman effect and an increase in signal variation caused by water. Furthermore, spectral intensities from RS will vary with time as the laser intensity changes which can be misleading and cause problems when interpreting data in real-time. To resolve this, a reference band (of a known concentration) is often also monitored e.g. that of the phenyl ring in styrene polymerisation.

1.4.6. *Mid-Infrared Spectroscopy*

The Mid-Infrared (MIR) region (4000 – 400 cm⁻¹) corresponds to fundamental molecular vibrations and contains the frequency range known as the ‘fingerprint region’ (1500-400 cm⁻¹). One major disadvantage of using IR techniques to monitor

polymerisation reactions is that water absorbs strongly in the IR region, leading to complications when highly aqueous matrices are concerned. ATR technology has allowed industry to overcome this challenge; not only do they allow IR spectroscopy in the presence of water but they also eliminate sample preparation which allows spectral changes to be monitored in real-time.⁴¹

IR is often combined with Fourier-transform (FTIR) which can provide key information; as was exemplified by Roberge and Dubé⁴² when they monitored monomer concentration and conversion during the homo- and co-polymerisation reactions of styrene and butyl acrylate (BA). In this work, they analysed the miniemulsion solutions every 2 minutes as the polymerisation progressed, each measurement taking 128 scans in the MIR region (4000-700 cm^{-1}). The chosen probe used light conduit technology rather than optical fibres which are more widely used. The results obtained through the in-line ATR-FTIR method were compared with off-line gravimetry and proton nuclear magnetic resonance ($^1\text{H-NMR}$) to assess the validity of ATR-FTIR for this application. The data from the ATR-FTIR analyses was treated with a simple univariate processing approach to estimate monomer conversion which proved unsuccessful, despite previous results suggesting that univariate calibration was sufficient for estimating monomer conversion in BA, MMA and vinyl acetate homo-, co- and terp-polymerisations.²⁸ A PLS method was then applied and the results were much more encouraging – particularly in the 1800-650 cm^{-1} region – further confirming the success of the calibration model for estimating monomer concentrations and, hence, conversion rate. Having previously shown that a univariate approach to data interpretation does work in the estimation of monomer conversion for polymerisation systems, the results from this study indicate that this may be dependent on the system under investigation.

1.4.7. *Near Infrared Spectroscopy*

Extending from 13000 – 4000 cm^{-1} , the NIR region provides information on overtones and combination bands and is therefore much weaker than MIR spectra which, coupled with the strong IR absorption bands of water and its sensitivity to temperature change, make NIR monitoring of suspension polymerisation difficult. Therefore, mathematical methods are almost always employed when using NIR, with PLS and PCA being the most widely-used.¹⁶ Cherfi et. al⁴³ combined NIR spectroscopy with a “standard” PLS regression to very successfully describe the monomer conversion and weight-average molecular weight during the solution polymerisation of MMA in toluene. This was done regardless of pure-batch or fed-batch conditions.

Other research shows that even highly aqueous systems can yield information with NIR spectroscopy.⁴⁴ This work showed that NIR could be used to describe the average polymer particle size during an emulsion polymerisation. The data used to build the calibration model was chosen to show how the particle size could be predicted independently of polymer content and monomer concentration. In addition, the authors demonstrated the success of NIR in process monitoring relies heavily on the development of reliable calibration models for each property of interest. The models have to be fitted from data (spectra) which represent the behaviour of the process in question. Prediction of particle size was successful but the prediction of other properties – particularly monomer concentration – was poor. In order to better predict these other properties, other calibration models must be developed using data which describe each property at different stages throughout the reaction. Fontoura et. al⁴⁵ showed that, through combination of NIR measurements and a Kalman filter estimator, the monomer conversion and the polymer-average molecular weight could be simultaneously monitored and controlled throughout a reaction.

1.4.8. *Acoustic Emission Spectroscopy*

Methods of in-situ particle size measurement face many challenges, especially in turbid or opaque media. Typically, laser diffraction methods such as focussed beam reflectance measurement (FBRM)^{46, 47} or particle video microscopy (PVM)⁴⁸ can be used, but are expensive and require complex algorithms to convert the measurements into particle size measurements. Acoustic measurements can be made non-invasively and are not subject to probe fouling, like laser diffraction methods.

Active and passive acoustic emission spectroscopies (AES) utilise the naturally occurring change in acoustic waves generated in a reaction vessel as the reaction progresses to infer key reaction properties such as reaction rate and particle size within the reaction matrix.⁴⁹ The features of acoustic waves generated in a reaction matrix vary depending on the properties of the reaction medium, through which these waves propagate.⁵⁰ Furthermore, AES is not hindered by opaque or turbid media. While this method can lack the sensitivity of other spectroscopic techniques,⁵¹ its low cost, ease-of-implementation, non-invasive and non-destructive nature have made it a highly useful tool in the pharmaceutical,^{52, 53} petrochemical⁵⁴ and engineering⁵⁵ fields, to name a few. Its application in polymerisation monitoring has shown it to be useful in the inference of hardening rates, viscosity changes⁵⁶ and particle size distribution (PSD).⁵⁷

Non-invasive active ultrasound measurements are theoretically a good option for the measurement of particle size *in-situ* but, in practise, are subject to several disadvantages – the biggest issue is the vessel jacket as most of the ultrasound gets trapped in the jacket wall.⁵⁸ The use of active ultrasound measurements for in situ measurement of particle size is not straightforward. Comparatively, the use of passive acoustics for non-invasive monitoring of particle size is low cost and offers a cheap non-invasive means for monitoring of particle size.

Table 1.2 - A summary table of relevant analytical techniques and their advantages and disadvantages in the monitoring of polymerisation.

Technique	Advantages	Disadvantages
Temperature sensors	<ul style="list-style-type: none"> • Simple • Quick • Invasive or non-invasive • Styrene polymerisation is exothermic • Fibreoptic tech available allows remote sensing in extreme environments 	<ul style="list-style-type: none"> • Non-invasive methods can be low accuracy • Fibreoptics increase sensitivity and accuracy, but are expensive and provide complex data at high temperature • Information obtained is fundamental but limited
Pressure and flow sensors	<ul style="list-style-type: none"> • Fibreoptic tech allows low-cost, simple yet durable sensors, even in harsh reaction environments • Multiple flow fronts can be detected at once (EDTR) • PT is simple with a high imaging rate 	<ul style="list-style-type: none"> • Complex computational methods are required to extract meaningful information • Ultrasonic sensors are inaccurate at high temperature • PT requires time-intensive planning for use in extreme

	<ul style="list-style-type: none"> • Coriolis can be very accurate • Multivariable transmitters allow real-time monitoring and control 	<p>reaction environments</p> <ul style="list-style-type: none"> • Subject to probe fouling
Gas chromatography	<ul style="list-style-type: none"> • Can quantify unreacted monomer • Accurate 	<ul style="list-style-type: none"> • Sampling run-time is too long for real-time control • Viscous samples clog instrument lines
Conductometry	<ul style="list-style-type: none"> • Can determine surfactant coverage in emulsion polymerisations 	<ul style="list-style-type: none"> • No information on the reaction chemistry or kinetics
Calorimetry	<ul style="list-style-type: none"> • Well-established • Reliable • Can predict polymer properties from emulsion polymerisations 	<ul style="list-style-type: none"> • Univariate output, making it a poor technique for co-polymerisation reactions
Gravimetry	<ul style="list-style-type: none"> • Well-established, relatively simple, accurate • Often used as offline method of monomer 	<ul style="list-style-type: none"> • Assumes completely even dispersion of all reaction constituents • Time and labour-intensive • Time-sensitive

	conversion measurement	
HPLC	<ul style="list-style-type: none"> • Sensitive, accurate, robust • Quantitative 	<ul style="list-style-type: none"> • Sample preparation required • Sample run-times are long • Time and labour-intensive
UV-Vis spectroscopy	<ul style="list-style-type: none"> • Well-established • Predicts weight fractions in copolymerisations • Monitors droplet size distribution 	<ul style="list-style-type: none"> • Often requires sample pre-treatment e.g. dilution
Raman spectroscopy	<ul style="list-style-type: none"> • Sensitive to C=C double-bond breakage seen during polymerisation • Fast sampling rate • Particle sizing is possible • Can easily take measurements in aqueous media 	<ul style="list-style-type: none"> • Susceptible to fluorescence • Complex reaction matrix can interfere with spectrum • Laser intensity can change over time, leading to misleading changes in Raman intensity • Probe fouling is an issue

<p>Mid-Infrared spectroscopy</p>	<ul style="list-style-type: none"> • Encompasses the ‘fingerprint region’ • Compatible with ATR technology • Fast, reliable, specific and accurate 	<ul style="list-style-type: none"> • Highly susceptible to interference from water • Can require sample preparation before measurement • Susceptible to probe fouling • Lots of work required to ensure method is accurate and reliable (suitability tests)
<p>Near Infrared spectroscopy</p>	<ul style="list-style-type: none"> • Use of MVA methods with NIR spectra can greatly improve results • Fast, cheap and reliable 	<ul style="list-style-type: none"> • Weak signals compared to MIR • Highly susceptible to aqueous interference • Complex and highly specific calibration models are required
<p>Acoustic emission spectroscopy</p>	<ul style="list-style-type: none"> • Fast, cheap, non-invasive • Particle size, distribution and density directly affects spectra 	<ul style="list-style-type: none"> • Much of the available data is lost in the vessel wall/jacket • Ambient machinery can interfere

This review highlights the challenges associated with polymerisation monitoring and the limitations of the analytical methods for doing so. Each technique shows promise in solving the challenges with this project, but a balance should be achieved between applicability, cost, ease of implementation, and most importantly speed, among other factors. The key for this project is the ability for a technique to provide the information in real-time, to allow for reaction control as well as monitoring. Online spectroscopic techniques such as MIR and Raman allow the fastest gathering of the large quantities of chemical information while remaining cheap and easy to implement and their potential for monomer conversion monitoring will be investigated in this project. Robust offline methods for quantification of monomer conversion – gravimetric analysis and HPLC – will also be used as confirmatory techniques to shore up models built with spectroscopic data. Furthermore, acoustic emission spectroscopy will be investigated as a fast, low-cost and reliable method of estimating particle size distribution compared to offline sieving analysis.

1.5. Project Aims

There are several economic and environmental drivers at the heart of this project. The tightening of product and process safety specifications and strict environmental constraints mean that innovative approaches to equipment implementation and plant operation must be developed to ensure efficient and sustainable production. Key information on solution composition, PSD, and residual monomer level is desired to allow process optimisation and intensification which could lead to the end of product post-treatment, reduce reaction run-time and lessen the production of off-specification product. The aim was to gain an understanding of how the reaction works and to investigate the potential applications of Raman spectroscopy in monitoring the process, with emphasis on the residual monomer level within the polymer product. Current monitoring techniques employed by BASF (Raman spectroscopy) have been successful at establishing residual monomer levels down to as low as approximately 2% wt. or 20,000 $\mu\text{g g}^{-1}$ (ppm). However, current safety

standards dictate that the upper threshold for residual monomer within the bead products is 0.1% wt. (1000 ppm).

To achieve this, it was first imperative to identify which analytical methods were best suited to monitoring this process, given the substantial challenge of obtaining this level of chemical information non-destructively and non-invasively from inside solid polymer beads in a turbid, heterogeneous suspension. Once identified and evaluated, these techniques were to be combined with modern statistical modelling methods to monitor this reaction for real-time process control at BASF. The complexity of the reaction matrix is reflected in the complexity of spectroscopic data obtained from it, the implementation of mathematical pre-treatment methods can help overcome this and allow meaningful data to be collected.

One key challenge in this is that the particles produced in this reaction can be of several millimetres in diameter, making conventional Raman spectroscopy difficult as their sampling size and penetration depth can be limited. However, the development of wide-area Raman probes has the potential to provide more reliable information from heterogeneously distributed sample media. They are, however, more difficult to implement, particularly at lab-scale. Therefore, their applicability and to what extent the information they provide is greater than that obtained with 'traditional' Raman probes was assessed.

The goal of this project in terms of residual monomer levels was to either have monitoring capabilities sensitive enough to detect and quantify styrene to this level or to build predictive models robust enough to predict when a reaction will yield products below this limit once a detection limit above 1000 ppm has been reached. Building on this, the project aimed to develop mathematical models which use the spectroscopic data to affect real-time process control measures. These models would be treated with an array of spectral pre-processing methods ranging from

basic techniques to novel approaches to extract the maximum valuable information from the spectral data and gain a deeper understanding – and thus control – of the reaction. The robustness of models built using these pre-treatment methods and their ease of applicability would serve as a measure of their potential for this application.

Finally, the determination of particle size and particle size distribution was to be investigated. Acoustic emission spectroscopy – a non-invasive, cheap alternative to labour-intensive and time-consuming particle sieving analysis or expensive and invasive imaging techniques – was to be applied to model mixtures and lab-scale suspension polymerisation reactions to establish what particle size information could be extracted and analysed potentially in real-time. The degree of correlation between acoustic data obtained and offline particle size or PSD information would indicate this technique's potential use in this environment. The ability to monitor and control PSD throughout a reaction is essential for controlling the rate of the reaction as a whole and much sought after by industry.

2. Theory and Instrumentation

Of the many spectroscopic techniques available, MIR, NIR, UV-Vis and Raman are by far the most well-understood and potentially useful for online real-time polymerisation monitoring. These techniques have all proved to be useful on lab-scale polymerisation reactions with the real potential for implementation on an industrial scale. UV-Vis spectroscopy often requires sample conditioning in the case of suspension and emulsion reactions. Although there is evidence of its use for monitoring a polymerisation reaction in toluene,⁵⁹ there remains more work to be done before it is an ideal technique for aqueous systems. NIR measurements require very complex mathematical modelling before any substantial information can be obtained. Once developed, however, the models and NIR measurements can yield a wealth of information. Raman and ATR-MIR measurements are well-established techniques routinely used in reaction conditions similar to those studied in this work and both are readily obtainable; therefore, they serve as ideal starting points for this investigation.

Furthermore, researchers at Strathclyde have a wealth of experience in the use of acoustic emission spectroscopy (AES) in monitoring several industrial chemical processes.^{49, 51, 60-62} The formation of solid particles in an agitated aqueous medium – such as in the polymerisation process in this study – lends itself very well to this method of non-destructive, non-invasive and high-throughput data collection, yet examples in literature appear almost non-existent. With the exception of a few patented viscosity measurement techniques,^{63, 64} this appears to be a widely underutilised polymerisation monitoring method with the potential to provide information on PSD, polymer bead hardening, batch failure and more. Therefore, this technique was also implemented in the monitoring of the reaction.

The quality of the models built from these monitoring techniques, however, is only as good as the reference data used to build them. It is therefore of great importance to establish robust and reliable methods of ascertaining definitive reaction information to provide the foundations on which complex models can be built using

spectroscopic data. In this work, the primary focus was the consumption of monomer to form polymer beads. One of the most common and well-known methods of accurately assessing this conversion is offline gravimetry, therefore it was used throughout this study as a reference method for the determination of polymer conversion.

2.1. Raman Spectroscopy

Raman spectroscopy (RS) is an ideal candidate for monitoring this reaction for several reasons: the highly aqueous nature of the reaction matrix causes no interference with RS as it would with other techniques such as MIR, the use of longer wavelength lasers can reduce fluorescence interference caused by inorganic additives (salts and surfactants typical of suspension polymerisations) and the carbon-carbon double-bond produces a sharp characteristic Raman band which can clearly be followed as the reaction progresses and these bonds are broken down. Furthermore, spectral acquisition times are incredibly short when compared to the time and labour-intensive offline techniques available such as gravimetric analysis, which is used routinely throughout industry. Indeed, RS has previously been used in studies of monomer conversion during the suspension polymerisation of styrene³⁹ and the results showed that not only is RS applicable for monitoring chemical properties such as monomer conversion but it may also be useful for the determination of physical properties such as PSD.

2.1.1. Vibrational Spectroscopy Theory

The overall energy of a molecule (E_{total}) is best described by separating it into three distinct additive components – the energy associated with the movement of electrons within the molecule (E_{el}), the vibration of the molecule (E_{vib}) and the rotation of the molecule (E_{rot}).

$$E_{\text{total}} = E_{\text{el}} + E_{\text{vib}} + E_{\text{rot}}$$

Equation 2.1

Spectroscopy involves irradiating a sample with light and studying how that light interacts with matter in the sample.⁶⁵ The frequency, ν , of the incident light is a measure of how many electromagnetic waves there are in the distance that the light travels in one second and is directly proportional to the amount of energy transferred to the molecule (Equation 2.2).

$$\Delta E = h\nu = h \frac{c}{\lambda} = E_2 - E_1 \quad \text{Equation 2.2}$$

Where:

- ΔE = the difference in energy between two quantized states, E_1 and E_2 ($E_2 > E_1$);
- h = Planck's constant, $6.62606957 \times 10^{-34} \text{ m}^2 \text{ kg} / \text{s}$;
- ν = the frequency of the light, s^{-1} or "Hertz" (Hz);
- c = the velocity of light, $3 \times 10^{10} \text{ cm s}^{-1}$ and
- λ = the wavelength of the electromagnetic wave, cm.

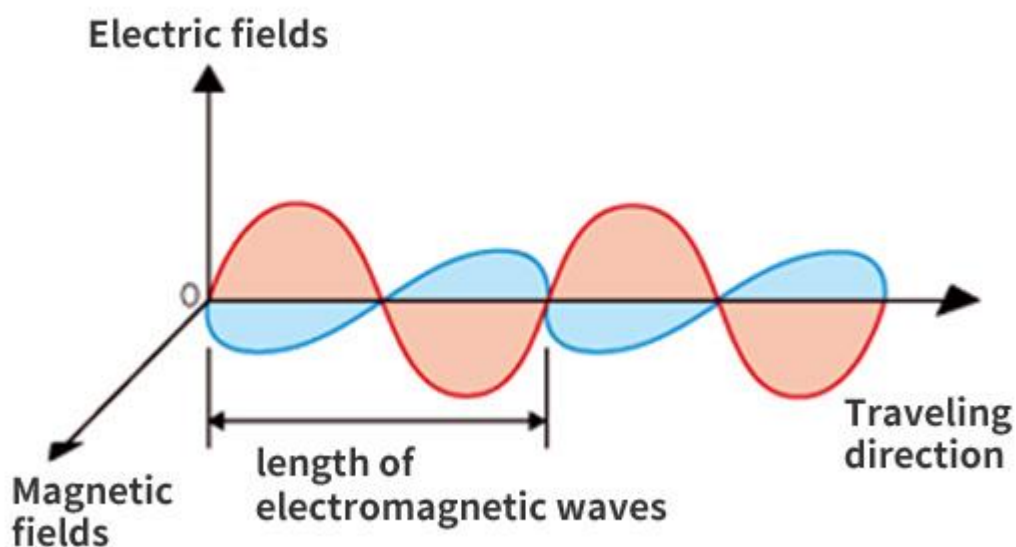


Figure 2.1 – An electromagnetic wave separated into electric and magnetic components showing the direction of propagation and wavelength.⁶⁶

More commonly in spectroscopy, the term ‘wavenumber’, $\tilde{\nu}$, is used and is defined by Equation 2.3.

$$\tilde{\nu} = \frac{1}{\lambda} \qquad \text{Equation 2.3}$$

Wavenumber, therefore, has units of cm^{-1} and can be related to the change in energy of the molecule by combining Equations 2.2 and 2.3:

$$\Delta E = hc\tilde{\nu} \qquad \text{Equation 2.4}$$

When the incident light photons come into contact with the sample, several events can occur including: (1) absorption of light energy by a molecule; (2) scattering of light by the molecule and (3) emission. The scattering of light is utilised in RS and the absorption of energy is the basis for IR spectroscopy. Vibrational transitions are observed in Raman and IR spectra and occur in the 10^2 - 10^4 cm^{-1} region of the electromagnetic spectrum. The electromagnetic spectrum – or, more accurately, electromagnetic radiation – ranges from gamma and cosmic rays, through ultraviolet (UV), visible, infrared (IR) and microwaves, to radio frequencies as shown in Figure 2.2.

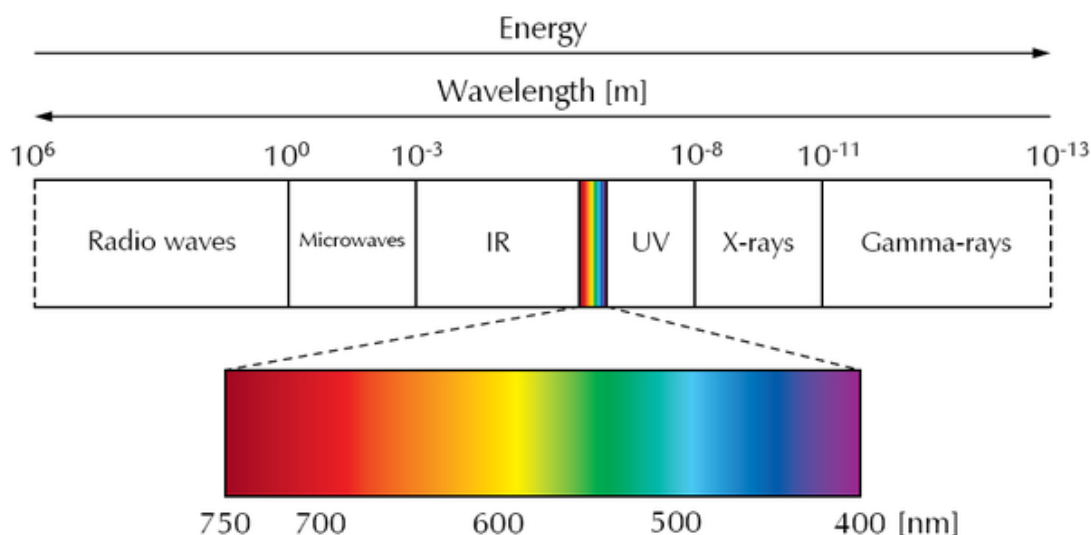


Figure 2.2 – Regions of the electromagnetic spectrum emphasising the visible light region.⁶⁷

The simplest way to describe the process of molecular vibration is to consider the harmonic oscillator model, where a diatomic molecule is presented as two bodies of different mass connected by a 'spring' at an equilibrium distance of r_0 (Figure 2.3). This 'spring' represents the electrons in the bond between the two bodies and the bodies themselves represent each nucleus in the molecule.

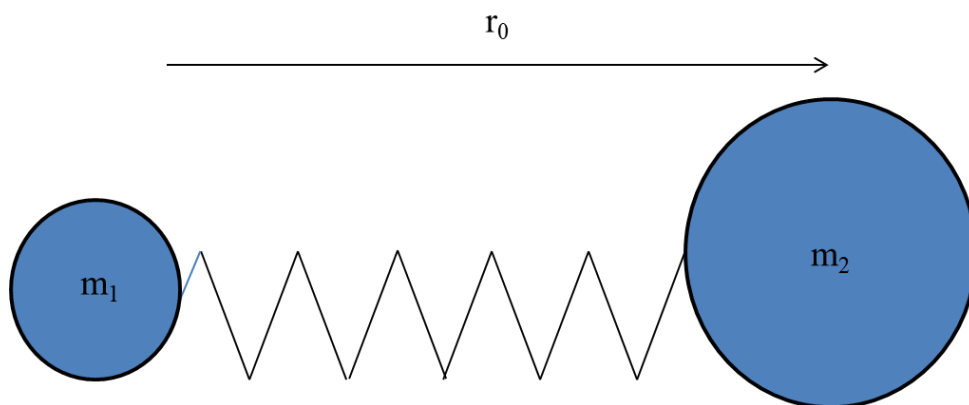


Figure 2.3 –Schematic of a simple diatomic molecule where nuclei are represented by m_1 and m_2 held together by a 'spring'.

As *both* nuclei are in motion, the mass of the system can be approximated to take this into account by combining m_1 and m_2 as per Equation 2.5:

$$\mu = \frac{m_1 m_2}{m_1 + m_2} \quad \text{Equation 2.5}$$

Where:

- μ = the reduced mass;
- m_1 = the mass of nucleus 1 and
- m_2 = the mass of nucleus 2

In this model, the force exerted on each nucleus as the molecule vibrates (i.e. as each nucleus moves from equilibrium position) can be calculated as a product of a constant, k , and its position in space, x , relative to its origin – i.e. the displacement (Equation 2.6).

$$F = -kx \quad \text{Equation 2.6}$$

Where:

- F = the force on each of the nuclei;
- k = the force constant and
- x = the displacement of the nucleus with respect to its origin.

The potential energy for this system, V , can also be calculated as per Equation 2.7:

$$V = \frac{1}{2} k(\Delta r)^2 = \frac{1}{2} kx^2 \quad \text{Equation 2.7}$$

Where:

- V = the potential energy of the system;
- k = the force constant and
- $\Delta r = x$ and is the change in the nuclear position from equilibrium, r_0 , to a new position, r .

Plotting this potential energy as the displacement, x , changes gives rise to a potential energy curve as described in Figure 2.4:

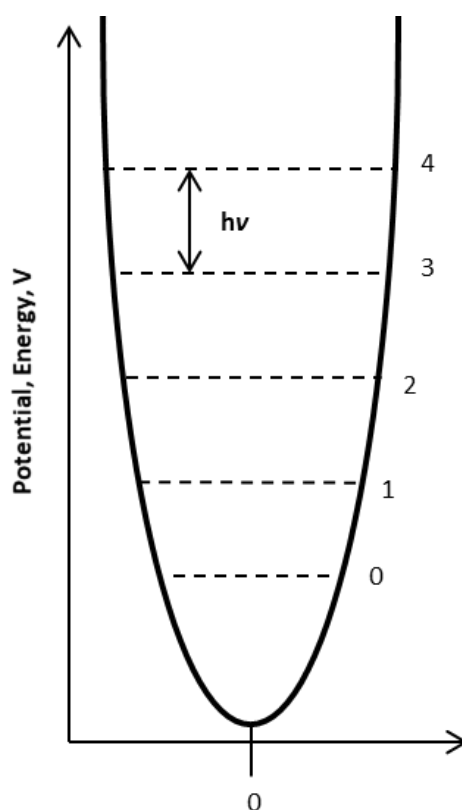


Figure 2.4 – Potential energy curve for a harmonic oscillator as a function of Δr .

The dotted lines represent the permitted vibrational energy levels for the molecule, which are all separated by the same value of $h\nu$. The value of each energy level can be calculated by:

$$E_n = (v + \frac{1}{2})h\nu$$

Equation 2.8

Where:

- E = the allowed energy of the system;
- v = vibrational quantum number (0, 1, 2, 3...);
- h = Planck's constant, $6.62606957 \times 10^{-34} \text{ m}^2 \text{ kg / s}$ and
- ν = the frequency of the vibration, s^{-1}

The absorption of energy from light photons at a value of $h\nu$ causes a change in the vibrational energy of the molecule, which is the mechanism at the centre of all spectroscopic techniques. As only absorption of energy in quantities of $h\nu$ take place, the vibrational energy change of a harmonic oscillator only takes place between adjacent energy levels i.e. from E_n to E_{n+1} . However, since the number of molecules existing in an excited state, $E_{n>0}$, will be low at room temperature (as described by Boltzmann's distribution law, Equation 2.9), only fundamental absorptions, those from E_0 to E_1 , are usually seen and the frequency of these fundamental transitions usually fall within the IR region of $4000\text{-}400 \text{ cm}^{-1}$.

$$N_1 / N_0 = \exp[-(E_1 - E_0) / kT]$$

Equation 2.9

Where:

- N_1/N_0 = the ration of molecules in energy level E_1 to those in E_0 ;
- k = Boltzmann's constant and
- T = the temperature, K

The harmonic oscillator model only holds true, however, when Δr is small, which is only true for a few molecules. In reality, larger deviations from r_0 occur, resulting in

anharmonicity of the system. This can be represented by a Morse potential curve as shown in Figure 2.5. Anharmonicity occurs due to the build-up of electron repulsion as atoms become closer together (as x goes towards 0) and the dissipation of energy as a bond is broken (as x increases).

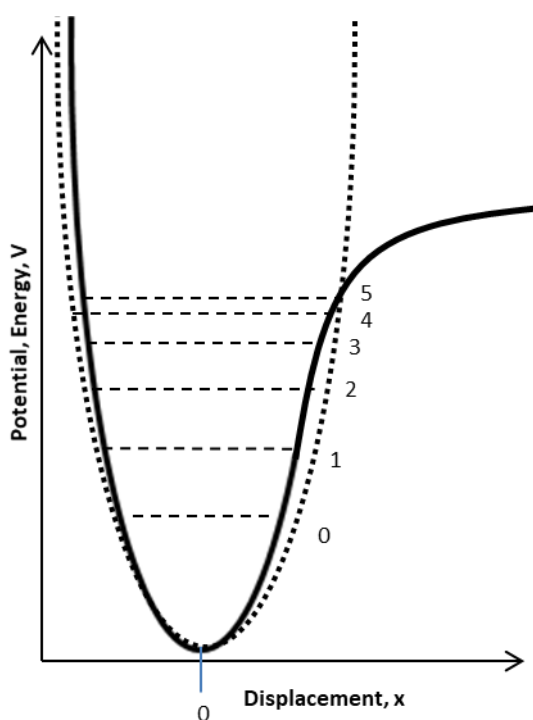


Figure 2.5 - Potential energy curve for an anharmonic oscillator as a function of Δr (black) compared to that for a harmonic oscillator (dotted).

This in turn affects the energy levels within the system which are no longer evenly spaced. Transitions from one energy level to one other than the adjacent level are now allowed, and such transitions are known as overtones. The intensity of these overtones is proportional to the anharmonicity of the system and these can be analysed using near-infrared (NIR) spectroscopy ($12500\text{-}4000\text{ cm}^{-1}$), which is in the region beyond the limit of MIR spectroscopy ($4000\text{-}400\text{ cm}^{-1}$) and not part of this study.

The calculation of the energy value of these energy levels is now described by Equation 2.10:

$$E_n = hv[(v + \frac{1}{2}) - x_e(v + \frac{1}{2})^2] \quad \text{Equation 2.10}$$

Where:

- v = any positive integer (0, 1, 2, 3...);
- hv = the energy per quantum of radiation and
- x_e = the anharmonicity constant.

Moving from diatomic to polyatomic molecules increases the number of fundamental vibrations; each of these vibrations being called a 'normal mode', which describes the collective motion of every atom in the molecule where they all move in phase with one another at a particular frequency. Linear molecules are capable of $3N-5$ normal modes, whereas non-linear molecules are capable of $3N-6$ (where N is the number of atoms in the molecule). This is because linear molecules' rotation about the molecular axis cannot be observed.

Raman and Infrared spectra are both used to observe the vibrational transitions. However, the physical origins of their spectra are very different: IR spectra arise from photons in the IR region which are absorbed by transitions between vibrational energy states of a molecule, whereas Raman spectra originate from the polarisation of the molecule's electron cloud by the incident light.

Raman spectroscopy (RS) is of high interest to those wishing to monitor and control industrial polymerisation reactions as it provides results quickly, is non-invasive and

non-destructive. It is also well-known that water has an extremely weak signal in RS and therefore the technique is ideally suited to monitoring highly aqueous matrices e.g. emulsion and suspension polymerisations. An intrinsic property of many polymerisation reactions is the reduction of a C-C multiple bond, which gives rise to a strong characteristic Raman peak which changes in intensity as the bond is reduced, allowing reaction progress to be easily inferred. Thus, RS has been applied to many areas of the polymer industry for monitoring and control purposes over the years.^{12, 68-70}

Since its discovery in 1928 by C. V. Raman,⁷¹ RS has become an invaluable analytical tool with many applications ranging from cell mapping⁷² to quantitative and qualitative analysis on the nanoscale.⁷³ When a photon from an incident light source interacts with a molecule, the light is either absorbed or scattered and it is this scattering of light that gives rise to the Raman effect. Most of this scattered light is elastic scattering, termed Rayleigh scattering, where the incident photon interacts with the electron cloud of the molecule and distorting it before scattering. Little to no energy is transferred to or from the photons from the molecule.

In this process, approximately only one in 10^6 of these photons interact with the molecule via an inelastic process known as Raman scattering. In Raman scattering, the incident photons cause an induced dipole in the molecule as internuclear distances are changed and the molecule becomes polarised. This occurs in one of two ways: the transfer of energy from the photon to the molecule (Stokes Raman scattering) or from the molecule to the photon (anti-Stokes Raman scattering). Stokes Raman scattering involves the excitation of the molecule from its lowest vibrational energy state to a virtual energy state for a very short time before relaxing to a higher vibrational energy level than the ground state (Figure 2.6(a)). Anti-Stokes Raman scattering occurs when a molecule in a vibrational energy level which is higher than the ground state is excited to the virtual energy level before quickly

relaxing to a lower level than before (Figure 2.6(b)). Thus, anti-Stokes Raman scattering gives much weaker signals than that of Stokes Raman scattering.

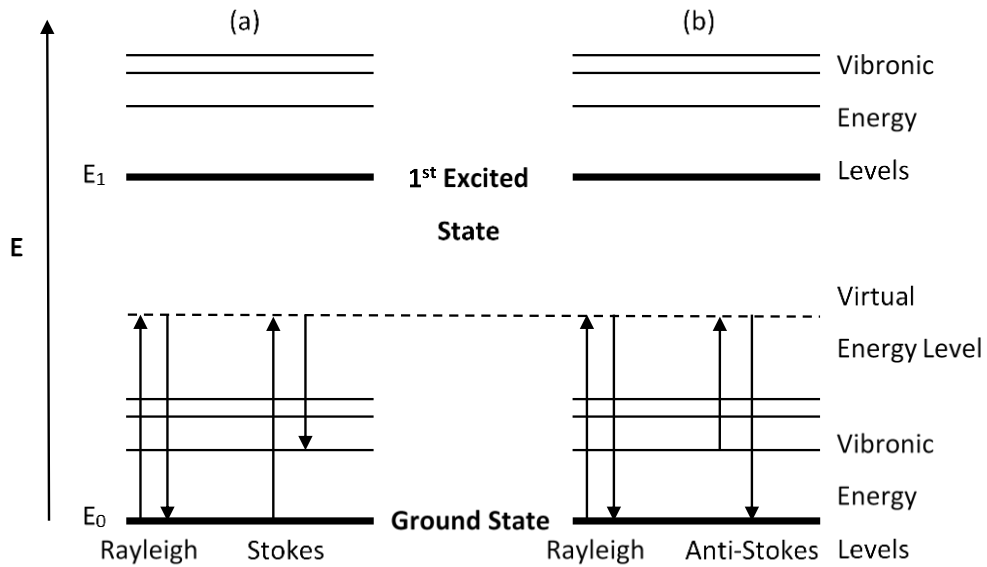


Figure 2.6 – Rayleigh scattering vs. (a) Stokes Raman scattering and (b) anti-Stokes Raman scattering.

This occurs because most molecules in a sample exist in the ground state at room temperature. The population of energy levels can be described as previously by the Boltzmann distribution (Equation 2.9). As it is generally more favourable for molecules to be in their ground state at room temperature, Stokes Raman scattering is more probable and therefore more intense than anti-Stokes scattering. However, RS is a relatively weak process as only one in 1 billion photons are scattered. Despite this inherent weakness, Raman spectroscopy remains a very specific, non-destructive and versatile technique with a wide variety of process analysis applications.

2.1.3. Raman MR Probes

Figure 2.7 shows a general schematic of a concentric fibre bundle probe, with 7 core 100 μm optical fibres, which are cemented into a cylindrical holder and then

polished. Probes typically use between 6 – 18 collection fibres as a single fibre only collects about 10-15% of the amount a multi-fibre bundle can. The excitation fibre delivers light into the sample and the surrounding collection fibres collect the Raman scattered photons. A microscope objective is typically used to focus the laser onto the excitation fibre.

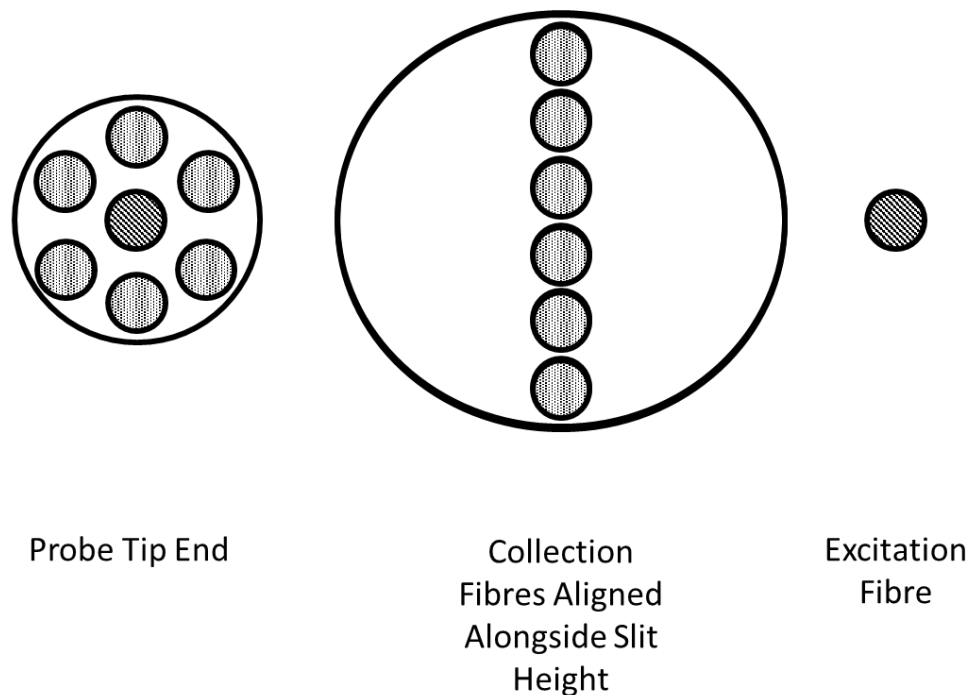


Figure 2.7 - General schematic for a concentric unfiltered fibre bundle or "n-around-1" probe and the filtered probe.

After travelling over at least a meter of fibre, the laser light generates an intense silica spectrum, causing significant background noise as well as fluorescence from the cladding holding the fibres together. These signals leave the incident fibre, reflect off the surface of the sample and are then collected along with the sample spectrum. As the signals travel back through the collection fibres, more noise is generated. This problem is mostly overcome by subtracting the background and this is most often adequate but sometimes it results in obscuring weak Raman signals.

The use of filtered optic probes – such as Kaiser’s micro-Raman (MR) probe – eliminates this problem by filtering out radiation at the laser wavelength before the laser light reaches the sample.⁷⁴ The collected light is also filtered and the remaining light is then focussed onto a single collection fibre. Furthermore, implementing microscope objectives allows the laser to be focussed on a smaller area, creating a higher power density at the sample, which can mitigate some of the Raman intensity lost when using lower powered lasers. It is important to balance the benefits of increased power density (increased Raman signal, the ability to analyse samples obscured by sample housings or packaging materials) with the inherent shortcomings (increased chance of fluorescence caused by contaminants, increased chance of sample degradation).

These MR probe heads are very versatile and allow non-contact as well as immersive sampling to be used. The advantage of using an immersion optic (IO) is that it can be immersed into a reaction vessel and directly measure the contents at any point during the reaction. The jacket on these vessels is usually so thick that a non-contact optic (NCO) cannot be used as the working distance of the laser is too short. The disadvantage, however, is that the immersion probe has a very short working distance and a smaller laser spot size – 60 μm for the immersion probe head as opposed to 100 μm for the NCO.

This results in a much smaller volume of the sample material being analysed and, thus, subsampling – a misrepresentation of the spectrum of a mixture due to inadequate sampling volume⁷⁵ – can occur, which is a particular problem for heterophase reaction monitoring. As the solid polymer particles start to form in the reaction, the information obtained by conventional Raman spectroscopy (i.e. with non-contact or immersion MR probe heads) becomes subject to subsampling. In terms of monitoring residual monomer levels in the beads, this means that with each scan, the probability of observing the residual monomer varies.

2.1.4. Raman PhAT Probes

Kaiser's PhAT probe was designed to alleviate the issue of subsampling in Raman solids analysis. Using a much wider spot size – up to 6 mm – this probe can measure a much larger volume of the sample and provides much more representative analysis. Figure 2.8 illustrates the much larger spot sizes and longer working distance achieved with the PhAT probe, resulting in much larger sampling volumes. The heterogeneous distribution of styrene throughout the polystyrene beads would normally result in variability and uncertainty in determining its concentration but, with the PhAT probe, this uncertainty is reduced greatly.

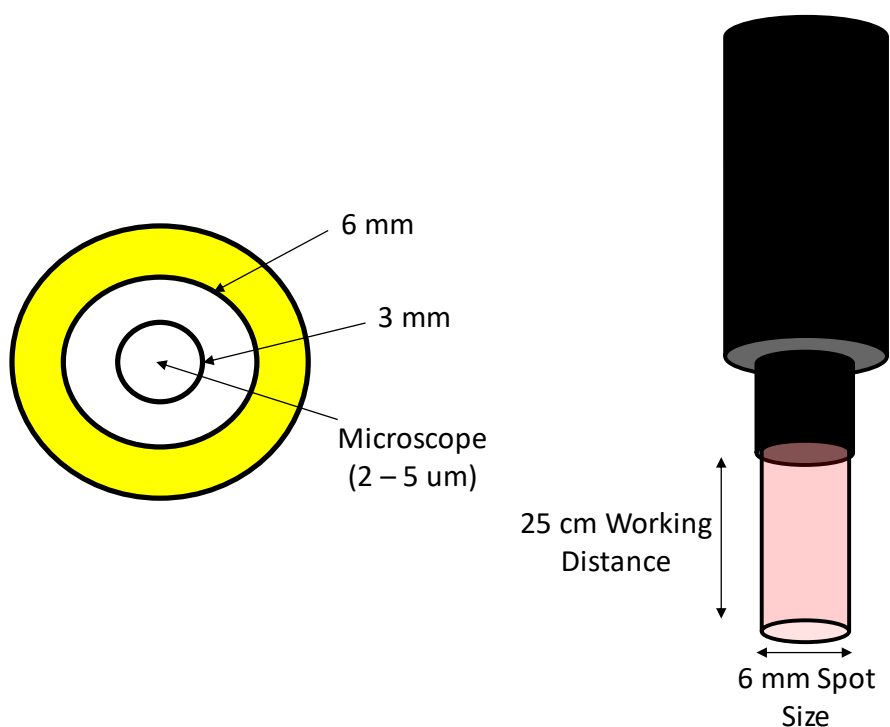


Figure 2.8 – Left: Schematic of spot sizes on a tablet (yellow circle) achieved from using different lasers; Right: Schematic of the Raman PhAT probe showing the wider illumination area and long working distance.

2.1.5. Optical Fibres

Process spectroscopy has greatly benefited from the advent of fibre-optic technology. Coupled with in-situ probes such as ATR probes, optical fibres allow analysers to be housed several (in some cases hundreds) meters away from the harsh reaction environments, thus eliminating the need for sample extraction and allowing analysis to be carried out at safe distances from potentially dangerous processes. A general schematic for a typical optical fibre can be seen in Figure 2.9:

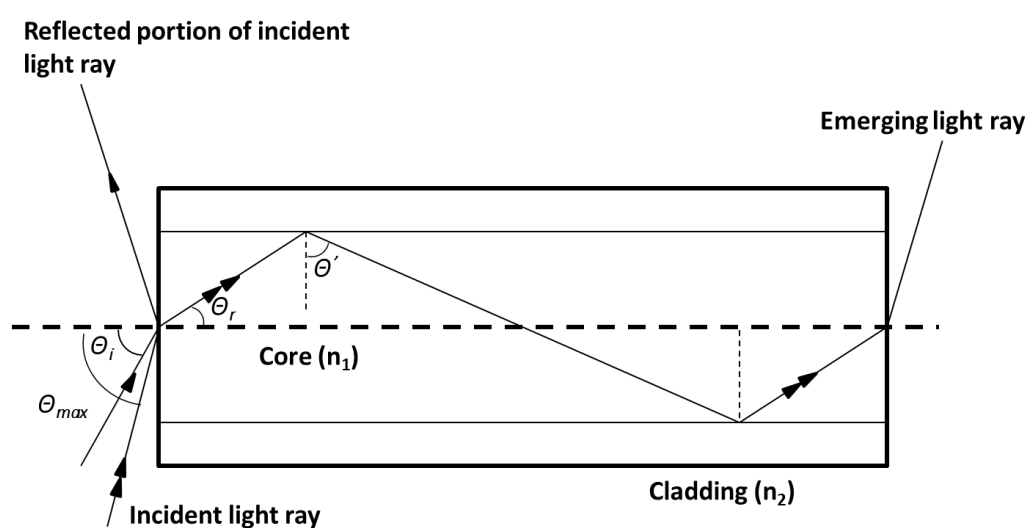


Figure 2.9 - Schematic of a cross-section through a typical optical fibre.

The cylindrical core material and the outer cladding material are chosen so that the core's refractive index (n_1) is greater than that of the cladding (n_2). As incident light enters the fibre, it is reflected at an angle of θ_r , which can be calculated in relation to the angle at which the incident light enters, θ_i :

$$\sin \theta_i = n_1 \sin \theta_r \quad \text{Equation 2.13}$$

For the light to propagate through the fibre to the analyser, total internal reflection must occur, for which the minimum value of θ can be calculated by:

$$n_1 \sin \theta_{\min} = n_2$$

Equation 2.14

Clearly, the choice of material is a key parameter in optimising the performance of these fibres. Unfortunately, MIR spectroscopy limits the selection of materials available to As_2S_3 chalcogenide and silver halide; the latter of which was used in this investigation.

2.2. Acoustic Emission Spectroscopy

Acoustics can be defined as the generation, transmission and reception of energy as vibrational waves in matter⁷⁶ and is generally thought of as the study of sound and vibrations.

Acoustic techniques have long been utilised by various industries such as agriculture,⁷⁷ pharmaceuticals⁷⁸ and oil and gas⁷⁹ for the monitoring of industrial processes. Forces exerted on the process matrix (e.g. through agitation) result in the elastic generation of sound waves which can exist in the sonic (20 Hz – 20 kHz), ultrasonic (>20 kHz) or infrasonic region (<20 Hz),⁷⁶ each of which can yield information about complex, changing processes. The advantages of these techniques are numerous for industrial process monitoring in that they can provide information in real-time and non-destructively, they can be completely or almost completely non-invasive, they are reliable, low cost and easy to implement. Acoustic sensors (transducers) can be safely attached to process vessels, allowing information to be gathered from potentially dangerous process environments.⁸⁰

Acoustic methods of process monitoring also hold several advantages over optical measurements. Opacity of the process matrix under investigation has no effect on its acoustic properties and therefore does not hinder acoustic monitoring methods.

Moreover, there is often no need for sampling windows and external sources of ultrasonic interference is limited by the intrinsic nature of ultrasonic waves in that they do not travel long distances.⁸¹⁻⁸⁴

Broadly speaking, acoustic monitoring technologies can be separated into two distinct classes: active and passive.

2.2.1. Active

Active techniques involve the generation of sound waves which then pass through the process matrix before being collected again and analysed, using the initial sound wave as a probe. This can be achieved by attaching one acoustic transducer to a reaction/process vessel wall, generating the probing sound wave, allowing the wave to travel through the reaction matrix and collecting the wave back again after it rebounds from within the vessel (so-called Pulse-echo, seen in Figure 2.10 a). Alternatively, a Pitch-catch set-up can be employed (Figure 2.10 b), whereby two separate transducers are placed on opposite sides of the vessel; one generating the probing wave, the other collecting it after passing through the process matrix.⁸⁴

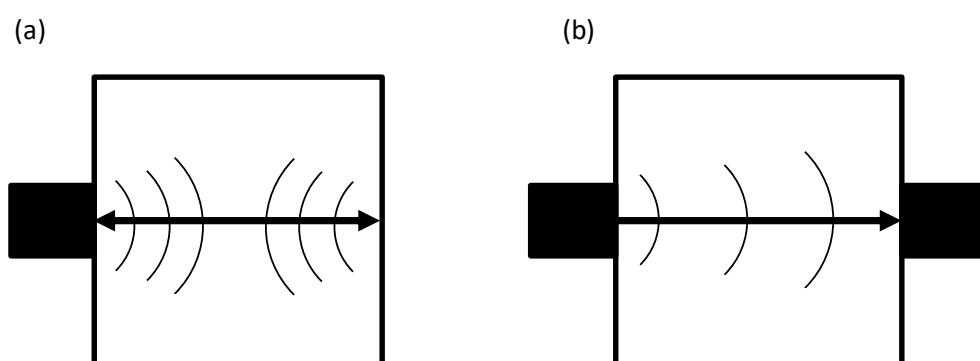


Figure 2.10 – Schematic for Pulse-echo (a) and Pitch-catch (b) methods of active acoustic monitoring techniques showing sound waves emitting from transducers (black boxes) and travelling through the system before collection. Adapted and modified from Bellamy, L. J.⁸⁵

Upon collection, the sound waves are then re-analysed and process information can be inferred from changes in their speed and attenuation when compared to the incident wave pulse.⁸⁶

2.2.2. Passive

Conversely, passive acoustic monitoring techniques only involve the collection and analysis of sound waves generated from within the process itself,⁸⁶ allowing information to be gathered without potentially disrupting the system being studied by inducing acoustic vibrations. Therefore, much use has been made of passive acoustic emission (AE) in the area of fault detection (e.g. pipe leakage),^{87, 88} but relatively little work has focussed on the use of passive AE to monitor physicochemical changes in the processes themselves (e.g. polymerisation or crystallisation).

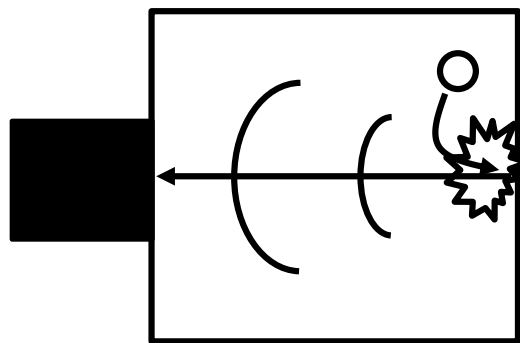


Figure 2.11 – Schematic for passive acoustic emission showing waves propagating from an internal acoustic event (e.g. a polystyrene bead striking the vessel wall) within the process vessel. Adapted and modified from Bellamy, L. J.⁸⁵

The acoustic waves generated by the process must then be collected, characterised and analysed to glean important process information. Solid, liquid and gaseous process matrices produce longitudinal waves – meaning that the energy of the wave propagates through the matrix parallel to the direction to the wave. This produces a series of rarefactions (regions of low-pressure, low density) and compressions (regions of high-pressure, high-density). However, not all waves generated are

longitudinal; solid matrices can also produce waves where the particle vibration direction is perpendicular to that of the wave (known as transverse waves or shear waves). This does not occur with gaseous or liquid sample matrices as they are of too low a viscosity.

Regardless of the longitudinal or transverse nature of the waves produced, they can be characterised by certain key parameters, each of which can be used to extract physicochemical information. Waves can be characterised by their speed, c , their wavelength, λ , and their frequency, f , all of which are related to one another through Equation 2.15.

$$c = \lambda f \qquad \textbf{Equation 2.15}$$

This equation allows the characterisation of key aspects of an acoustic wave, which can provide vital information regarding the inner workings of complex processes and systems. Physicochemical process data relating to particle size, shape and density can be inferred as acoustic waves are formed through particle collisions (with the vessel walls, agitator/impeller and even one another) and these can be inferred through analysis of the acoustic waves generated throughout the process. Furthermore, key parameters related to the operation of the process (e.g. mixing speed) can also be determined from monitoring of AE.⁵²

However, the entirety of the information provided by an acoustic wave may not be of any physicochemical or operational significance. There remain several other potential sources of AE which could convolute the analysis and obscure results such as impeller movement or the flow of oil or water through the vessel jacket. It is therefore important to thoroughly analyse the AE signal for the regions which carry the most significant information and separate it from inconsequential interference.⁸⁹ Through doing so, it is possible to elicit information on the physical state of a system

as the speed of acoustic waves is affected by B, the elasticity (bulk modulus) and ρ , the density of the sample via Equation 2.16:

$$c = \sqrt{\frac{B}{\rho}} \quad \text{Equation 2.16}$$

In this case, B is the adiabatic bulk modulus of a liquid. In the case of a solid sample, B is replaced by E, Young's modulus.

In this study, passive acoustic signals were collected with a piezoelectric transducer, which converts acoustic waves into electric signals, which in turn can be collected and interpreted to obtain information on the system. Materials which can generate an electrical charge proportional to the amount of mechanical stress applied to them are described as piezoelectric.⁹⁰ The piezoelectric effect is reversible, allowing the same materials to be used in generating and collecting acoustic waves. In a passive AES measurement, the acoustic wave generated by the system causes the piezoelectric material in the transducer – affixed to the side of the vessel – to vibrate and generate an electrical signal that can then be collected and interpreted.

There are several piezoelectric materials that be used to make AES transducers, and combinations of these materials can be used to tailor the transducer to be sensitive to a specific frequency of noise, owing to the fact that piezoelectric materials have natural response frequencies depending on their mechanical and electrical properties as well as their thickness.⁹¹ Materials such as polymer films, monocrystalline bulk materials and piezoelectric ceramics are encased in a housing which is fixed to the vessel wall (usually using a resin or physical binding) with a coupling such as a silicon-based vacuum grease, which minimizes the attenuation of the sound waves as they travel between the vessel wall and the piezoelectric material within the transducer.

Broadband transducers are sensitive to a wide range of noise frequencies as opposed to resonant transducers, which resonate only at a small range of frequencies. The data generated by broadband transducers is therefore inherently more complex but it allows the inference of particle concentration as well as size as both factors affect the signal in different ways,⁶² although recent studies have shown the benefits of including a low frequency-sensitive transducer as well as broadband signal collection for these measurements.⁹²

Acoustic signals generated by the system are very susceptible to attenuation as they travel through the reaction media, the vessel jacket and the coupling material and so a signal preamplifier is normally used before the signal is passed to an oscilloscope. It is important to consider the acoustic impedance of a material as this dictates the proportion of the signal that is reflected from its surface.⁸² Therefore, if the impedance values of two materials are very different, a higher proportion of the acoustic wave is reflected rather than transmitted. The material in the transducer (e.g. ceramic) must be acoustically matched to the vessel material in order to optimise the transmission of acoustic signal to the detector. This signal is then passed through a preamplifier, which provides the impedance matching and allows the signal to travel down long cables to the oscilloscope, which in turn displays the signal in the time domain and allows the data to be stored digitally.

Once collected, the power spectrum of the signal can be generated in the frequency domain using Equation 2.17:

$$Power = \frac{fft(s) \times conj[fft(s)]}{\text{Number of Points}} \quad \text{Equation 2.17}$$

Where:

- fft = Fourier transform of the time domain signal, s
- $conj$ = the complex conjugate

The shape of the calculated power spectrum is determined by the dynamics of the system being analysed. In this work, a “soft ceramic” lead zirconate titanate (PZT5H) was used.

2.3. High Performance Liquid Chromatography^{93, 94}

High performance liquid chromatography (HPLC) is a well-established method for the separation, identification and quantification of analytes from mixtures, based on their affinity with the HPLC column. The general principle of HPLC is shown in Figure 2.12:

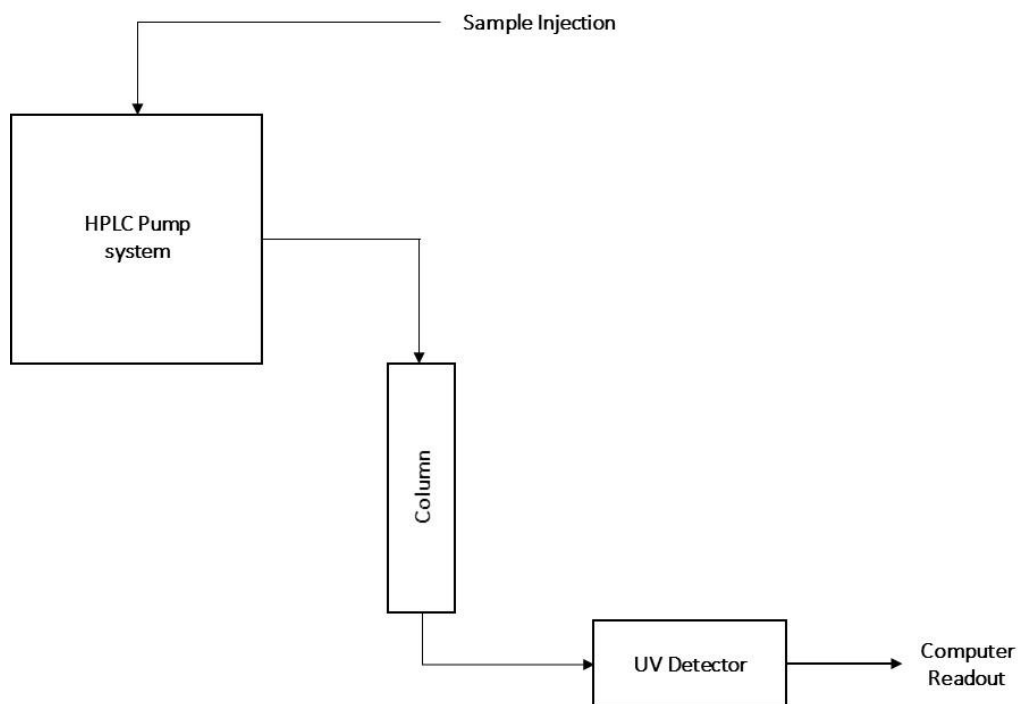


Figure 2.12 – General schematic of a HPLC system showing the sample path from injection, through the column, to detection.

A sample – carried by a liquid mobile phase – containing one or several components through a column coated in a solid stationary phase. As analytes pass through the column in solution, they interact with functionalised particles coated to the inner walls of the column. Depending on the degree of interaction with the stationary phase, the analytes then exit the column at different times before passing through an analyser (most often UV), allowing them to be identified and quantified based on analyses of known standard solutions.

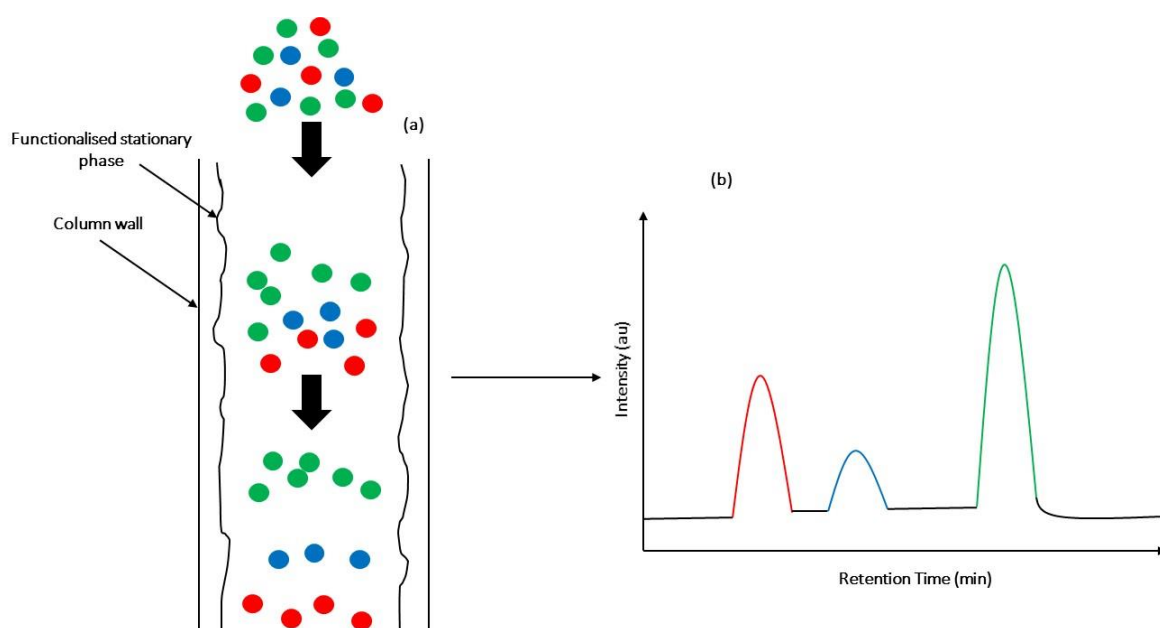


Figure 2.13 – General schematic of (a) a sample passing through an HPLC column and separating analytes (red, blue and green circles) and (b) the resulting chromatogram as the separated analytes pass through the UV detector.

Figure 2.13 shows in more detail the sequence of events as the sample passes through the HPLC column to the detector. The analytes flow through the column and interact to different degrees with the stationary phase – green particles have a strong interaction, blue particles a weaker interaction, and red particles the weakest interaction – causing the analytes to elute from the column at different times. This results in three distinct peaks in the UV chromatogram produced, with the peak height and area proportional to the concentration of each analyte in the original

sample solution. If standard samples of known content and concentration can be analysed also, this allows the analytes in the unknown sample to be identified and quantified.

While the technique is highly sensitive, robust and accurate, time and labour-intensive suitability testing is required to ensure this. Methods must go through rigorous development, optimisation and qualification before being fit for purpose.

2.4. Multivariate Data Analysis^{95, 96}

Multivariate analysis (MVA) is a tool for finding patterns, trends and relationships between multiple variables simultaneously, and it allows the prediction of the effects of changing one variable on the others. MVA uses graphical approaches to allow analysts to examine structures hidden within large, complex datasets, and to visually identify the factors which influence the results. These methods are used routinely across various scientific industries including medical diagnostics,^{97, 98} oil and gas,⁹⁹⁻¹⁰¹ pharmaceuticals¹⁰² and polymers.^{16, 103-105}

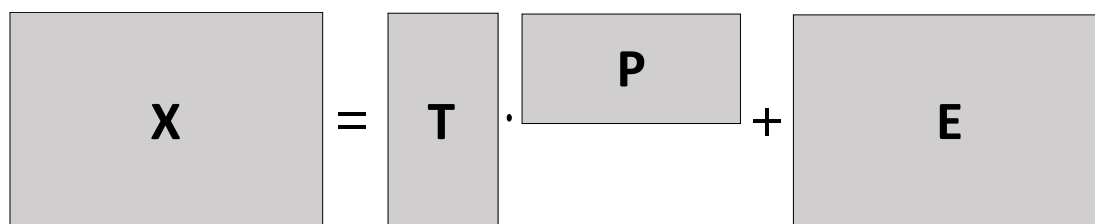
Two of the most common multivariate methods of assessing the variation within a dataset are principal component analysis (PCA) and partial least-squares (PLS) modelling. PCA is an exploratory data processing technique that has become indispensable in the field of data analysis and can be used to establish relationships and correlations between variables or samples when datasets are large and complex, such as in industrial reaction monitoring. Its simplicity and ease-of-implementation make it a powerful tool for recognising patterns and trends within complex datasets and for sample classification. This is a quick way of establishing which variables contribute most to the variation within a dataset e.g. spectral regions that change the most throughout a reaction. Furthermore, sample-to-sample variation can provide insight into reaction progression and trajectory (endpoints, deviations, intermediates, etc.).

Combining spectral data with quantitative offline analysis can be done to build PLS models, which can then be used to provide quantitative information using spectral data only. By building a model using several datasets and then training the model using separate datasets, the predictive power of the model and its robustness can be assessed using various criteria.

2.4.1. Principal Component Analysis

In modern data analysis, PCA is a routinely-used tool used in a wide variety of fields, from advancing green chemistry¹⁰⁶ to fault detection in military aircraft.¹⁰⁷ Its aim is to mathematically reduce large datasets to a few simple vector components – ‘principal components’ – each of which describe some amount of the total variation within the original data.

To achieve this with spectral data, spectral matrices are decomposed to give scores, loadings and residual errors, as described in Figure 2.14:



The diagram shows the equation $X = T \cdot P + E$ where each term is enclosed in a gray rectangular box. The boxes are arranged horizontally from left to right, separated by an equals sign, a dot, and a plus sign.

Figure 2.14 – Schematic representation of PCA.

Where:

- **X** is the $m \times n$ spectral data matrix (samples x wavenumbers).
- **T** is the $m \times i$ scores matrix (samples x principal components), containing information on the sample-to-sample variation in the original matrix.
- **P** is the $i \times n$ loadings matrix (principal components x wavenumbers), which allows us to infer the magnitude of influence over the spectral data each variable (in this case, wavenumbers) has.

- **E** is the $m \times n$ residual unaccounted-for variability – e.g. measurement error – associated with the spectral data (samples \times wavenumbers).

The data within **X** is first mean centred to ensure that the first principal component (PC) represents the variance within the dataset and not simply the average of all the spectra. Each subsequent PC is orthogonal to the first, meaning that they are constrained by the first PC and more PCs are required to describe all the variation within the data. The scores within **T** each represent a sample spectrum, showing how similar or different to one another they are. Furthermore, the loadings in **P** show the correlation between individual wavenumbers across the data. In reaction monitoring, there are multiple sets of scores and loadings required to describe the data. The first PC would describe most of the variation, with each subsequent PC describing less and less. To avoid overfitting a PCA model, it is best to restrict the number of PCs to a maximum number of realistic sources of variation within the data (i.e. the number of spectroscopically active components in the reaction).

2.4.2. Partial Least Squares

Partial least-squares (PLS) regression allows the estimation regression coefficients in linear models containing a large number of correlated variables. In contrast to the qualitative nature of PCA, PLS regression can be used to quantify the correlation between a multivariate dataset (**X**) and reference data (**y**, e.g. % conversion) and can be used to predict these responses if given a data matrix within the calibration range of the model. To do this, the sample data matrix is deconstructed to give scores and loadings matrices – similar to PCA. In PLS however, the maximum covariance between spectral data and gravimetric response is calculated (**X** and **y** in Figure 2.15):

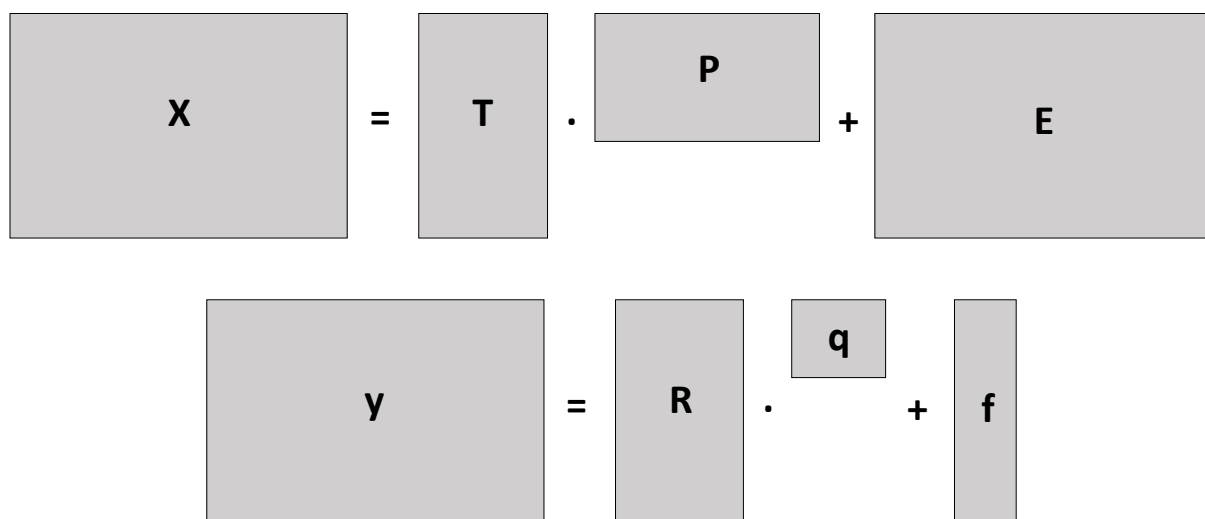


Figure 2.15 – Schematic representation of PLS modelling.

Where:

- **X** is the $m \times n$ spectral data matrix (samples x wavenumbers)
- **T** is the $m \times i$ scores matrix (samples x latent variables)
- **P** is the $i \times n$ loadings matrix (latent variables x wavenumbers)
- **E** is the $m \times n$ residuals matrix
- **y** is the $m \times n$ reference data matrix (samples x % monomer conversion)
- **R** is the $m \times i$ scores matrix (samples x latent variables)
- **q** is the loadings vector
- **f** is the $m \times 1$ residuals vector

Maximising the covariance between **T** and **R** also maximises the correlation between the two, allowing a PLS model to predict the scores for the **y** data using the scores from **X**. The predicted **y** scores matrix (**R**) can then be used to calculate values of **y**.

2.5. Spectral Preprocessing¹⁰⁸

Data preprocessing essentially involves the removal of irrelevant variation from a given set of data. In spectroscopy terms, this can allow the separation of physical

sources of variation (e.g. scattering caused by particle size differences, instrument drift, etc.) and chemical sources of variation (e.g. analyte concentration).

Advances in analytical technologies and computer processing power have resulted in the ability to generate and manipulate massive quantities of data with ease, allowing greater insight into the chemistry of even complex sample matrices. However, a consequence of this is an increased uptake of chemically irrelevant information. Complex sample matrices and advanced analytical methods such as spectroscopy result in very large datasets which can become convoluted and can obscure key information about a reaction or chemical process. As a result, there have been many attempts at decoupling this irrelevant data through data matrix manipulation and many of these techniques have become widely used industry standards. With these, however, there are limitations in their applicability e.g. when assumptions and compromises must be made, when important data is excluded alongside the irrelevant information or when the methods become so advanced as to be time-consuming and complicated.

2.5.1. Savitzky-Golay Derivatisation

Savitzky-Golay (SG) smoothing is a polynomial smoothing method commonly used in signal preprocessing to improve the signal-to-noise ratio of spectral data. This technique uses least-squares fitting of a smooth polynomial function to spectral data using a sliding window of a defined width, w . Datapoints within the defined window are treated by evaluating the polynomial function at the midpoint of w before moving the window one datapoint to the right and evaluating the polynomial at the midpoint again. This is repeated until the entire spectrum has been smoothed. The definition of w and the degree of the polynomial are key to SG smoothing, as larger values of w give stronger smoothing and increased degrees of polynomial allow more complex curves to be fitted. However, strong smoothing – while giving better signal-to-noise ratios – can distort the signal, especially spectral data with sharp defined peaks. Similar effects are seen when using low order polynomials. Conversely, higher

order polynomials and small window sizes will preserve the shape of the original spectra but will remove less noise.

A variation on this polynomial smoothing is the use of first and second derivatives. Derivatisation of spectral data can eliminate baseline offset – as the derivative of a constant is zero – and works similarly to polynomial filtering, in that it uses a sliding window; however, the derivative of the polynomial function fitted to the data within the window is produced in this instance. This technique is also useful for sharpening and narrowing peaks which otherwise might become lost in a complex sample. Furthermore, this technique retains the quantitative nature of peaks in a sample spectrum.

However, care must be taken to avoid amplifying and sharpening noisy data. This technique, while useful, can incur low signal-to-noise ratios especially with noisy complicated datasets.

2.5.2. (Extended) Multiplicative Scatter Correction and Standard Normal Variate Transformation

Standard normal variate (SNV) transformation and multiplicative scatter correction (MSC) are similar techniques, often used in tandem to ascertain which gives better results for a given dataset. MSC eliminates baseline offset and can correct path length differences caused by changes in PSD. Changes in PSD can affect the levels of diffuse and specular reflectance reaching the collection fibres of a spectroscopic probe, thus affecting baseline offset between samples. Furthermore, penetration depth of laser light can change depending on the size and uniformity of the particles, which affects the path length and, thus, the spectral signal.

These issues are solved Equations 2.17 and 2.18. Firstly, a linear regression of each spectrum, \mathbf{x}_i , is made against a reference spectrum, \mathbf{x}_r , such as the mean spectrum of a set of training or calibration spectra:

$$\mathbf{x}_r \approx \beta_0 + \beta_1 \mathbf{x}_i \quad \text{Equation 2.17}$$

Least-squares coefficients, β_0 and β_1 are estimated initially before being used to calculate the MSC-corrected spectrum, \mathbf{x}_i^* :

$$\mathbf{x}_i^* = \beta_0 + \beta_1 \mathbf{x}_i \quad \text{Equation 2.18}$$

This method was further extended¹⁰⁹ to more effectively separate the chemical and physical effects on the spectra. This extended multiplicative scatter correction (EMSC) uses knowledge about the analytes' spectra to enhance the robustness of the method.

SNV transformation works similarly, but the mean of each spectrum is subtracted, and its length normalised to 1 as per Equation 2.19, where the mathematical similarity to MSC can be seen.

$$\mathbf{x}_i^* = \beta_0 + \beta_1 \mathbf{x}_i \quad \text{Equation 2.18}$$

Where:

- $\beta_0 = -\bar{\mathbf{x}}$
- $\beta_1 = 1/\|\mathbf{x}_i\|$
- $\|\mathbf{x}_i\|$ = the norm of \mathbf{x}

2.5.3. (Modified) Optimal Path-Length Optimisation and Correction

The modified optimal path-length estimation and correction (OPLECM) method introduces multiplicative parameters to the linear estimation of spectra (row vector \mathbf{x}_k in Equation 2.19):

$$\mathbf{x}_k = \left[p_k \sum_{i=1}^{n_s} c_{k,i} \mathbf{r}_{s,i} + q_k \sum_{j=1}^{n_p} m_{k,j} \mathbf{r}_{p,j} \right] + \mathbf{d}_k, k = 1, 2, \dots, K$$

Equation 2.19

Equation 2.19 shows the approximation of K heterogeneous spectra as a linear combination of the contribution of the constituents in the solution and oil phases where:

- \mathbf{x}_k is the measured spectrum of the k th sample
- $c_{k,i}$ is the concentration of the i th analyte in the solution phase of sample k
- $m_{k,j}$ is the mass fraction of the j th analyte in the oil phase of sample k
- $\mathbf{r}_{s,i}$ is the spectral response per unit concentration of the i th analyte in the water phase
- $\mathbf{r}_{p,j}$ is the spectral response per unit concentration of the j th analyte in the oil phase
- n_s and n_p denote the number of constituents in the water and oil phases, respectively
- \mathbf{d}_k represents model deviation
- p_k and q_k are multiplicative effects of scatterers in the water and oil phases, respectively, and describe the effect these scatterers have on the spectra of other constituents in each phase

The key to OPLEC and its subsequent modifications and improvements is the determination of these multiplicative effects, p_k and q_k , as they have confounding effects on the values of $c_{k,i}$ and $m_{k,j}$, respectively. This is the limitation of standard

multivariate linear calibration methods, as they do not account for these multiplicative effects when modelling relationships between \mathbf{x}_k and $c_{k,l}$ or $m_{k,j}$.

Through a series of matrix manipulations and mathematical treatments,¹¹⁰ multiplicative parameter vectors \mathbf{p} and \mathbf{q} can be derived using Equation 2.20 (only the derivation of \mathbf{p} is shown for simplicity, \mathbf{q} is derived in the same way):

$$\min_{\mathbf{p}} f(\mathbf{p}) = \frac{1}{2} \mathbf{p}^T \left((\mathbf{I} - \mathbf{U}_s \mathbf{U}_s^T) + \text{diag} \left(\frac{\mathbf{c}_i}{w} \right) (\mathbf{I} - \mathbf{U}_s \mathbf{U}_s^T) \text{diag} \left(\frac{\mathbf{c}_i}{w} \right) \right) \mathbf{p},$$

such that $-\mathbf{p} \leq -\mathbf{1}$

Equation 2.20

This key step allows OPLECm to accurately estimate the number of spectroscopically active components in a system, J , which has significant impact on the performance and reliability of models built using it. Previous versions (OPLEC) relied on estimating the J value or using a time-consuming, iterative optimisation process where the value of J was changed several times to assess the optimal parameters for model building. This is discussed in detail in chapter 4.

Furthermore, Equation 2.20 provides the multiplicative parameter vector, \mathbf{p} , which can then be used in a dual calibration model with a set of calibration spectra, \mathbf{X} , (Equations 2.21 and 2.22) using a multivariate linear calibration method such as PLS.

$$\mathbf{p} = \alpha_1 \mathbf{1} + \mathbf{X}\beta_1$$

Equation 2.21

$$\text{diag}(\mathbf{c}_i) \cdot \mathbf{p} = \alpha_2 \mathbf{1} + \mathbf{X}\boldsymbol{\beta}_2$$

Equation 2.22

Linear calibration of these two models would give estimations for parameters α_1 , $\boldsymbol{\beta}_1$, α_2 and $\boldsymbol{\beta}_2$. The concentration of the i th constituent, $c_{test,i}$ in the water phase of a test sample spectrum, \mathbf{x}_{test} using these two calibration models as per Equation 2.23:

$$c_{test,i} = \frac{\alpha_2 + \mathbf{x}_{test}\boldsymbol{\beta}_2}{\alpha_1 + \mathbf{x}_{test}\boldsymbol{\beta}_1}$$

Equation 2.23

2.6. Raman Instrumentation

A Kaiser RXN-1 Raman spectrometer with an MR, non-contact optic (NCO) probe (Kaiser Optical Systems Inc., Ann Arbor, MI, USA) was used. This probe had a 1 cm working distance and an approximate laser spot diameter of 100 μm . An Invictus diode laser with a wavelength of 785 nm was operated at 350 mW at source. Data was acquired using HoloGRAMS software (Kaiser Optical Systems). Before each analysis, the spectrometer was calibrated using a cyclohexane standard and the HoloGRAMS built-in calibration wizard. To avoid over or under-filling the detector, acquisition parameters (exposure time and accumulation number) were set to achieve the optimum detector fill (60-70%). Each experiment required different parameters to achieve this depending on the chosen sampling method and probe (e.g. *in-situ* reaction monitoring using an immersion optic probe head required 10 acquisitions for 12 s each to achieve the optimum detector fill – these parameters will be stated for each experiment).

For the comparison of narrow and wide area beams, a PhAT probe developed by Kaiser Optical Systems Inc., Ann Arbor, MI, USA and first reported by Kim et. al.¹¹¹ was used. This probe was also equipped with an Invictus diode laser with a 785 nm

wavelength, operating at 350 mW at source. Similarly, the spectrometer was calibrated before each analysis using a cyclohexane standard and the built-in HoloGRAMS calibration wizard. This work was performed at Clairet Scientific in Northampton with the help of Paul Dallin and John Andrews.

2.7. Reactor Equipment

Polymerisation reactions were carried out in a Radley's 1 L jacketed glass reaction vessel, using a Radleys RS37 Digital Plus stirrer motor to control stirrer speed and a Huber Technologies temperature control unit (Figure 2.16) which was monitored and adjusted manually to keep the temperature at $80 \pm 0.5^\circ\text{C}$ throughout the reaction.

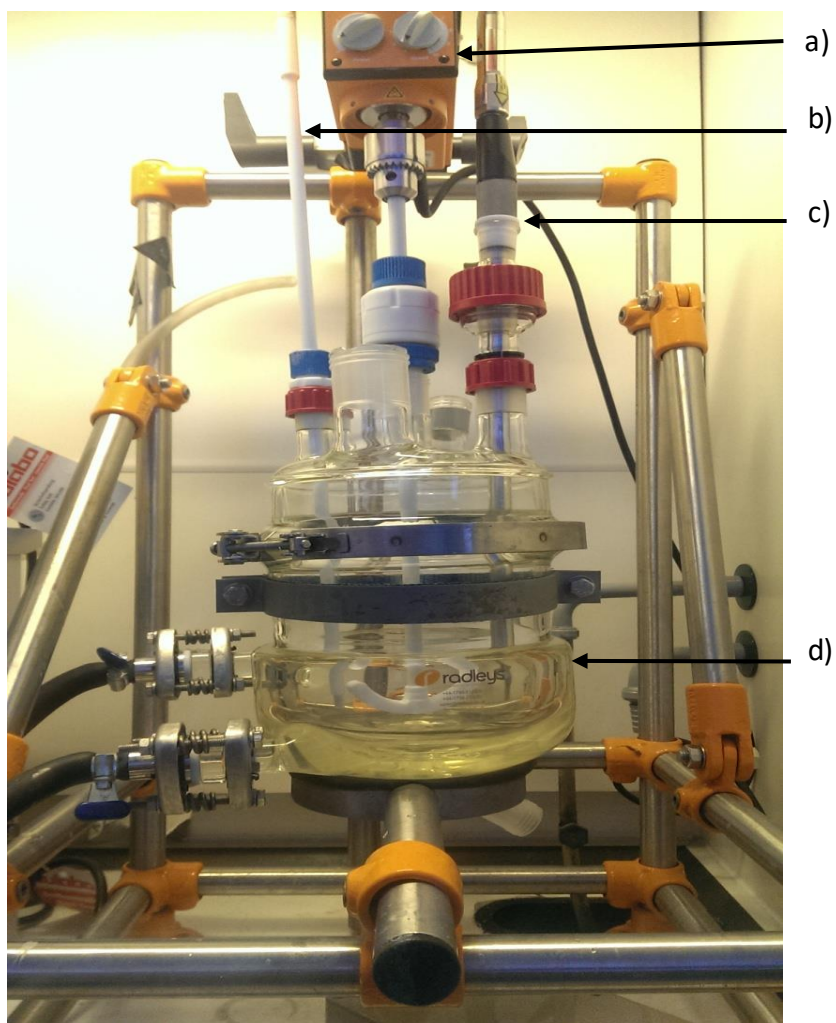


Figure 2.16 – Reactor set-up showing a) Radley's stirrer/motor control unit, b) immersion temperature probe, c) Kaiser immersion optic Raman probe and d) jacketed 1L Radley's reaction vessel.

3. Quantification and Monitoring of Residual Styrene Within Polystyrene Beads

3.1. Introduction

The transition from monomer droplet to polymer bead results in some unreacted monomer being trapped inside the bead product, which can leak out over time and as such is the focus of ever tighter health and safety legislature to which Industry must abide. This formed the basis for part of this project. In this chapter, the applicability of Raman spectroscopy for monitoring the level of monomer left within the beads as the reaction progressed to a level of 0.1% or lower was assessed. To achieve this, several polystyrene (PS) bead samples were provided with differing residual monomer (RM) levels – as quantified by HPLC. The HPLC data were then compared to offline Raman data collected from the same samples to establish a degree of correlation.

As it is difficult to control the RM of the bead products during a reaction, existing PS beads were ‘spiked’ with monomer to provide a set of ‘standards’ with differing RM levels. The stability of these samples was verified via RS to ensure the additional monomer remained within the polymer bead. The effects of particle size on RS was also investigated.

Furthermore, the application of RS using different laser spot sizes was investigated. Developments in Raman technologies have resulted in laser spot diameters ranging from microns to centimetres, allowing sampling depths and volumes to improve as well as system robustness.⁷⁵ A MR probe with an immersion optic (IO), a non-contact optic (NCO) and a non-contact wide-area illumination/pharmaceutical area testing (WAI/PhAT®) optic were used.

3.2. Instrumentation and Materials

3.2.1. HPLC

A Waters 2690 HPLC system coupled to a Shimadzu SPD-6A variable wavelength UV detector (set at 254 nm) and Chromeleon software was used in this work (Figures 3.1 and 3.2). Styrene, acetonitrile, SDBS and tetrahydrofuran (THF) were supplied by Sigma-Aldrich UK.



Figure 3.1 – Waters 2690 HPLC system.¹¹²



Figure 3.2 – Shimadzu SPD-6A variable wavelength UV detector.¹¹³

3.2.2. EPS Beads

Several batches of polystyrene beads were provided by BASF. The first of these batches were split into three groups based on their mean particle size as per Table 3.1. These were then used as the basis for generating in-house 'standards' of different RM content.

Table 3.1 – Categorisation of provided EPS beads by mean particle diameter and corresponding RM content as determined by HPLC at BASF.

Category	Mean Particle Diameter (mm)	Residual Monomer Content (ppm)
Small	0.827	72
Medium	1.003	4837
Large	1.334	5462

Further batch of EPS beads were provided, each with very low RM content for the purposes of establishing a limit of detection (LOD) on various configurations of Raman optics. Beads were provided with 0.036, 0.116, 0.124, 0.143, 0.21, 0.309 and 0.718% v/v residual styrene.

3.3. Experimental

To successfully monitor the progress of this reaction, it is vital that any techniques used be assessed in their efficiency at detecting styrene. To do this, the spectral regions associated with styrene must be studied in two key environments where styrene is expected to be present for the understanding and optimisation of the polymerisation process: free in aqueous solution and trapped residually in the polymer beads produced.

3.3.1. Polystyrene Bead Impregnation

Several different batches of EPS beads produced by BASF were provided along with details of their residual monomer contents, which had been obtained by HPLC. Each batch had a different average particle size and overall PSD although close similarities between some batches did exist (Table 3.2 and Figure 3.3).

Table 3.2 – Analytical data of 4 different polystyrene bead batches as provided by industrial partners. Shown is the particle size determined by sieving and the residual monomer content determined by HPLC.

Batch No.	Average Particle Size (mm)	Styrene Content via HPLC at BASF (ppm)
1	1.364	4781
2	1.334	5462
3	1.003	4837
4	0.807	72

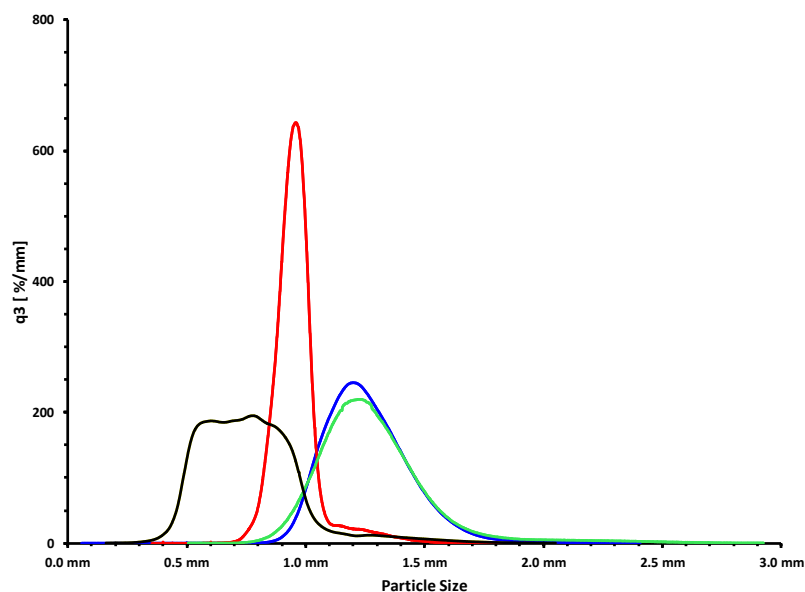


Figure 3.3 - Particle size distributions of EPS bead batches 1 (cyan), 2 (blue), 3 (red) and 4. Data provided by industrial partners.

Data provided by BASF (Figure 3.3) shows that the PSD and RM content of EPS beads made by suspension polymerisation was varied. Whilst batches 1 – 3 had similar RM contents, batch 3 had a narrower distribution with smaller average bead sizes. Batch 4 had the lowest RM level as well as the smallest average bead size with the widest distribution. Such variability in EPS batches could affect spectroscopic measurements, and this was investigated. HPLC data provided quantitative information on the monomer content of EPS beads, and it was therefore of interest to establish some correlation between spectroscopic and HPLC measurements. However, the beads were insufficiently different in monomer content and so a method was developed for impregnating the beads with additional styrene.

Samples of EPS beads with different residual styrene levels were created in-house. These could then be analysed by offline RS and HPLC to establish any correlation between the two techniques. To do this, a bead impregnation method was developed with varying success as described in Table 3.3.

Table 3.3 – Experimental conditions for polystyrene bead impregnation method development performed in a 250 mL Radleys jacketed reaction vessel. Impeller speed was kept at 400 rpm in each experiment.

Volume water (mL)	Volume styrene (mL)	Weight Surfactant (g)	Weight pSty Beads (g)	Bead Batch Number
250	0.6	2.6661	8.887	3
250	0.8	2.6661	8.887	3
250	0.8	2.6661	8.887	3
250	0.6	2.6661	8.887	3
250	0.4	2.6661	8.887	4

In each case, the desired amount of surfactant was fully dissolved in 250 mL of water. The polystyrene beads were then immersed in the solution whilst stirring at 400 rpm and the solution sampled continuously with an immersion Raman probe until the height for the styrene derivative peak remained constant. Once this was achieved, the required amount of styrene was added into the solution, which was then stirred and sampled continuously until the styrene derivative peak height remained steady. Once the experiment was over, the beads were collected from solution and left to dry overnight. They were then collected in a glass vial and sampled using the NCO Raman probe (Figure 3.4). Finally, an HPLC method was implemented with instruction from BASF to accurately quantify the monomer content of the beads produced.

3.3.2. EPS Bead Impregnation Verification via High Performance Liquid Chromatography

HPLC is a quantitative method regularly used in the off-line analysis of monomer content of polystyrene beads. Such a method was already in use at BASF and details

were provided to enable the analysis to be performed at Strathclyde. The method was developed to be linear for styrene between 0 and 10 ppm in THF (Table 3.7 and Figure 3.15). Therefore, bead samples were dissolved in THF until within this range and then the original styrene content could be inferred using linear regression from a standard curve, accounting for the dilution factors.

Standards were prepared by dissolving approximately 0.1 g of styrene in 40 mL of THF, before transferring the solution to a 100 mL volumetric flask. The solution was then made to volume using THF washes from the original beaker the styrene was dissolved in, resulting in ~1000 ppm styrene solution. This was then diluted to give a 100 ppm solution, which could then be used as a stock solution to prepare a range of standards (e.g. by pipetting 5 mL of this stock standard to a 50 mL volumetric flask and making to volume with THF, a 10 ppm solution was prepared). This was done to generate styrene standards of 10, 20, 40, 50, 60, 70 and 80 ppm.

Samples of polystyrene provided by BASF or collected during a reaction could then be dissolved in THF and analysed alongside the standard samples, using linear regression analysis to obtain the styrene content of the samples. Approximately 0.05 g of polystyrene beads were dissolved in 15 mL of THF in a 25 mL volumetric flask, which was made to volume once the beads had dissolved. If the HPLC results were within the calibrated range, the styrene content could be calculated. Otherwise, smaller or larger sample weights could be used until the result fell within the linear range. Sample weight and dilution factor were taken into account in the calculation of styrene content. The error associated with the sample preparation (multiple dilutions, pipetting errors) is not insignificant and is one of the main disadvantages of this method. Furthermore, samples taken before the solidification of polymer beads are difficult to weigh accurately and prepare reliably for HPLC analysis.

The HPLC method was as follows:

Instrument – Waters 2690 HPLC

Column – Phenomenex Luna 3 μ C18 (150 x 4.6 mm)

Mobile phase – Acetonitrile:water (60:40) degassed before use.

Flow rate – 1 mL/min Isocratic

Detector wavelength (λ) – 254 nm

Injection volume – 15 μ L

Retention Times

Styrene – ~6.2 mins

3.3.3. EPS Bead Impregnation Verification via Offline Raman

Samples of EPS beads impregnated with styrene were left to dry overnight and then collected in a glass vial. The vial was then placed in a shuttered sample housing (Figure 3.4) and analysed using an NCO Raman MR probe head and HoloGRAMS software, programmed as per Table 3.4:

Table 3.4 – HoloGRAMS settings for non-contact Raman analysis of dry impregnated EPS beads.

Parameter	Setting
Exposure (s)	20
No. of Accumulations	10
Interval (s)	0

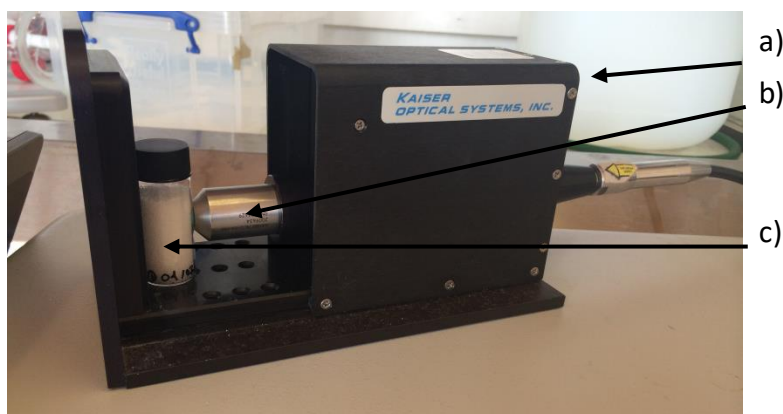


Figure 3.4 - Offline EPS bead analysis set-up showing: a) shuttered sample housing unit, b) Kaiser NCO Raman MR probe head and c) glass vial containing EPS beads.

3.6.4. Effect of EPS Bead Size on Raman Spectroscopic Measurements

As shown in Figure 3.1, a suspension polymerisation reaction can produce EPS beads of varying particle size, often resulting in a wide PSD, which can affect Raman signals.¹¹⁴ Therefore, it was necessary to investigate the effect of particle size on detection limit calculations. This was done by sieving the impregnated EPS bead samples into 3 sizes (Table 3.1) and establishing the correlation between HPLC and RS analysis of RM content for all 3 sizes. The effect of mean particle size on the correlation could then be assessed.

3.6.5. Wide Area Illumination Study

Small and wide area Raman probes were used to analyse polystyrene beads of two sizes. Due to the short working distance of the NCO (3.3 cm), the sample tube had to be as close to the probe end as possible – as seen in Figure 3.5. To facilitate this, a glass plate was placed on the end of the probe – pointed upwards – and the sample tube was secured to the plate directly above the probe lens. The glass plate was supported by the Raman sample housing. As the sample housing had to be left open during spectra acquisition, the opening was covered to block out any external light sources.

A sulphur disc was used as a Raman scattering standard for the sample depth studies and was placed in the sample tube on top of the bead sample.

Small Sample Volume

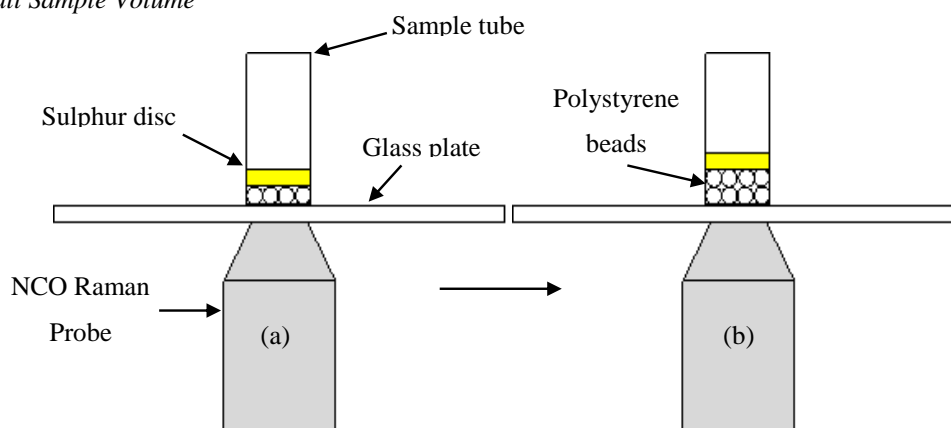


Figure 3.5 – Schematic of small area probe sample depth study set-up showing sample tube with increasing sample depth going from (a) to (b).

The sample tube was filled with polystyrene beads at a depth beginning at 1 mm and the sulphur disc was then placed on top of the beads directly above the probe end. The sample area was closed off as per Figure 3.4 and spectra were acquired with 2.5 seconds exposure and 5 accumulations per spectrum. This was repeated 5 times and the average of those 5 spectra was used for analysis. The sulphur disc was then removed before another 1 mm depth of beads was added. The sulphur disc was then placed on top of the polystyrene again, this time 1 mm further from the probe as before and scanned again. This was repeated for several depths of polystyrene beads.

Large Sample Volume

The large area laser – the PhAT probe – employs a 6 mm diameter beam with a 254 mm working distance and a 50 mm depth of field. This was set up as per Figure 3.6:

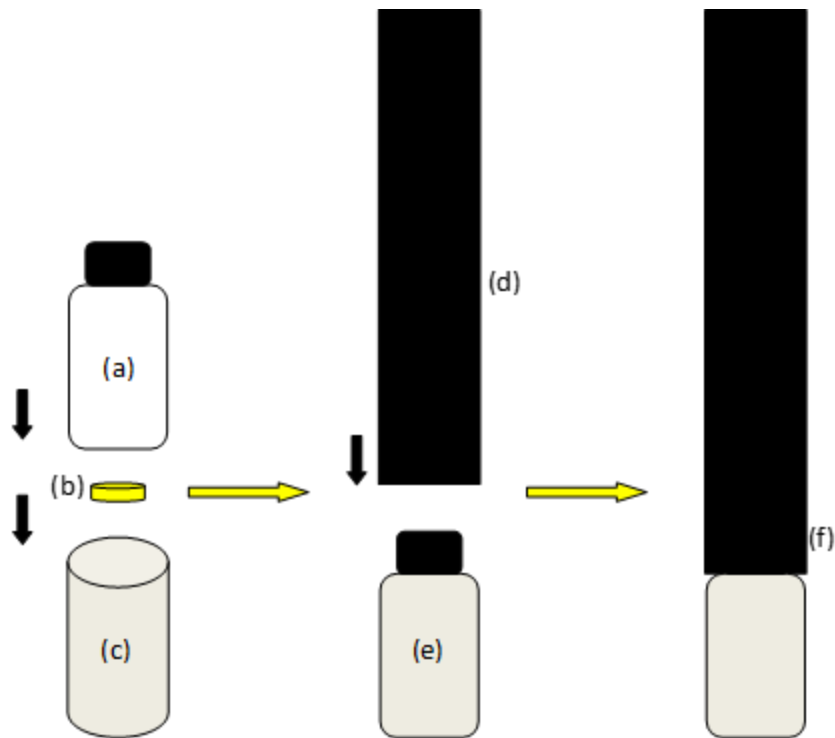


Figure 3.6 – Schematic of wide area probe sample depth study set-up showing (a) glass vial with no lid and x mm of EPS beads, (b) sulphur disc placed between bottom of the vial and (c) a foil jacket, (d) the 203 mm collimated beam housing sitting above (e) the jacket and sample vial and (f) the completed system ready for spectral acquisition.

The sample vial was filled with a layer of polymer beads starting at a depth of 3 mm for larger beads and 1 mm for smaller beads. This was then placed in a foil jacket with the sulphur disc secured between the vial and the jacket in the centre of the base of the vial. The collimated beam housing was then lowered so it sat directly on top of the sample vial, securing it in place. The sample was then ready for spectral acquisition which was done using 1.25 seconds exposure time and 5 accumulations per spectrum. These parameters were found to give a similar detector fill (60-70%) as the MR probe at 2.5 seconds with 5 accumulations and this was repeated 5 times before adding a further layer of polystyrene beads and repeating the process, each

time increasing the depth of polystyrene sample between the probe and the sulphur disc under the vial.

3.6.6. Detection Limits of Styrene in EPS Beads via Raman MR and PhAT Probes

EPS beads provided by BASF with differing RM content were analysed by Raman MR and PhAT probes both offline and in water. Dry beads were analysed in glass vials as per section 3.6.3. using either the MR and PhAT probe heads. These beads were also submerged in 250 mL of water in a glass reaction vessel with agitation at 300 rpm and analysed in-situ using the IO probe head – immersed in the water with the beads – and the PhAT probe – pressed up against the vessel wall from the outside.

3.6. Results and Discussion

3.6.5. Detection of Styrene via MIR Spectroscopy

Figure 3.7 shows the MIR spectrum obtained from a 10 mL vial of neat styrene with strong absorbance bands at 694, 771, 902 and 987 cm^{-1} and smaller bands at 1018, 1203, 1280, 1411, 1450, 1496, 1573, 1604 and 1627 cm^{-1} . Table 3.6 shows the possible interpretation of these peaks. The four intense peaks between 1000-600 cm^{-1} indicated that styrene could be identified using MIR. It was then important to ensure that the styrene could be monitored in the intended reaction environment. The highly aqueous nature of the reaction matrix was expected to cause difficulties for MIR analysis, the extent of which had to be investigated, so samples with different water/styrene ratios were prepared and sampled as before. In a typical polymerisation reaction, styrene would initially make up roughly 60% of the total solution volume, a water/styrene sample of a comparable nature (50% v/v) was analysed. Figure 3.8 shows this spectrum and compares it to that of pure styrene and a 10% v/v styrene in water solution. This dilute solution is representative of the conditions towards the end of a reaction.

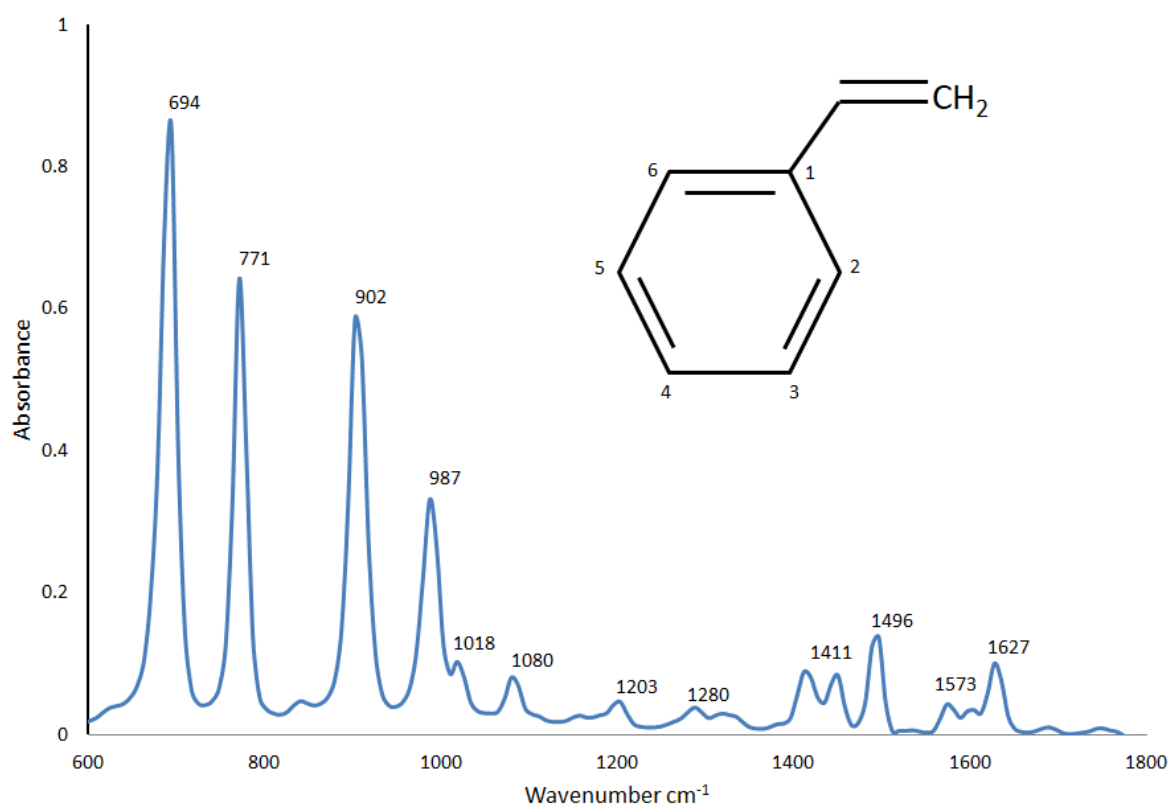


Figure 3.7 – The 600 – 1800 cm⁻¹ region of the average (n = 51) MIR spectrum of pure styrene using an ABB MB3000 FTIR spectrometer (Clair Scientific, Northampton, UK) coupled with polycrystalline silver halide optical fibres. Measurements were made with a resolution of 16 cm⁻¹ and subtracting an air background.

Table 3.5 - MIR band assignments for the spectrum of pure styrene¹¹⁵

Peak Frequency (cm ⁻¹)	Assignment
694	Olefinic CH wag
771	Mono-substituted benzene CH wag
902	Vinyl CH wag
987	Vinyl CH wag
1018	2,4,6 radial carbon in-phase stretch. Aromatic.
1080	2,4,6 radial carbon in-phase stretch. Aromatic.
1203	2,4,6 radial carbon in-phase stretch. Aromatic.
1280	2,4,6 radial carbon in-phase stretch. Aromatic.
1411	Unassigned
1450	Aromatic ring semi-circle stretch
1496	Aromatic ring semi-circle stretch
1573	Aromatic ring quadrant stretch
1627	Weak aromatic C-H stretch overtone

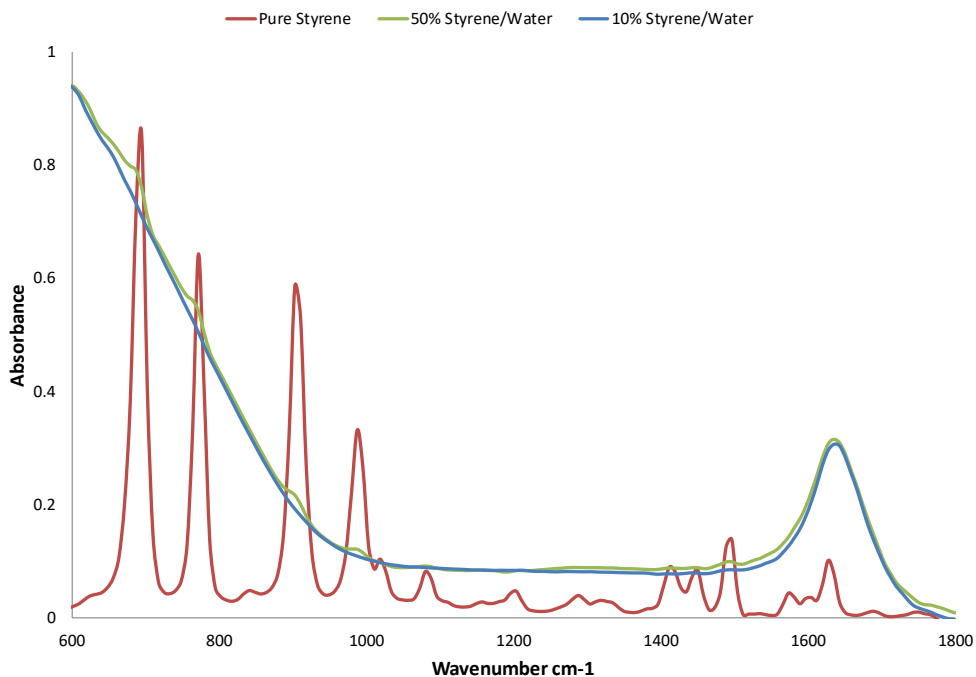


Figure 3.8 – Average ($n = 51$) MIR spectra of pure styrene (red), 50% styrene (green) and 10% styrene (blue) mixtures. All spectra shown have a resolution of 16 cm^{-1} and a subtracted air background.

Even at relatively high concentrations of styrene (50% v/v), the broad water band from $1000\text{-}600 \text{ cm}^{-1}$ all but completely obstructs the distinct styrene bands. As the aim is to monitor monomer levels at very low concentrations, it was important to also investigate the impact of water on the styrene spectral bands at such a level. Figure 3.8 shows the contrast between spectra of 100, 50 and 10% styrene/water and highlights the challenge associated with using MIR for this process. It is evident that at 10% styrene – still well above the levels at which this project aims to monitor styrene – the spectrum becomes swamped with water bands, obscuring the styrene peaks completely.

From this work, it was concluded that no further use of MIR would be considered as the highly aqueous reaction matrix caused too much interference and completely obscured the spectral region necessary for analysing styrene content in water.

3.6.6. Detection of Styrene via Raman Spectroscopy

Analysis of the Raman spectrum of each individual reaction component highlights the suitability of the technique for this application as well as the collective complexity of the reaction media.

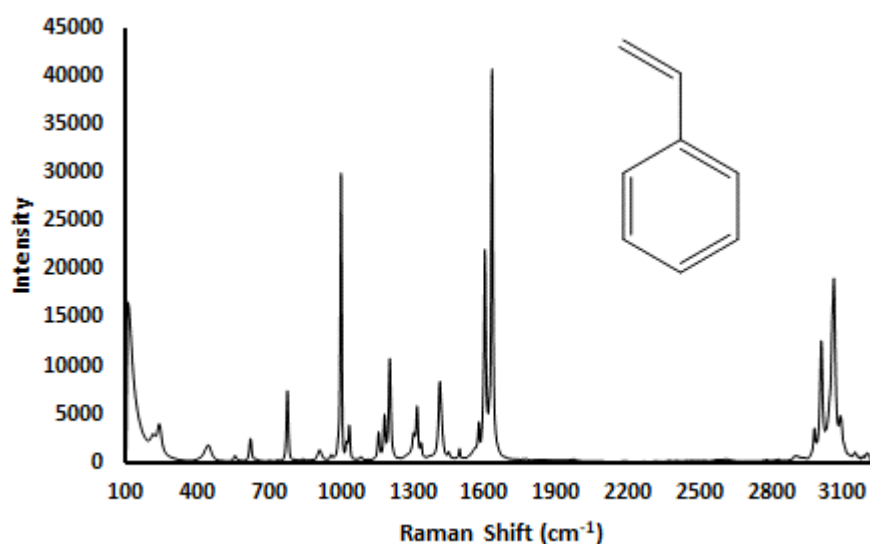


Figure 3.9 – Average (n = 5, 1.5 s exposure) Raman spectrum (785 nm, 100-3240 cm⁻¹) of neat styrene in a glass vial using an NCO MR probe head in a shuttered housing.

In contrast to MIR spectra, the bands observed in Raman spectra are sharper and are indicative of more symmetrical and polarisable groups within the molecular structure. Key features shown in Figure 3.9 include the C-C_{aliphatic} stretch at 770 cm⁻¹, the aromatic ring breathing seen at 1000 cm⁻¹, the aliphatic C-C ring chain vibrations at 1600 cm⁻¹, and the distinct C=C stretch seen at 1630 cm⁻¹. Peaks around 3000 cm⁻¹ corresponding to C-H stretching are weaker in the monomeric form of styrene and would be expected to become more intense with polymerisation.

The differences in the Raman spectra of styrene and polystyrene highlight the key spectral regions that enable Raman monitoring of the polymerisation reaction (Figure 3.9 and 3.10):

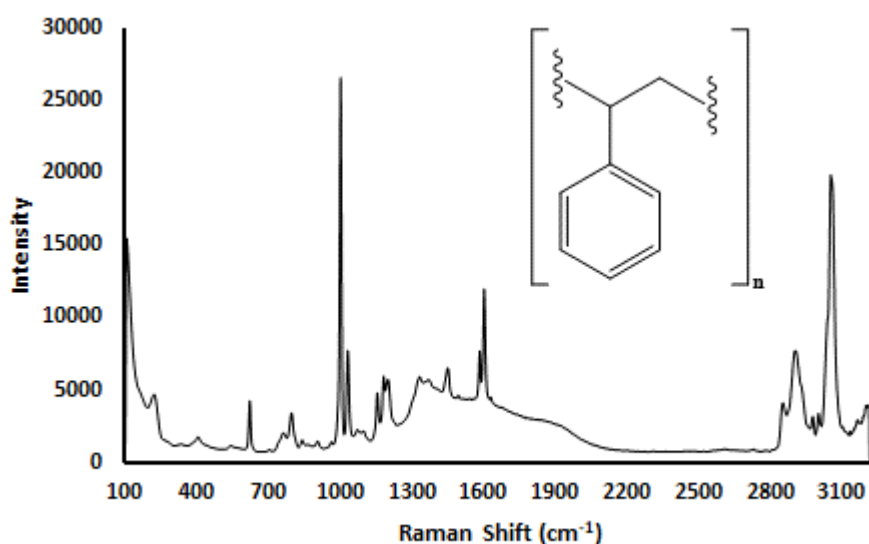


Figure 3.10 – Average (n = 5, 2 s exposure) Raman spectrum (785 nm, 100-3240 cm⁻¹) of polystyrene beads in a glass vial using an NCO MR probe head in a shuttered housing.

Comparison of Figures 3.9 and 3.10 show the diminishing intensity of the C=C peak at 1630 cm⁻¹ and corresponding increase in the intensity of the C-H stretching peak ~3000 cm⁻¹ as C=C bonds are broken during polymerisation. Furthermore, the influence of impurities and inorganic components of the polymerisation process can be seen from the fluorescence in the 1200-2200 cm⁻¹ region (Figure 3.10).

Fluorescence can also be seen in the Raman analysis of other components of the reaction matrix. Figure 3.11 shows the Raman spectrum of initiator – DBPO – and Figure 3.12 shows the Raman spectrum of the surfactant – TCP.

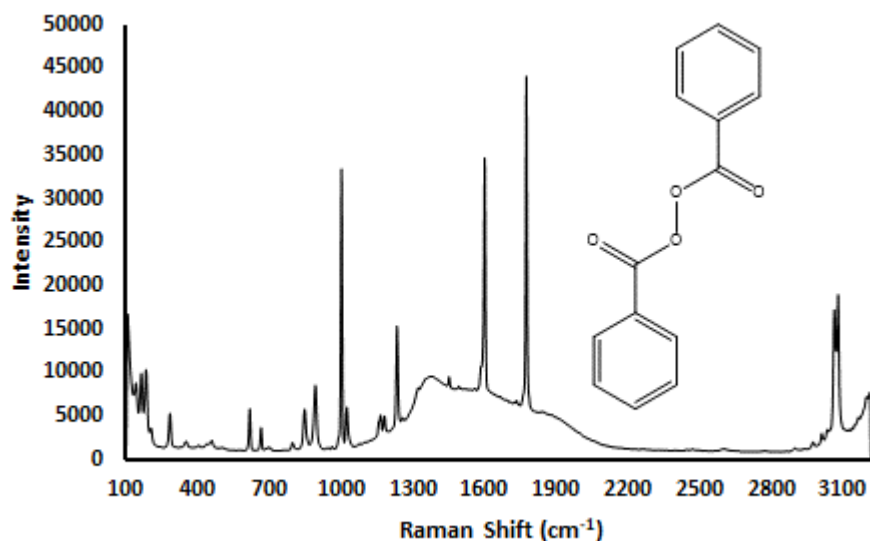


Figure 3.11 – Average ($n = 5$, 2 s exposure) Raman spectrum (785 nm, 100-3240 cm^{-1}) of crystalline DBPO in a glass vial using an NCO MR probe head in a shuttered housing.

In Figure 3.11, the aliphatic ring breathing can be seen again at 1000 cm^{-1} , as well as C-C ring chain vibrations at 1600 cm^{-1} , and an intense carbonyl C=O stretching band at 1775 cm^{-1} . Again, fluorescence caused by impurities in the reagent powder can be seen in the 1200-2200 cm^{-1} region.

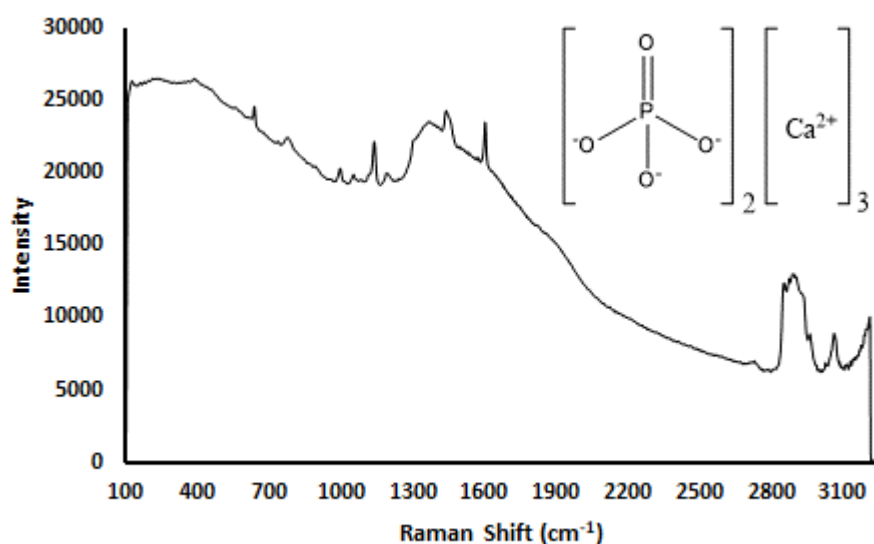


Figure 3.12 – Average (n = 5, 1 s exposure) Raman spectrum (785 nm, 100-3240 cm⁻¹) of crystalline TCP in a glass vial using an NCO MR probe head in a shuttered housing.

Figure 3.12 highlights the interference caused by inorganic compounds present in the reaction matrix. The spectrum of the inorganic crystals in their raw form is dominated by fluorescence, showing almost no distinguishable Raman bands. The low concentration of this component in the reaction matrix should mitigate this interference.

By examining each reaction components' Raman spectra (Figures 3.9-3.11), the strong C=C peak at 1631 cm⁻¹ was observed for neat styrene alone which can be, indicating that this peak was then used throughout as a basis for monitoring changing levels of styrene in different environments. The change in this region with time throughout a reaction can be seen in Figure 3.13:

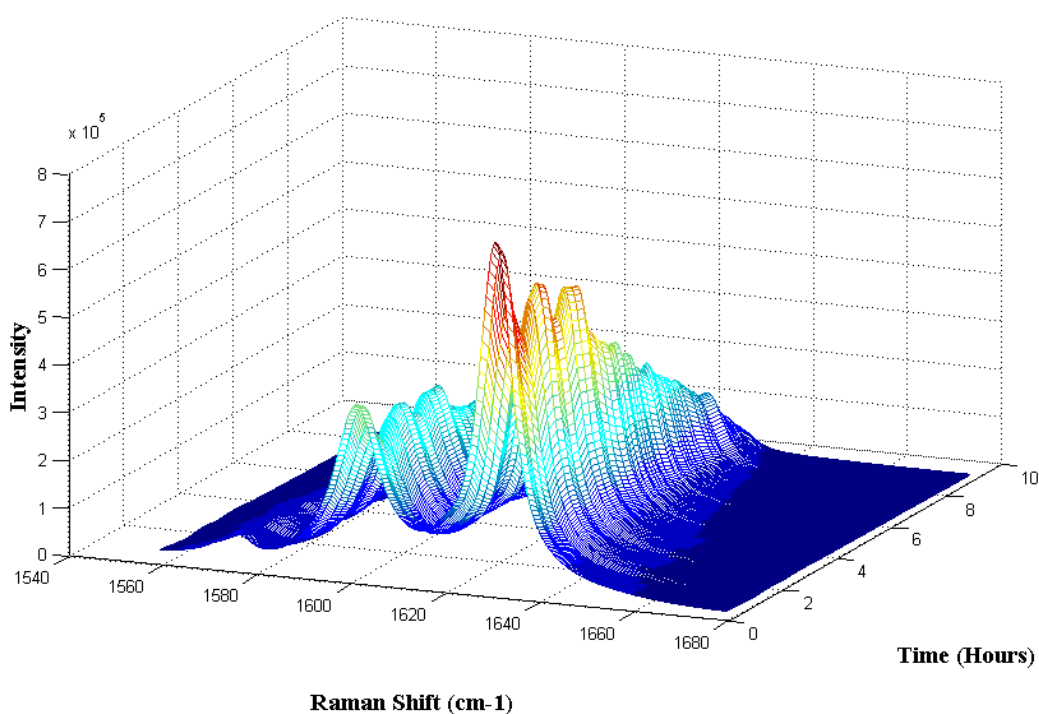


Figure 3.13 – A 3D representation of the 1548-1680 cm^{-1} region of the Raman spectra (785 nm laser) taken hourly throughout a reaction using an immersion optic probe head. Each spectrum was an average of 10 acquisitions of 12 s each.

The intense, sharp band C=C band at 1630 cm^{-1} can easily be followed as the reaction progresses, making it an ideal region to study for monitoring. However, as the reaction nears its endpoint, this distinct peak becomes harder to discern as the concentration of unreacted monomer gets smaller. Furthermore, the formation of solid particles as the reaction progresses and the contribution from each reaction component increases the complexity of the spectra collected throughout. It is often beneficial to employ first or even second derivatisation of the collected data to minimise baseline shift and interference caused by fluorescence, and to amplify smaller peaks that can otherwise be lost in noisy spectra. This is especially useful when sharp defined peaks are present, such as in the Raman spectra collected in this work. Figure 3.14 shows the effect of taking the first order derivative of the Raman spectra of styrene:

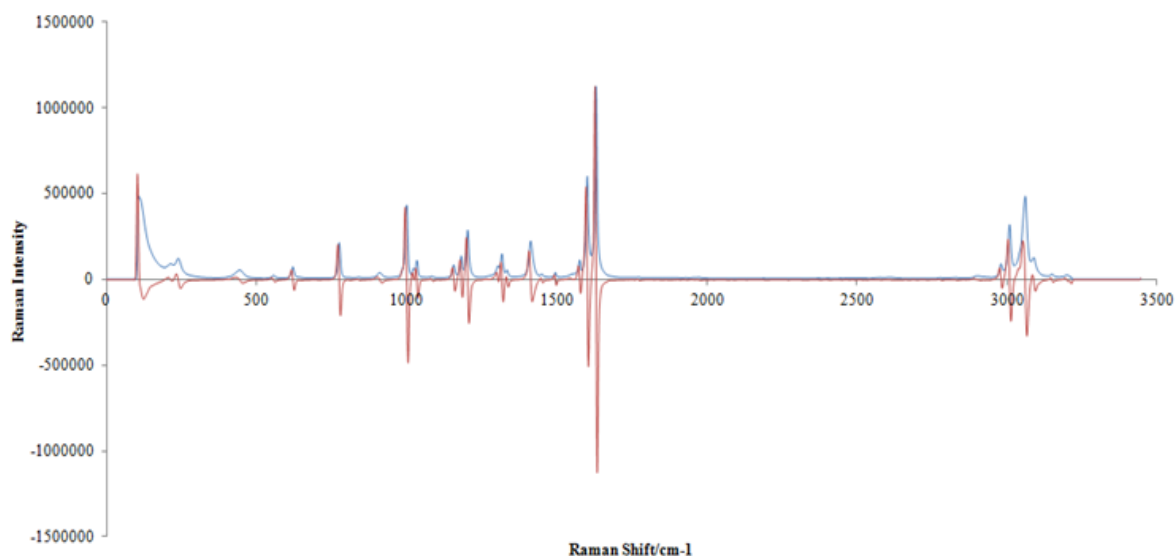


Figure 3.14 – Average Raman spectra of styrene (n=10, blue) and its first derivative (red) using an NCO Raman probe (785 nm, 20 s exposure per acquisition). Derivatisation was carried out using the Savitzky-Golay function on Matlab using a 31-point window. Spectra obtained with an NCO MR Raman probe.

The point at which the peak reaches its maximum (1631 cm^{-1}) in the raw spectrum is equal to 0 in the first derivative; therefore, it was no longer viable to use this point as a measure of styrene concentration. To account for this, the height of the peak in the region before this 0 point (i.e. the maximum slope of the peak in the raw spectrum, occurring at 1627 cm^{-1}) was then used throughout the investigation to establish and monitor styrene concentration.

3.7.3. Detection of Styrene in EPS beads via Raman Spectroscopy

Due to the nature of the reaction, some monomer remains residually in the polymer beads formed after the reaction is complete.¹¹⁶ This styrene can then be removed by other chemical processes, such as foaming with a foaming agent (e.g. pentane). However, by being able to monitor the level of residual styrene, it would be possible to optimise and control the polymerisation in real time. Impeller speed, initiator

concentration, surfactant concentration, temperature fluctuations and particle size distribution can all affect the residual monomer content of the product. By controlling the component concentrations, temperature and mixing speed while monitoring particle size and monomer level, it should be possible to know the residual monomer content of beads produced.

Figure 3.15 shows the presence of the same peak used before as being indicative of styrene in the Raman spectrum of polystyrene, indicating that RS can be used to see the residual styrene in polystyrene beads.

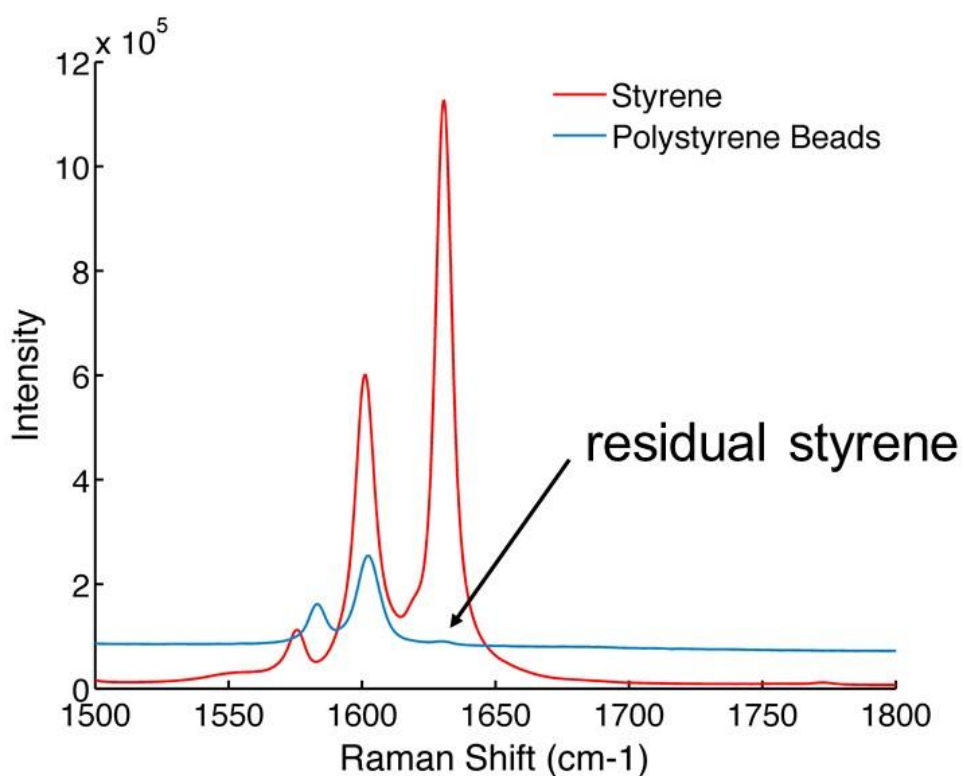


Figure 3.15 – Average Raman spectra (n=5, 20 s per acquisition) of styrene (red) and polystyrene beads (purple) indicating the styrene peak at 1631 cm⁻¹. Spectra were acquired using an NCO through a glass vial.

By knowing the styrene content of the beads from HPLC, it is possible to look at the styrene signal achieved with RS and establish some correlation between the two. However, given that 3 of the batches of beads have relatively similar residual styrene levels – and, thus, relatively similar Raman intensities for the styrene peak – there is insufficient data with which to establish this detection limit in polystyrene beads.

As described in Section 3.3.1, polystyrene bead samples were created which contained differing levels of residual styrene. The result of these experiments is exemplified in Figure 3.16 illustrates the first successful impregnation experiment on batch 3 polystyrene beads. It can be seen from the derivative peak height that the styrene level has increased – the peak maximum has increased from approximately 50 to 500. This experiment was performed by adding 6% w/w of styrene to the vessel. The sample was then re-tested one week later to ensure that added styrene was not lost over time.

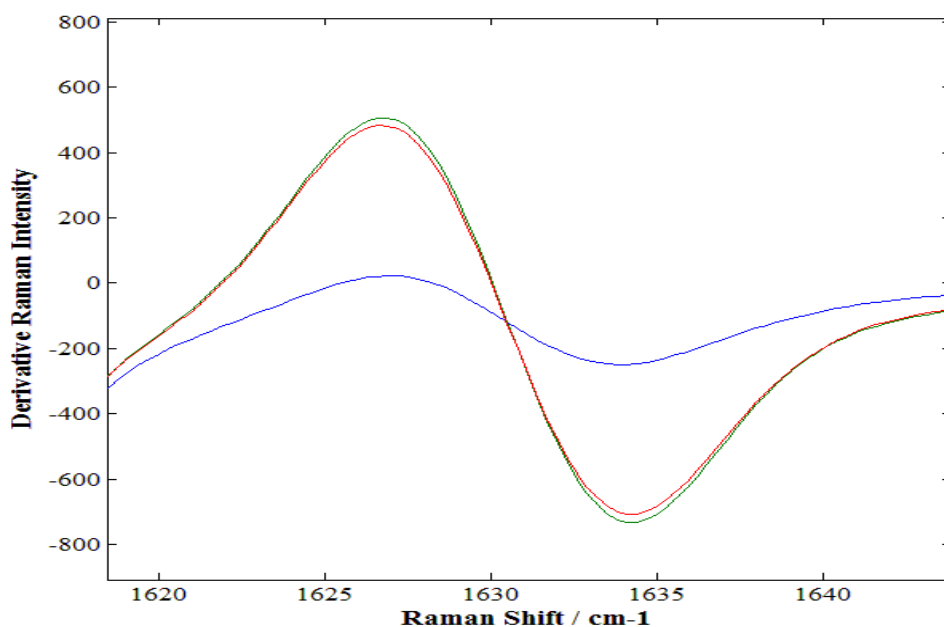


Figure 3.16 - Derivative offline Raman spectra of batch 3 polystyrene beads as received (blue), successfully impregnated (green) and one week after the experiment (red). Spectra are averaged from 10 accumulations of 10 s exposure each.

Also highlighted in Figure 3.16 is the influence of noise on the calculated derivative spectra, as the inflection point (where the slope is steepest) does not occur at zero. Noisy data causes this and it can be mitigated by further smoothing the data prior to derivatisation, but this can lead to over-smoothing and loss of meaningful peaks as well as noise.

Successful experiments with batch 3 beads were performed with 8 and 6% w/w styrene being added to the vessel – with subsequent quantification of styrene had adsorbed onto or into the beads. Furthermore, some successful experiments were carried out with low amounts of styrene on batch 4 beads. It was expected that these beads, having already low monomer levels, would be more susceptible to adsorbing smaller levels of styrene, which was confirmed with a successful 4% styrene experiment.

After several iterations of this experiment, the production of polystyrene beads with different amounts of residual styrene was achieved. Through this work, samples with different amounts of styrene could now be analysed as 'standards' using RS and HPLC.

To quantify the styrene content of samples via HPLC, a standard curve had to first be produced by dissolving known amounts of styrene in THF and plotting the instrument response against the known monomer content (Table 3.6, Figure 3.17 and Figure 3.18).

Table 3.6 – Standard curve data for quantifying styrene in ppm from the area under the curve in the HPLC response.

Styrene Content (ppm)	Peak Area (mV x min)
0	0
10	53.4132
20	106.0714
40	191.2884
50	250.4036
60	291.6325
70	324.5473
80	362.9852

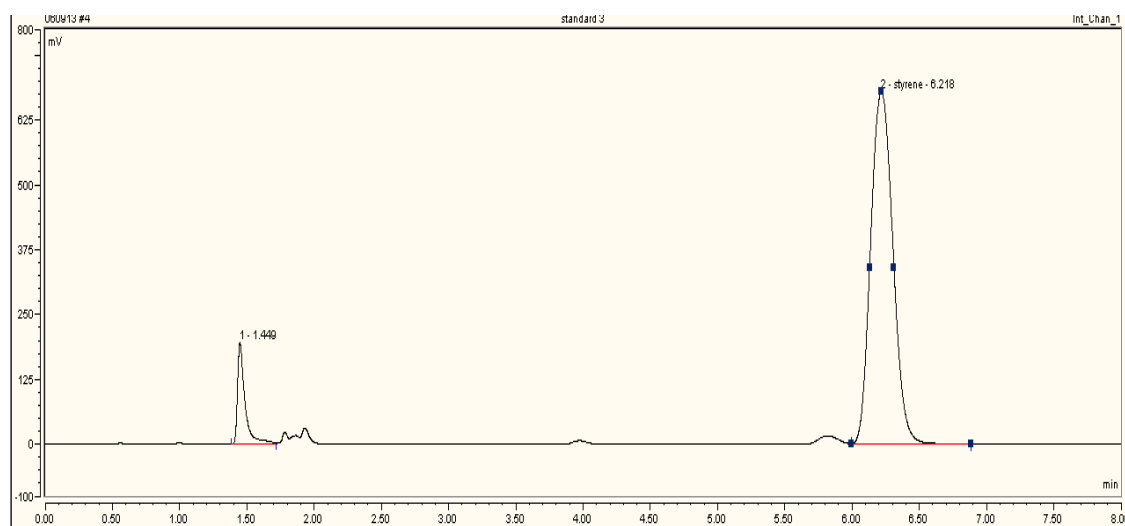


Figure 3.17 – Screenshot of a typical HPLC trace from a 40 ppm standard solution analysed using a Waters 2690 with a Shimadzu SPD-6A variable wavelength UV detector and Chromeleon software.

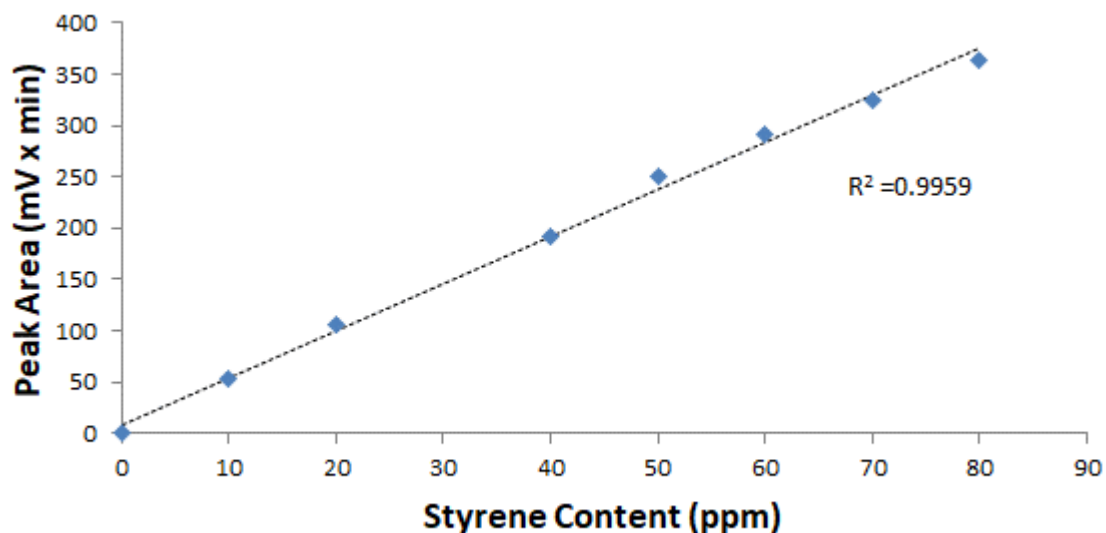


Figure 3.18 – Calibration curve for a series of styrene/THF mixtures after HPLC analysis. The linearity of the 1630 cm^{-1} peak area from 0 to 80% v/v styrene is shown by the R^2 value.

The linear response from 0 – 80 ppm meant that samples could be manipulated (varying the initial sample weight or using different dilutions of sample solution) to give a response within this range. The original sample weight and any dilution factors could then be used to accurately calculate the residual styrene content of the sample. To test the reliability of the method, polystyrene samples of known monomer content provided by BASF were analysed using this method (Table 3.7).

Table 3.7 – Residual monomer content of polystyrene beads provided by BASF showing (left) the known monomer content as provided by BASF via HPLC and (right) the monomer content calculated by Strathclyde following implementation of the HPLC method.

Data Provided by BASF (ppm)	Data Obtained at Strathclyde (ppm)
72	73.8
4837	4618

The comparable results from HPLC analysis at BASF and Strathclyde show that the implementation of the BASF method at Strathclyde was successful and, thus, results obtained by this method were reliable. However, the multi-step sample preparation provides multiple opportunities for errors to be introduced – either from operator error in handling, weighing or diluting, or instrument and equipment error such as in volumetric glassware or pipettes. The error associated with this method is not trivial and is one of the main disadvantages of using HPLC as a reference, along with the slow rate of analysis.

Following the generation of a set of ‘standard’ polystyrene samples spiked with varying residual monomer levels, these could then be analysed via HPLC and their monomer content related to the intensity of the C=C peak in the derivatised offline Raman signal obtained using the NCO.

Table 3.8 - Residual styrene contents of batch 3 polystyrene beads from HPLC (left) and Raman spectroscopy (right).

Styrene Content via HPLC at Strathclyde (ppm)	1630 cm ⁻¹ Raman Peak Intensity (MR)
4577	40.57
16473	506.12
18936	566.62
26539	802.99
30994	973.56

Table 3.8 shows the residual styrene contents of the successfully impregnated beads as measured by HPLC and RS at Strathclyde. Through HPLC, the residual styrene content is quantified, allowing a correlation to be established between first order derivatised Raman measurements and residual styrene content, as illustrated by Figure 3.19:

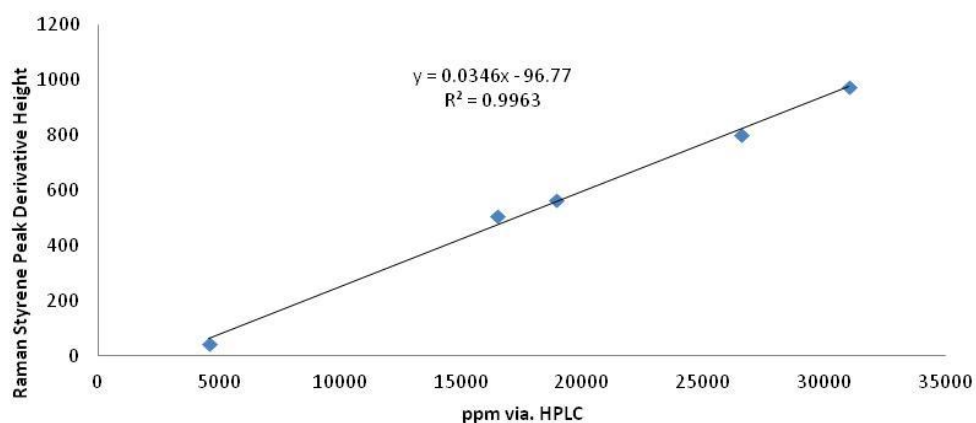


Figure 3.19 - Residual styrene content of batch 3 polystyrene beads measured via HPLC plotted against that measured via offline Raman spectroscopy followed by first-order derivatisation.

The linearity of this data shows the potential of RS for monitoring the styrene content of polystyrene beads. Calculating the LOD as per Equation 3.1 gives a result of 3940 ppm, around 0.4% styrene.

$$\text{LOD} = 3 \times \text{SD}_{\text{Blank}}/\text{slope} \qquad \text{Equation 3.1}$$

Where:

- SD_{Blank} = The standard deviation of the Raman signal at 1630 cm^{-1} in a blank solution. Due to the lack of polystyrene bead samples with no styrene present (a true blank), the SD of the styrene peak at 1630 cm^{-1} in the 4577 ppm beads was used
- Slope = The slope of the line of best fit through the data

It has been demonstrated that applying a first order derivative to the spectral data collected in these experiments has the potential to meet the challenges of the project, as it allows residual C=C bonds to be seen even in low RM EPS bead products at a level close to that desired by industrial partners. By applying a second order derivatisation of the data and plotting the intensity of the negative peak at 1630 cm^{-1} (Figure 3.20), the LOD calculated is 486 ppm (approx. 0.05% styrene. Second order derivatisation further improves the signal-to-noise ratio of the data and mitigates fluorescence and baseline drift in the spectra. It is often beneficial to investigate multiple orders of derivatisation on spectral data.

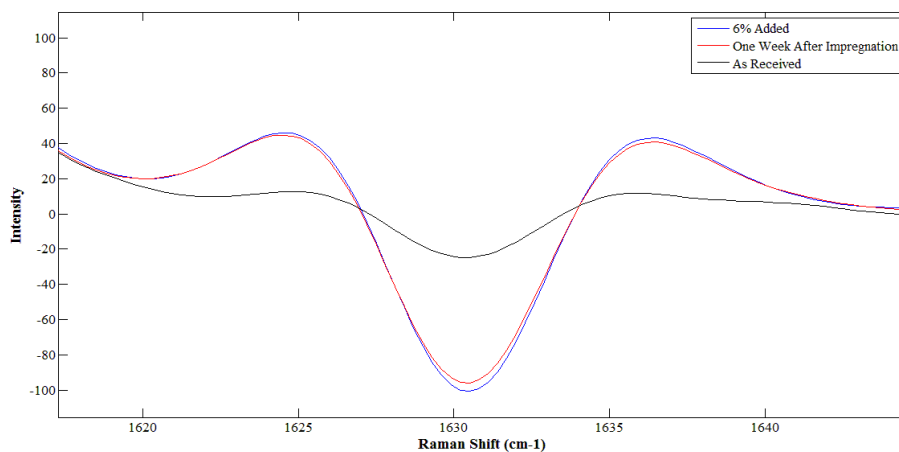


Figure 3.20 - Second order derivatisation of offline Raman spectrum of EPS beads as received from BASF (black), with additional styrene added (blue) and one week after addition of styrene (red).

Table 3.9 – Varying second order Raman peak magnitudes from different EPS bead samples with corresponding RM levels determined via HPLC.

Monomer via HPLC (ppm)	Magnitude of 2 nd Derivative at 1630 cm ⁻¹
4577	26.66
16473	100.84
18936	108.88
26539	146.14
30994	173.77

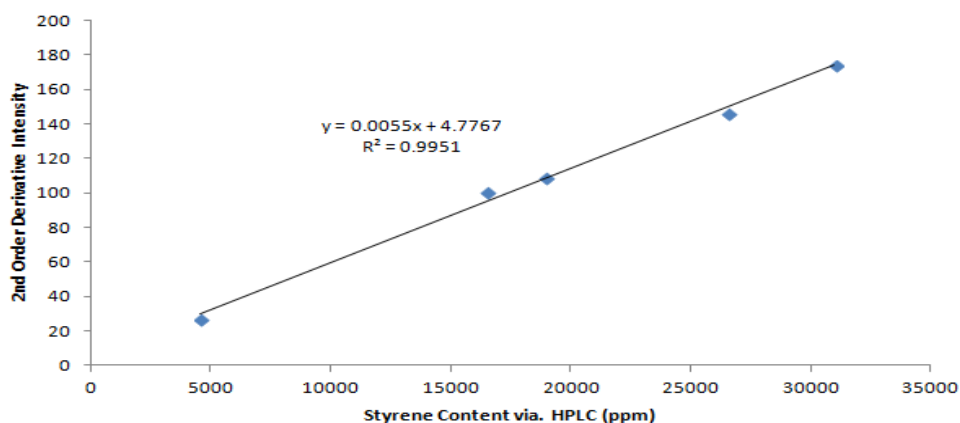


Figure 3.21 - Second order peak magnitude at 1630 cm⁻¹ from offline Raman spectrum of different bead batches with differing RM content as determined via HPLC.

By increasing the order or derivatisation, a lower LOD that satisfies one of the key objectives of this study is achieved; the detection of residual monomer within EPS beads below 0.1%. The use of derivatised offline spectroscopic measurements of collected reaction products has shown the potential for Raman spectroscopy to solve this challenge in industry. However, though successful in proving the ability of the chosen analytical methods to solve the industrial problem, there are several inherent issues that should be addressed to make this solution more practical and beneficial to industry. First, this method requires offline measurements after the reaction is complete rather than providing information on the reaction's progress. Also, the narrow spot diameter of the probe used – while ideal for monitoring well-mixed solutions – can cause subsampling when solid particles are formed. Finally, the PSD of the samples analysed can affect the spectral data. Each of these problems should be addressed in order to better design an analytical method suited to its industrial requirements.

3.7.4. Effect of EPS Bead Size on Raman Spectroscopic Measurements

Particle size changes are an inherent feature of these reactions and this has been shown to affect the Raman signal.^{114, 117-119} However, much of the literature available concerns particles in the nanometre range, whereas the suspension polymerisation reactions in this study produced beads of a much larger diameter. This work was carried out by Meghan Sanders and the effects of particle size on the Raman data can be seen in Figures 3.22 – 3.25:

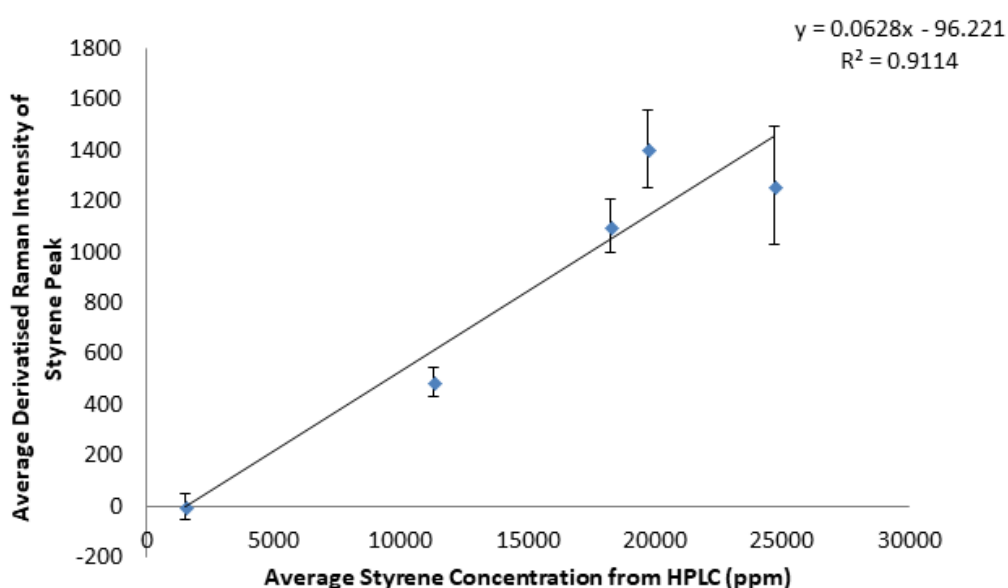


Figure 3.22 – Correlation between residual monomer measurements made via HPLC and offline Raman spectroscopy of small EPS beads (0.827 mm mean diameter, Raman spectra averaged from 5 acquisitions, 20 s exposure per acquisition). Error bars indicate one standard deviation.

The error associated with Raman measurements increases as the styrene content of the smallest beads also increases (Figure 3.22), possibly owing to increased variability in measuring more intense derivatised peaks. This is also seen in the loss of linearity towards the top end of the concentration range analysed.

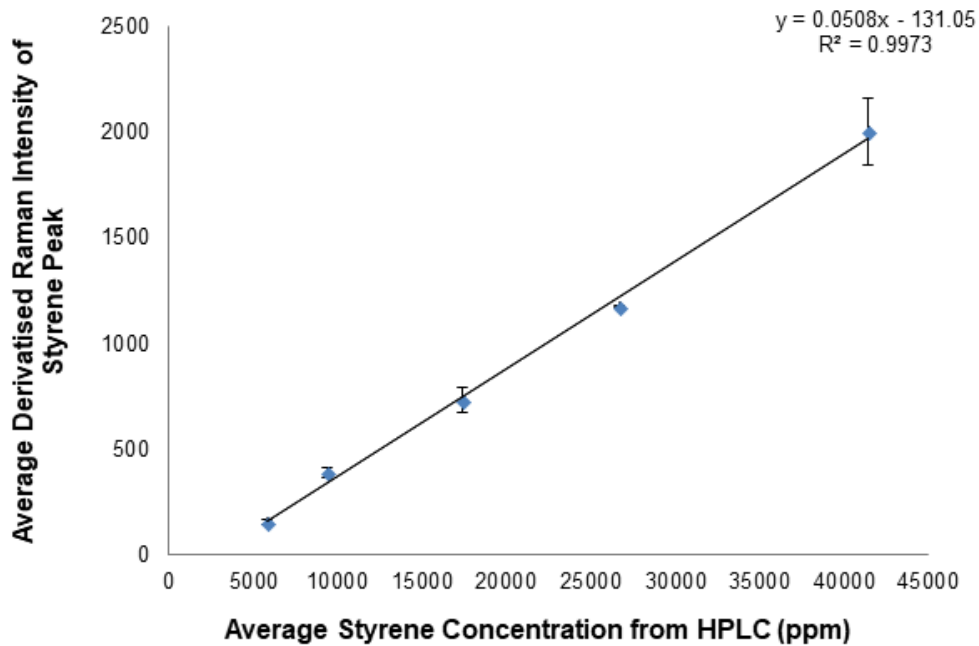


Figure 3.23 - Correlation between residual monomer estimations made via HPLC and offline Raman spectroscopy of medium EPS beads (1.003 mm mean diameter, Raman spectra averaged from 5 acquisitions, 20 s exposure per acquisition). Error bars indicate one standard deviation.

Mid-sized beads provided less variability than other sizes analysed across the entire concentration range studied (Figure 3.23). Increased linearity and lower errors associated with Raman measurements suggest a more homogeneous dispersion throughout the sample. Furthermore, Figure 3.3 shows this batch of beads as having a narrower size distribution than the others in this experiment. This allows a more evenly distributed sample, resulting in a more uniform propagation of light through the beads.

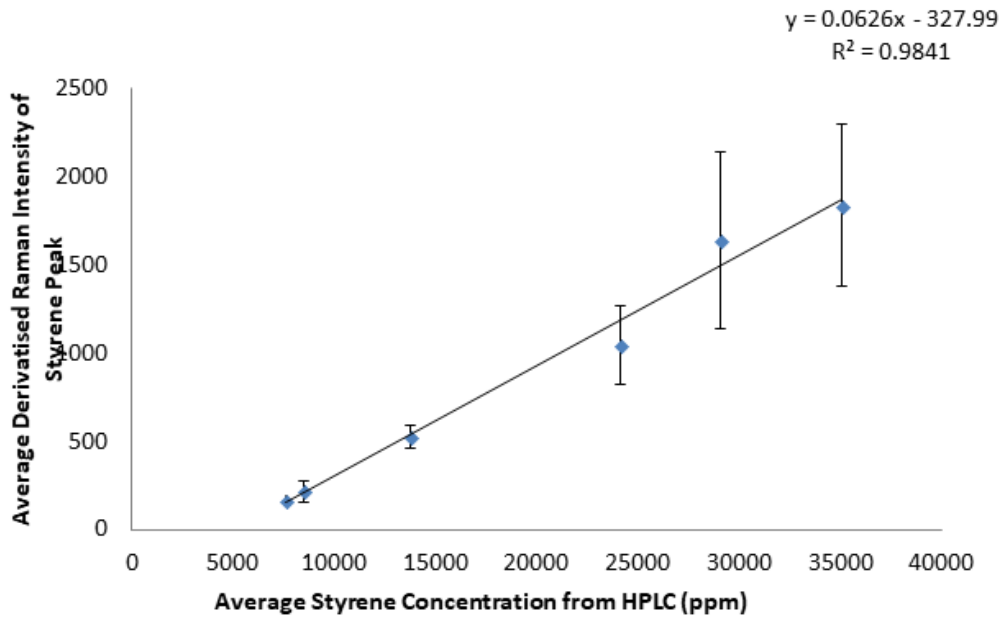


Figure 3.24 - Correlation between residual monomer estimations made via HPLC and offline Raman spectroscopy of large EPS beads (1.334 mm mean diameter, Raman spectra averaged from 5 acquisitions, 20 s exposure per acquisition). Error bars indicate one standard deviation.

Finally, larger beads show similar variability to smaller beads, most likely caused by their comparably wide PSD. Irregular distribution of EPS beads means that the Raman scans sample a wider variety of bead sizes each time, resulting in larger standard deviations from the average spectra. This is most exemplified at the higher end of the concentration range analysed, suggesting that this variability is increased as the intensity of the measured peak increases.

Changing particle size not only affects the intensity of the Raman signal, but the variability of Raman measurements as well. Error bars on Figures were calculated from the Raman signal of 5 repeat measurements and it can be seen – particularly for the smallest and largest beads at higher RM levels – these errors are large. This is likely due to heterogeneity in the sample. Whereas mid-sized particles produced more consistent results. Furthermore, examination of results from beads of similar

RM content (around 25000 ppm, highlighted in Figure 3.21) reveals an increase in Raman signal with decreasing particle size, consistent with other works examining the C-C Raman signal.¹²⁰ However, datapoints shown here are only similar in RM content, not identical, and this is subject to variability in the Raman spectra (y-direction) as well as in the HPLC measurements (x-direction).

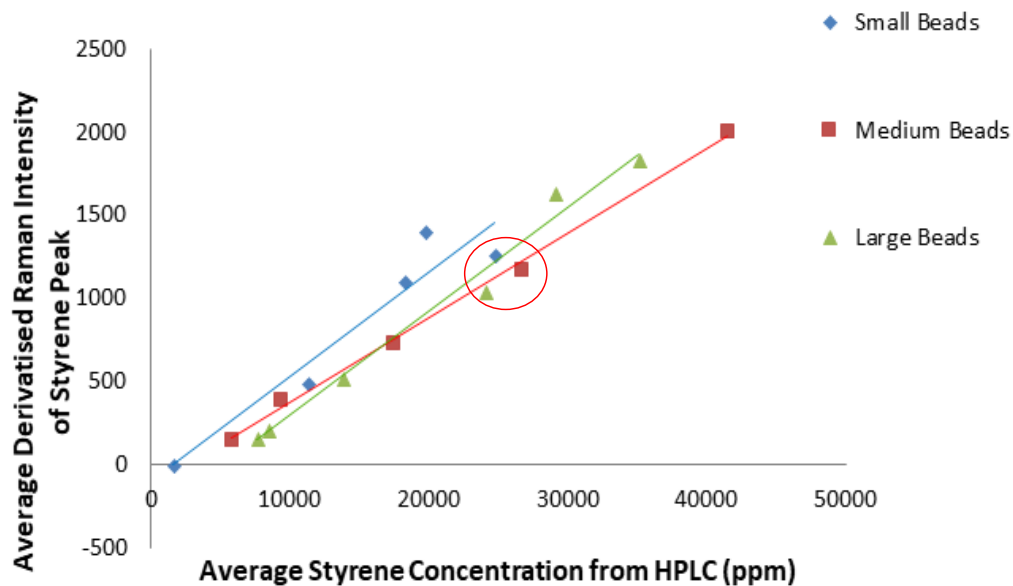


Figure 3.25 – Correlation between residual monomer estimations made via HPLC and offline Raman spectroscopy of all EPS bead size fractions. The area circled indicates the Raman response for all bead sizes with a similar residual monomer level as determined by HPLC.

Particle size changes result in changes in particle concentration, which in turn can affect Raman spectra collected using small area probes. These probes only capture a small snapshot of the reaction matrix to any given time, and the majority of the data collected comes from the very top layer of the particle being analysed. The linearity of the data from these model systems shows the potential for RS to be used for the determination of RM in EPS beads; however, employing more complex methods of data acquisition and analysis such as the use of different laser spot diameters, the analysis of samples taken from real polymerisation reactions, the assessment of *in-*

situ measurements and the employment of data pre-processing methods in conjunction with multivariate analysis (MVA, see Chapter 4) would allow not only the challenge of low residual monomer detection to be met, but the ability of this to be determined in real time throughout the reaction's progress to be explored.

3.7.5. Wide Area Probe and Information Depth Study

The non-contact MR Raman probe used throughout this study uses a focussed beam with a very narrow spot diameter of approximately 100 μm . This results in a very small sampling volume, normally sufficient for solution monitoring if the solution is sufficiently agitated. When solids are introduced, the small sampling volume can result in subsampling – an issue often seen in Raman analysis of solids or multiphase liquids, which can be caused by changing sample position, sample heterogeneity, or laser power density. These factors result in only a small, unrepresentative sample being taken.

To mitigate this, wide-area Raman probes with larger spot sizes have been developed, ranging from 3-7 mm in diameter. The increase in laser diameter while maintaining laser power results in the spreading of power density, as well as increasing the sample area being illuminated with each spectrum measured.^{121, 122} As the process under investigation involves the in-situ formation of solid beads, it was thought that a wide-area probe – a PhAT probe – may provide more information than a standard non-contact optic and an investigation was carried out with a 6 mm spot diameter.

The maximum depth at which each probe can acquire information was investigated using a sulphur disc as a Raman scattering standard. The standard was placed in front of each laser and the amount of sample between the standard and the laser was increased incrementally until the signal from the standard diminished towards 0.

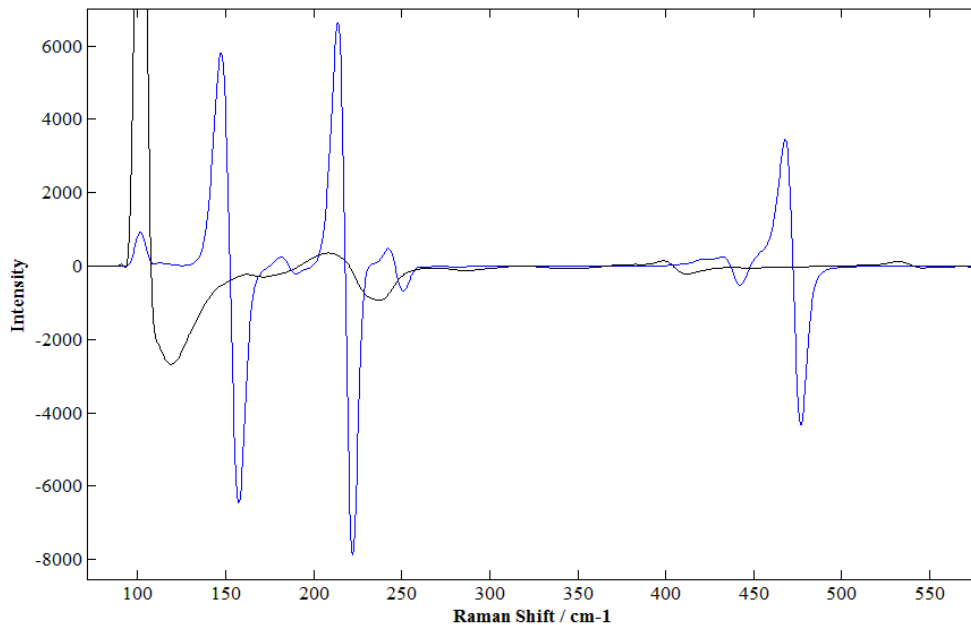


Figure 3.26 - Overlay of derivatised Raman spectra of sulphur disc (blue) with polystyrene beads (black) in 100-550 cm^{-1} region.

The two peaks present at ~ 147 and 214 cm^{-1} (Figure 3.26) would possibly be affected by the polystyrene but the peak at $\sim 468 \text{ cm}^{-1}$ is ideal for monitoring the sulphur disc. This peak was used to estimate the sampling depth of each probe. By observing the change in this peak signal as the sample depth increased and noting at which depth the signal became almost zero, the sampling depth of the laser was calculated. Knowing the laser's spot size, the sample volume for each probe could be calculated. It is assumed that the laser light is cylindrical; therefore, the laser spot area can be calculated directly from the laser spot diameter.

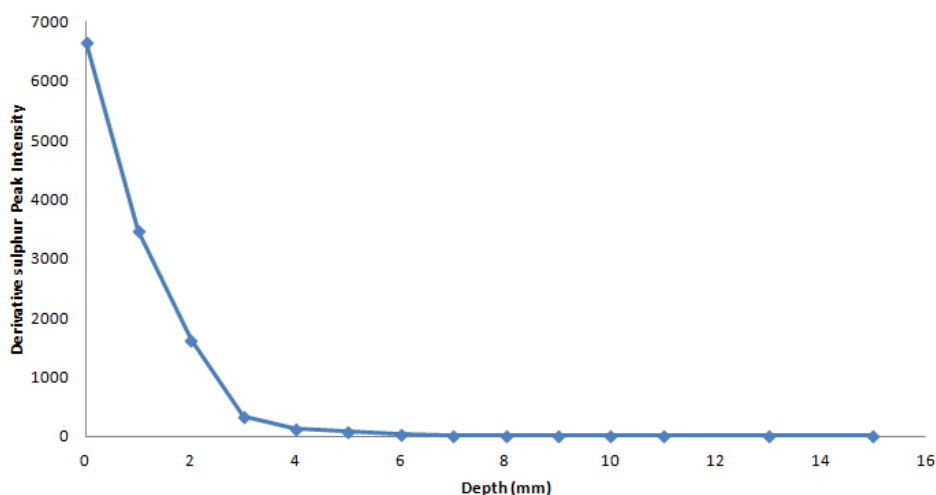


Figure 3.27 – Sulphur peak (468 cm^{-1}) intensity changing with increasing depth of large (1 mm) diameter polystyrene beads using an NCO MR Raman probe with a $100\text{ }\mu\text{m}$ spot diameter.

Figure 3.27 shows the sampling depths at which the signal from the sulphur disc could be seen using an MR probe with an NCO. What is shown is that the Raman signal arising from the sulphur disc standard can be seen up to a depth of approximately 7 mm when using larger beads, with most of the signal coming from the first 2-3 mm. This sampling depth of 7 mm combined with a laser spot diameter of $100\text{ }\mu\text{m}$ yields a sampling volume of 54.98 nL.

It is also important to determine the depth at which the sample becomes infinitely thick i.e. the minimum depth at which a laser must reach to ensure the data generated from its interaction with the sample is truly representative of the whole sample. This is done by observing the increase of the polystyrene signal as the sample depth increases. To do this, a Raman band for polystyrene which is unaffected by sulphur must be identified (Figure 3.28):

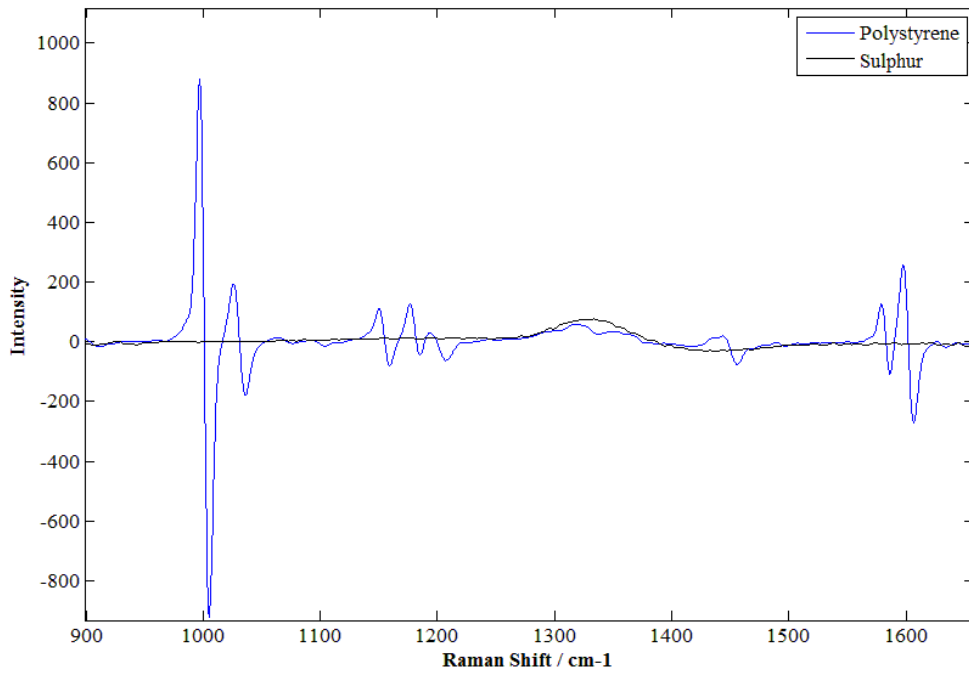


Figure 3.28 - Overlay of derivatised sulphur (black) and polystyrene (blue) spectra taken using an NCO MR Raman probe indicating a polystyrene peak at 997 cm⁻¹.

The peak in the styrene spectrum at approximately 997 cm⁻¹ is the largest peak corresponding to polystyrene which is also unaffected by the sulphur disc. Therefore, it is this peak that will be monitored to establish infinite thickness in the same way as sample depth was identified. With increasing sample depth, the polystyrene Raman band is expected to also increase up until a point where the laser light can penetrate no further. After this point, the Raman band from polystyrene would be expected to remain almost constant and this is known as the depth of infinite thickness, which can be seen in Figure 3.29:

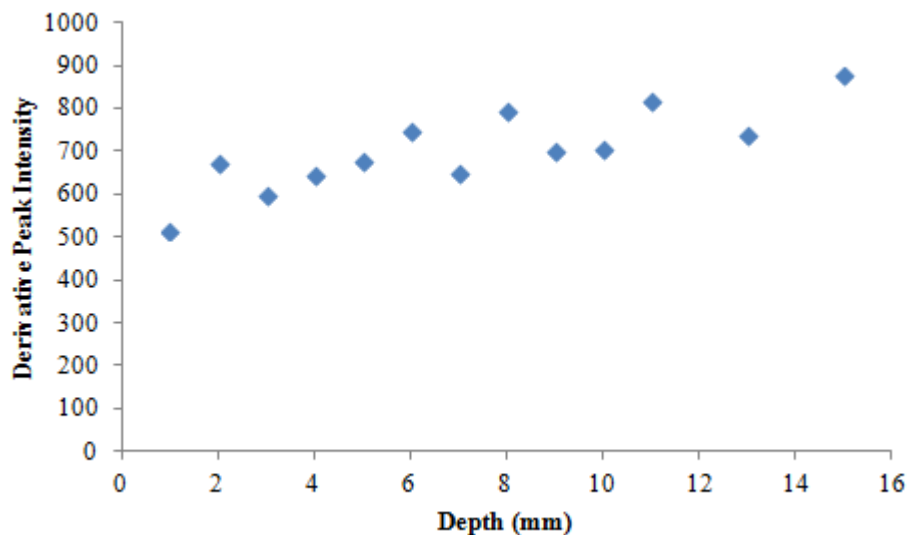


Figure 3.29 - Changing polystyrene peak height with increasing sample depth using NCO MR Raman probe and large (1 mm) polystyrene beads.

It is difficult to assign the depth at which the sample becomes infinitely thick due to the high variability in the peak height measured. There is an increase with sample depth, as is expected, but without a clear point at which the signal becomes steady it is difficult to establish the depth of infinite sample thickness in this case.

Comparing these results to those achieved with the same beads but using a PhAT probe with a 6 mm spot diameter ($r = 3\text{mm}$), a much greater sampling volume can be achieved (Figure 3.30).

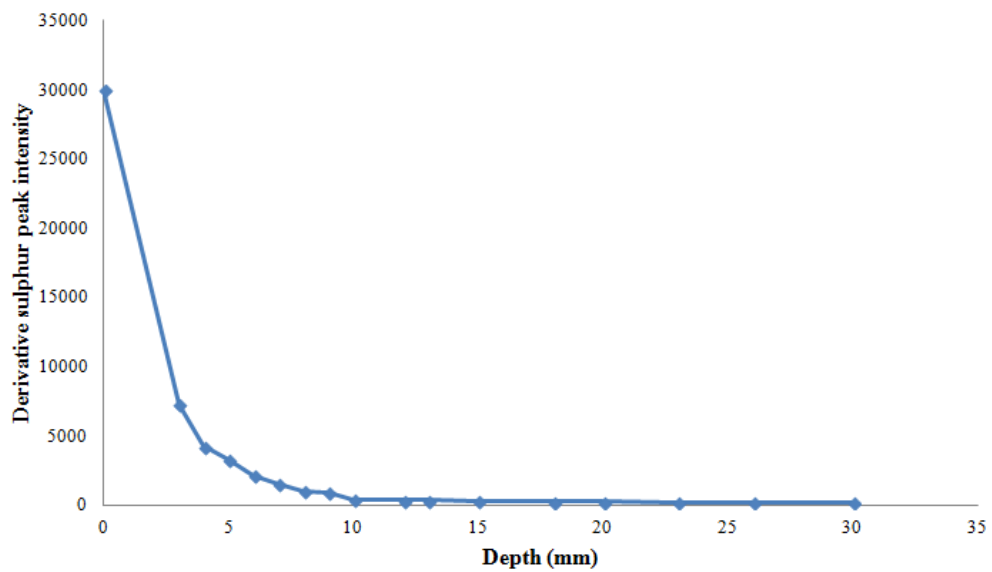


Figure 3.30 – Sulphur peak (468 cm^{-1}) intensity changing with increasing depth of large (1 mm) diameter polystyrene beads using a PhAT Raman probe with a 6 mm spot diameter.

The signal from the sulphur peak diminishes with increasing sample depth up to a depth of 15 mm, giving a sampling volume of $424.12 \times 10^3\text{ nL}$. Thus, by increasing the laser spot size from $100\text{ }\mu\text{m}$ to 6 mm, the sampling volume has increased by a factor of 7700.

Assigning the depth of infinite thickness is much simpler using the PhAT probe, as can be seen from figure 3.31:

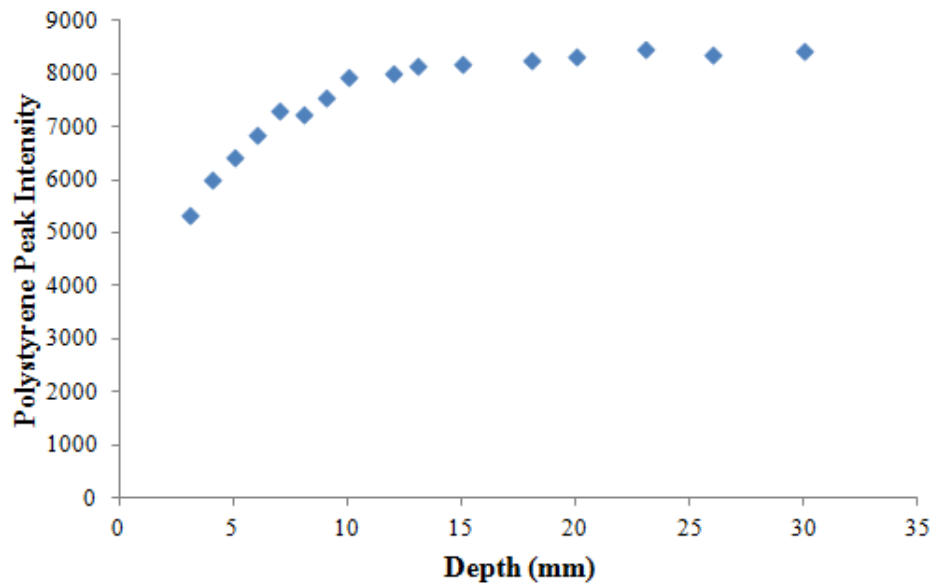


Figure 3.31 – Changing polystyrene peak height with increasing sample depth using a PhAT Raman probe and large (1 mm) polystyrene beads.

Here, at a depth of 23 mm, the data begins to level out, showing no more increase in polystyrene signal. This is a greater depth at which the sampling depth is achieved, which is consistent with other studies in this area.¹²³ This is because the sulphur reference layer is used to estimate information depth – the Raman signal used to determine this is only generated in the plane of the reference material before propagating back through the sample to the detector. Whereas, by using the polystyrene peak to obtain the depth of infinite thickness, the Raman signal used is generated throughout the entire depth of the sample and thus the signal decreases slower than the exciting laser intensity.¹²⁴ As a result, the depth of infinite thickness – i.e. using the signal generated by the sample material – is a more accurate reflection of the depth of material samples by the probe.

The 1 mm beads used for these experiments were from batch 2, which has a very narrow PSD. Diffuse reflectance of light should decrease with increasing particle size¹²⁵, resulting in greater contribution to the Raman signal. In contrast, smaller beads should increase the amount of diffusely reflected light, which should decrease

the penetration depth of light into the sample and result in a much weaker Raman signal from the sulphur standard. Figure 3.32 shows the sampling depth achieved using smaller beads with an average particle size of 0.8 mm.

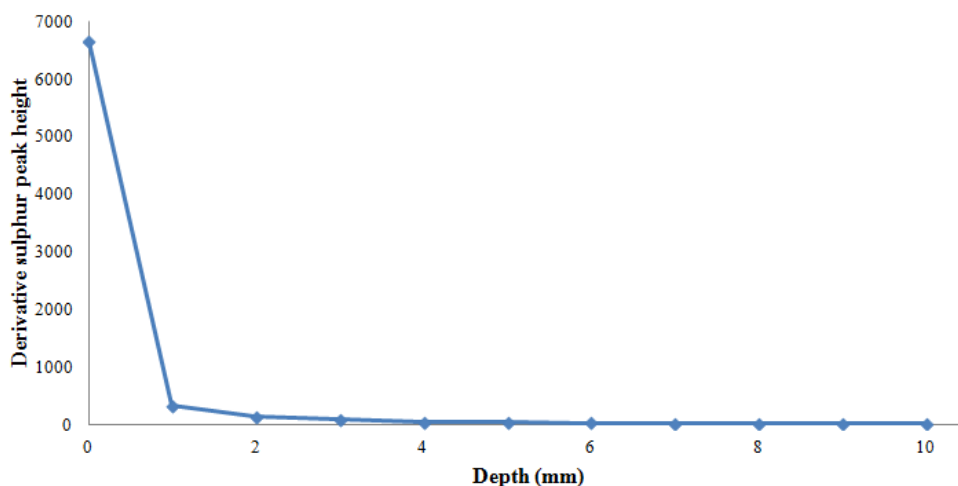


Figure 3.32 - Derivative peak of sulphur standard diminishing as the depth of sample between the standard and the laser increases. A non-contact MR Raman probe and 0.8 mm diameter beads were used.

The signal strength has diminished greatly from that obtained when using slightly larger beads. At a sample depth of just 1 mm, the Raman signal of the sulphur standard has diminished more than tenfold. Furthermore, the sulphur disc standard can only be seen to significantly diminish up to a depth of 4 mm, giving a sample volume of 31.42 nL. It should be noted that both small and large bead size MR experiments were performed on the same day as were both small and large bead size PhAT probe experiments. The MR and PhAT probe experiments, however, were not performed on the same day.

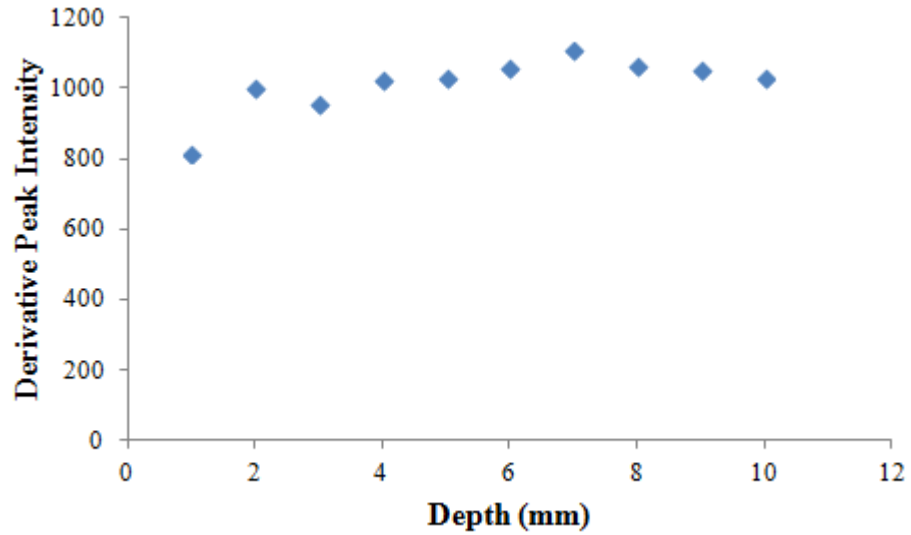


Figure 3.33 - Changing polystyrene peak height with increasing sample depth using a NCO MR Raman probe and small (0.8 mm) polystyrene beads.

It can be seen from Figure 3.33 that there is difficulty in ascertaining the depth of infinite thickness with the MR probe for smaller beads as there was for larger beads. It would appear, however, that this sample is infinitely thick after 4 mm, almost equal to the sampling depth seen in Figure 3.32.

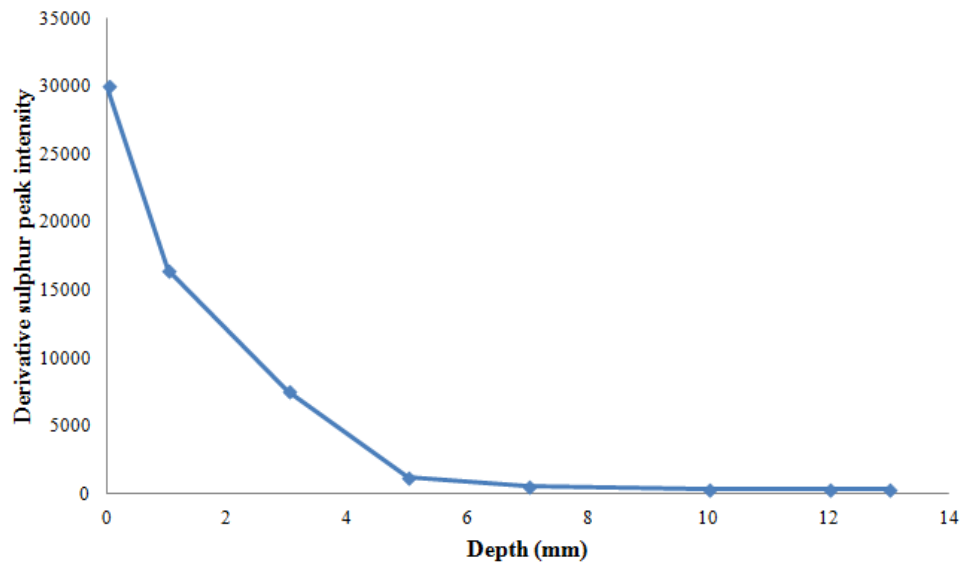


Figure 3.34 - Diminishing sulphur peak intensity as the depth of 0.8 mm diameter beads between the standard and the non-contact PhAT Raman probe laser was increased.

Figure 3.34 illustrates the sampling depth achieved with 0.8 mm beads using the PhAT probe. The depth at which the sulphur peak reaches a steady intensity is around 10 mm, 6 mm deeper than that achieved with the same beads using the MR probe. For the PhAT probe, this depth gives a sample volume of 197.92 μL ; around 6300 times that of the MR probe.

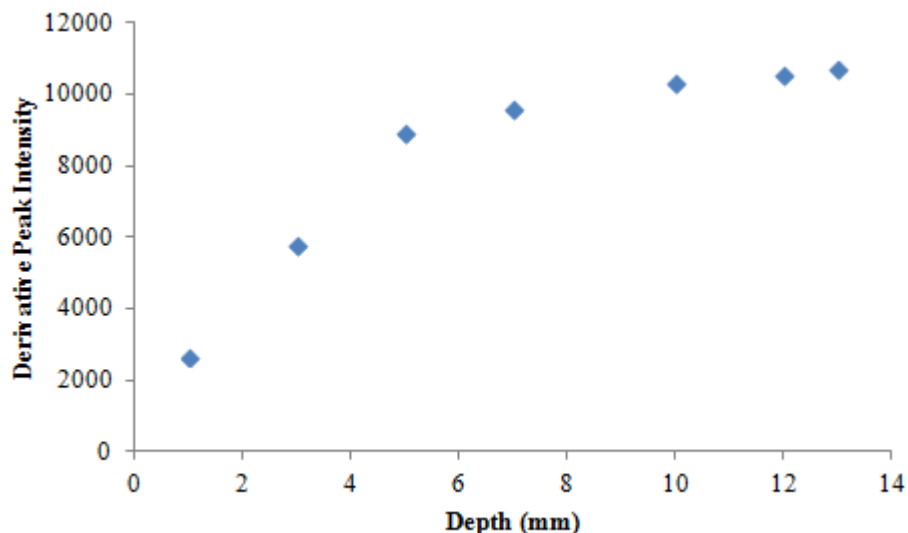


Figure 3.35 – Changing polystyrene peak height with increasing sample depth using a Raman PhAT probe and small (0.8 mm) polystyrene beads.

Figure 3.35 shows again that the depth of infinite sample thickness can be determined for smaller particle sizes using the PhAT probe; this was difficult to ascertain using the NCO MR probe. Here, it appears that infinite sample thickness occurs at around or greater than 13 mm although this is only an estimation due to the lack of greater sample depths. This, again, is greater than the depth achieved with the same bead size using the MR probe and is also greater than the sample depth obtained through using the sulphur disc standard.

Overall, through experiments with larger and smaller particles, the PhAT probe provides between 6000-7000 times greater sampling volume than the MR probe in just half the time. Work carried out by Wikström et al⁷⁵ shows similar results, where a PhAT probe with a 3 mm spot diameter produced a sampling volume 1300 times that of a 150 µm MR NCO probe.

Almost exclusively throughout this experiment, the PhAT probe provides a much more intense Raman signal than the MR probe when sampling equivalent sample depths. From the acquisition parameters, it can also be seen that the PhAT probe achieves these spectral intensities in just half the time – 6.25 s as opposed to 12.5 s for the MR probe. Furthermore, the uncertainty encountered when establishing the depth of infinite sample thickness on the MR probe – given that this method is more accurate than using a reference layer – suggests that a PhAT probe may be better suited for retrieving information from the solid polymer beads.

3.7.6. Detection Limits of Styrene in EPS Beads via Raman MR and PhAT Probes

Table 3.10 shows the LOD values calculated from the data acquired using different Raman optic configurations.

Table 3.10 – Detection limits resulting from immersion, PhAT and non-contact Raman probes with EPS beads.

Beads	Probe	Concentration/(%w/w)
Dry	MR with non-contact optic	LOD = 0.1
	PhAT probe	LOD = 0.01
In water	MR with immersion probe	Can detect 0.21
	PhAT probe	Can detect 0.718

The advantages of using larger laser spot diameters is seen here, as the LOD of the PhAT probe provides offline results an order of magnitude lower than the MR NCO; however, in-situ measurements highlight some of its limitations. The strong signal from the glass vessel wall through which the PhAT probe had to measure meant that

establishing a LOD for this data was not possible. The success of the offline results highlights the effectiveness of this method, suggesting that the implementation of the immersion PhAT probe could significantly improve these results.

This work has demonstrated the ability of Raman spectroscopy to measure residual styrene monomer in EPS beads below the limit desirable by industry leaders. Despite the multiple scatterers present within the reaction media, there are key Raman shift frequencies that make it a useful technique for monitoring this reaction. The breakdown of C=C bonds has a sharp, specific Raman signal that allows the monomer product to be seen even at low residual levels in the polymer product. Offline measurements of this signal in EPS beads show good correlation with HPLC analysis, which is time-consuming, destructive and prone to sample handling and dilution errors. However, offline Raman measurement does not come without its own challenges which must be overcome to make this method suitable for industry. The low level of residual monomer in the polymer beads means that, towards the end of the reaction, the distinct C=C peak becomes difficult to discern. Shown here is the potential benefits of smoothing and derivatisation of the spectra to overcome this. Furthermore, small laser spot size of conventional Raman instruments can lead to sample degradation from the high laser power density or subsampling from the small sampling volume at infinite thickness. The investigation into WAI probes has demonstrated that increasing sampling volume provides the instrument with the capability to avoid this issue, suggesting that the use of immersion probes within a constantly agitated sample medium – thus increasing the sampling volume – could be beneficial.

3.9. Conclusions and Further Work

It has been demonstrated that the study of suspension polymerisation reactions could benefit greatly from further application of Raman methodologies. The detection and quantification of unreacted monomer held within the polymer product is of foremost importance, owing to ever tightening Health and Safety and Environmental regulation. Current methods for this such as HPLC are time-consuming, labour-intensive and as such do not allow for real-time analysis and process control, leading to costly run-times or batch rejection.

The potential for *in-situ* Raman analysis of such a complex, multi-phase and dynamic system such as suspension polymerisation is of increasing interest to the polymer industry. The ability for RS to determine the RM level of polymer product could potentially lend itself to predictive modelling, several methods of which have proven useful in the polymer industry¹²⁶ – although again there is a lack of available studies of suspension polymerisation. In theory, RS could be employed throughout a reaction and estimations of the RM level could be used to monitor the reaction trajectory. Studies in reaction trajectory reveal that key criteria can be monitored and used to estimate future values.¹²⁷ By relating Raman measurements to offline HPLC analyses and building a large quantity of historical data, a model could be built which could take *in-situ* RS data and predict when a threshold of RM content would be reached.

Finally, an investigation into the use of the WAI probe head with immersion capabilities could be of great benefit to industry, as demonstrated in this work. Offline results show WAI probes to have far greater sensitivity due to their significantly increased sampling depth and volume, allowing the determination of unreacted monomer levels lower than the target value by an order of magnitude.

The remaining challenge is to apply the successful Raman measurements *in-situ*. For this work to be of value to industry, there is a need for real-time information on the reaction progress to allow for process control and waste reduction. To provide this, online and offline reference measurements must be made throughout the reaction, providing a data profile for modelling reaction behaviour. This incurs many new challenges, including offline measurement and increased spectral complexity, which require novel approaches in data processing and model building.

4. In-Situ Polymerisation Monitoring via Raman Spectroscopy and Spectral Data Preprocessing Investigation

4.1. Introduction

Methods of determining the rate of monomer conversion throughout polymerisation reactions can be time-consuming, labour-intensive, destructive, and fail to provide information on the chemical composition in real-time. The advent of fibre-optic technologies has resulted in spectroscopic techniques becoming more frequently used, primarily due to their short sampling time and often minimally invasive implementation.

As discussed in Chapter 3, physical variations in the sample matrix can obscure the chemical information gained from spectroscopic analysis. Offline measurement of reaction products has shown the effect PSD has on the spectroscopic data in this study, and this effect is amplified when measurements are made in a dynamic reaction environment. The changing size and viscosity of particles produced, as well as the organic and inorganic reaction components contributing to the overall reaction spectrum, means that spectral pre-treatment is necessary to deconvolute the data and give maximum information. Furthermore, more robust offline measurements must be made to allow a complete profile of the reaction progress from beginning to end. Previous work has shown HPLC to be accurate and robust, but only applicable once solid particles are produced.

In this chapter, the effectiveness of various preprocessing methods at removing the contribution of physical variations from the sample spectrum was investigated. The correlation between *in-situ* Raman measurements and offline gravimetry to measure monomer conversion was established using PLS modelling, with the application of various spectral preprocessing techniques evaluated based on several key model criteria.

Furthermore, a study of two similar offline gravimetric analysis methods was performed. Offline gravimetric analysis of the reaction matrix is a routinely used method for determination of monomer conversion in academic studies and provides reliable confirmatory results to which novel methods can be compared.^{68, 128-131} In this study, samples were removed from the reaction matrix and analysed using two different methods, the variability and reliability of the results were then evaluated based on industrial expertise and a literature comparison. The application of HPLC as an offline measurement method of residual monomer content is also evaluated.

4.2. Instrumentation and Materials

Suspension polymerisation reactions were performed using the Radleys equipment described in Section 2.4.

PCA, PLS modelling and preprocessing methods were implemented using MATLAB software, Mathworks, Massachusetts, United States (version 2015b) with PLS_Toolbox, Mathworks, Massachusetts, United States (version 70).

4.3. Experimental

4.3.1. *Suspension Polymerisation Reactions*

A series of 10 suspension polymerisation reactions was carried out under different conditions as per Table 4.1. The parameters chosen were known to influence the reaction progress and PSD of the EPS products and they were altered each time to provide a wide dataset with which to build models. Each parameter was given at least three different levels to represent a low, medium and high level. Other stirrer speeds and component weights were attempted but resulted in reaction failure and so were not included in this investigation.

Table 4.1 - Reaction conditions of 10 suspension polymerisation reactions. All reactions performed in a 1 L Radley's reaction vessel.

Reaction (R)	Stirrer Speed (rpm)	DBPO (g)	TCP (g)
1	200	3	2.5
2	250		2
3			2.5
4			
5	300	3	1.5
6			
7		3.5	2.5
8			
9			3
10		4	

Each reaction was performed following the same general set-up sequence:

- The temperature of the reaction vessel was set to 80°C, the stirrer speed was set and 400 g of styrene (with dissolved DBPO) was added;
- Once this temperature was reached, approx. 8 g of EPS beads were added to 'seed' the reaction;
- Once seed beads had dissolved, 650 mL of water with the desired weight of TCP was introduced;
- The vessel was then sealed, and the system was left to reach temperature (80 ± 0.5°C);
- Once the initiation temperature was reached, the timer was started, and sampling begun;
- After 1 h 15 min, a 1.5 mL aliquot of 1% SDBS solution was introduced by pipette through an aperture in the vessel;
- The reaction was then left to run to completion (approx. 8 hours)

Throughout these reactions, Raman spectra were acquired using an IO probe (Section 4.3.2.) with simultaneous sample extraction for offline gravimetric analysis (Section 4.3.3.).

4.3.2. Reaction Monitoring via Raman Spectroscopy

A Kaiser MR probe head with an immersion attachment was inserted through an aperture in the vessel lid, which fixed the probe depth for the entire reaction. For cleaning, the aperture was loosened, allowing the probe to be returned to the same depth after each removal.

Spectra were acquired at a rate of 12 s exposure for 10 acquisitions (a total of 2 min) every 10 minutes.

4.3.3. Reaction Monitoring via Offline Gravimetry

As discussed previously, offline HPLC while accurate is time-consuming and labour-intensive. Furthermore, samples taken during a reaction before the formation of solid EPS beads are viscous and at high temperature, making them difficult to prepare and analyse without specialised, dedicated HPLC instrumentation. This presents a challenge in generating reliable and accurate offline data throughout a suspension polymerisation reaction; a key component in model building and establishing correlation with online, real time measurements.

Another technique that is often employed as a method of establishing monomer conversion throughout these reactions is offline gravimetry, which requires no specialised instrumentation and involves no complex sample preparation while still offering reliable and accurate results. There are different variations on the method used for this analysis, the two most common of which were investigated in this study.

Method A involved removing approximately 5 mL of reaction matrix immediately after acquiring Raman spectra and introducing it to 1 mL of 1% hydroquinone solution in an aluminium pan to quench the reaction. Both the pan and the volume of hydroquinone solution had been weighed beforehand. To ensure the reaction had stopped completely the pan containing the sample was then put into a freezer for approximately 2 minutes before being weighed once more. Once the cool weight was obtained, the sample was placed in an oven at 45°C for several days to evaporate any solvents.

The solid samples were taken from the oven and weighed once a day until an approximately constant weight was reached. Then, the theoretical weights of all known solid constituents – surfactant, stabiliser, hydroquinone and initiator – were subtracted, leaving the weight of polystyrene in the sample. This was then taken as a percentage of the theoretical weight of polystyrene at 100% conversion to give the estimated % conversion at each sample point.

Method B is a very similar process but with some key differences, as have been discussed in previous studies.⁶⁹ Primarily, the choice of reagents used to quench the reaction in the removed sample is different, and the sample is weighed immediately after removal and while still hot. The same volume of sample is removed but is immediately taken and weighed before adding 5 mL of 0.1% w/w para-benzoquinone (pBq) in toluene to quench the reaction. This is then placed in the oven and weighed once a day to establish conversion as per Method A.

The aqueous solution of hydroquinone in Method A incurs problems; the hydroquinone – while soluble in the organic phase – is also soluble in the aqueous phase, which constitutes a large part of the sample. Further still, diffusion of the inhibitor into the polymer particles becomes more difficult towards the intermediate stages of conversion as the particles become very viscous. The use of pBq allows

faster diffusion into the beads as it is more hydrophobic than hydroquinone; therefore, faster quenching of the reaction in the sample is possible and a more accurate estimation can be achieved.

While Method B is reportedly the better of the two, it involves the use of chemicals which require more care when handling in the lab. Furthermore, the weighing of a hot sample taken straight from the reaction vessel can cause variable and possibly erroneous results. Therefore, results from both methods were assessed to ascertain which was more suitable for this study.

In each case, the sample weight, W_{Sample} , was calculated by subtracting the weight of the aluminium pan the sample was collected in, W_{Pan} , from the weight of the hot sample taken directly from the vessel, W_{Hot} . The theoretical weight of all reaction components except polystyrene within the sample, $W_{Components}$, then had to be calculated by calculating each individual component's theoretical weight in the sample and summing the. An example calculation of the DBPO content of the sample is shown in Equation 4.1:

$$W_{DBPO,Sample} = W_{Sample} \times \left(\frac{W_{DBPO,Total}}{W_{Rxn}} \right)$$

Equation 4.1

Where:

- $W_{DBPO,Total}$ = the total weight of DBPO added to the reaction matrix;
- W_{Rxn} = the total weight of the reaction media

The weight of polystyrene in the sample at t , $W_{Poly,t}$, could then be inferred from subtracting $W_{Components}$ from the total weight of all solids, W_{Solids} , collected in the pan once a consistent dry weight was reached. Finally, the theoretical weight of polystyrene in the sample at 100% conversion, $W_{Poly,100\%}$, was calculated simply by

dividing the total weight of styrene in the matrix by W_{Rxn} to give a weight of styrene per gram of reaction media. This could then be used to estimate the level of conversion at t using Equation 4.2:

$$\text{Conversion}_t (\%) = \frac{W_{\text{Poly},t} \times 100}{W_{\text{Sample}} \times W_{\text{Poly},100\%}}$$

Equation 4.2.

An example of this calculation from one reaction performed can be seen in Figure 4.1, where the conversion after 15 minutes is calculated. Shown here is the result of taking an 8.54 g sample from the reactor at $t = 15$ minutes, resulting in an estimated conversion of 6.3%, given a total styrene content of 413.5 g. This procedure was performed at periodically throughout the reaction to build up a reaction conversion profile over time for each reaction in the study.

<i>t</i>	Time (h)	weight (g)										Conversion _t %	
		<i>W_{Pan}</i>	<i>W_{Hot}</i>	<i>W_{Dry}</i>	<i>W_{Sample}</i>	<i>W_{Solids}</i>	<i>W_{Components}</i>	<i>W_{Poly,t}</i>					
1	0.25	3.3759	8.5492	3.5742	5.1733	0.1983	0.0703	0.1280				6.321	
	water	650	mL										
	styrene	456.4018	mL										
	styrene	413.5	g		total solids (non polymer)				5.599073	g			
	TCP	2.5104	g		total solids per g (non polymer)				0.005198	g			
	DBPO	3.0611	g		Total weight				421.5776	g			
	PS beads	8.0776	g		Polystyrene (100% conversion)				0.391373	g			
	Toluene (g)	149.2	g		Polystyrene (100% conversion per g)								
	Toluene Volume (mL)	172.4855	mL										
	p-Benzoquinone in toluene(g)	1.4984	g		Styrene								
	Toluene Volume per Sample (mL)	5	mL		TCP								
	total before SDBS	1077.149	g		DBPO								
	Water from SDBS	0.972427	g		p-Benzoquinone								
	SDBS (g/100mL)	2.7573	g		SDBS								
	SDBS (mL)	1	mL		Toluene								
	SDBS (g)	0.027573	g										
	total after SDBS	1077.177	g										

Figure 4.1. – Weights and volumes of reaction components and sample components of the sample taken at *t* = 15 minutes. Values were used to calculate the % conversion at this timepoint.

4.3.4. Multivariate Analysis –PCA and PLS Modelling

The results from the offline and *in-situ* methods were then used to build PLS models to establish the potential for Raman measurements to determine monomer conversion. To do this, datasets had to be selected to be used to calibrate the model, while leaving other datasets out for model validation.

To highlight which datasets could be used as validation data, PCA was performed and the results of the first 3 principal components were plotted. This highlighted which reaction data fell in the same general trend as the others and which data deviated. The reaction datasets that deviated most from the trend would serve as the validation data for a model calibrated using the rest of the data, resulting in a model covering the widest possible variance in the data.

Once the appropriate validation and calibration datasets were determined, the calibration data was then combined and used to build a PLS model, which was then applied to the validation data to assess the model's predictive ability. PLS regression allowed the correlation between spectral data and conversion established by gravimetry to be quantified.

The key aim of this chapter is to assess the effect of a variety of data pre-treatment methods – from widely used industry standards to modern novel techniques – on these PLS models and their ability to accurately predict the degree of monomer conversion from *in-situ* Raman spectra.

PCA was performed by first stacking all data taken during each reaction on top of one another, using each reaction as a separate class (Figure 4.1). The data was then preprocessed using mean centring (MC) – from here on referred to as 'no preprocessing' as MC is the last step in every model built in this work – or MSC followed by MC before performing PCA with PLS_Toolbox.

Data used in PLS analysis was treated in a similar fashion, stacking reaction data one on top of the other before preprocessing and analysis (Figure 4.2); however, only spectra that were taken simultaneously with gravimetric sampling were used, resulting in approximately half the number of spectra used for PLS as were taken throughout each reaction. PLS modelling was used to evaluate the correlation between the spectral data and conversion estimates and the predictive ability of each model was then evaluated by using eight sets of reaction data for calibration and the remaining two for validation. To further ensure the model was sufficiently robust, contiguous block cross validation was used, keeping number of blocks equal to the number of reactions used in the calibration dataset. The performance of the model was evaluated based on the correlation coefficient, R^2 , the number of latent variables (LVs) required to build the model and the error of prediction (RMSEP).

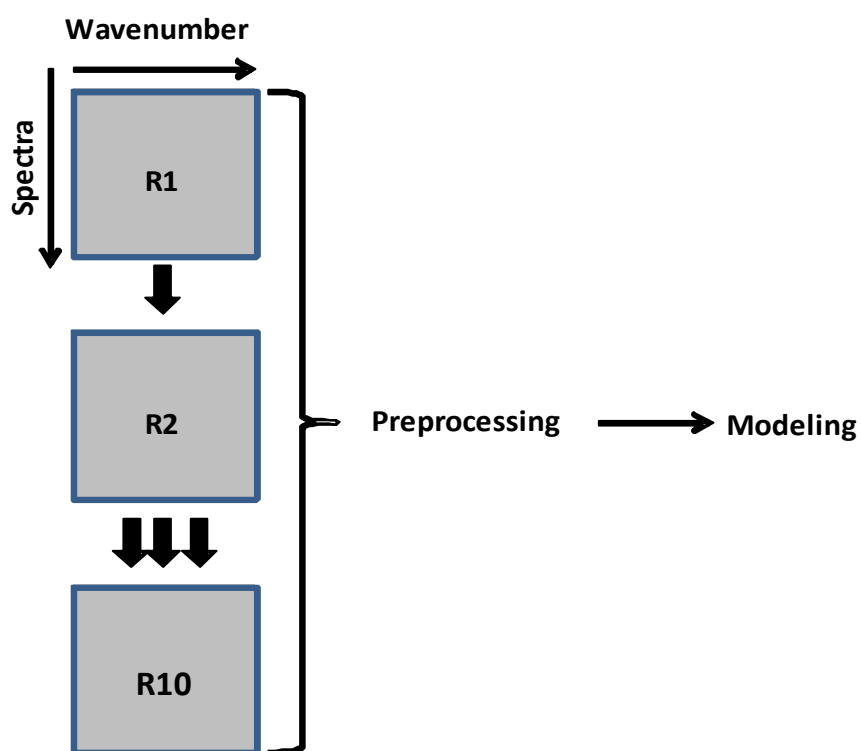


Figure 4.2 – Schematic of data processing method used to perform PCA on spectral data.

Of the various pre-processing methods applied to the data in PLS modelling, OPLEC and OPLECm were the most novel and interesting for this application as they were developed to correct spectral data in the presence of multiple scatterers. In order to ensure the maximum benefit was gained from using this method of spectral pre-treatment, some parameter optimisation work was required.

4.3.5. OPLEC Parameter Optimisation

The application of optimal path-length estimation and correction (OPLEC) involves the definition of the parameter **J** – the number of spectroscopically active components in the sample matrix which contribute to the overall sample spectrum.¹³² The reaction matrix of a suspension polymerisation contains several constituents with varying levels of influence on the overall sample spectrum and so it was important to establish an optimum value of **J**, resulting in the best model. Furthermore, the dual calibration strategy adopted by OPLEC to give predictions corrected after the removal of multiplicative effects involves the building of two separate PLS models, each with the same number of LVs. To ensure that the most robust model is built from the OPLEC pre-processed data, the effect of changing this number of LV used in both PLS models in the dual calibration was also investigated and an optimum value identified.

This was done by setting the value of **J** to 1 and performing the dual calibration using only 1 LV in each of the PLS models, before calculating the resulting corrected predictions. Subsequently, the value of **J** was kept constant whilst performing several iterations of the dual calibration, each time increasing the number of LVs used in each model by one until a value of 15 had been tested. This process was performed five times, increasing the value of **J** by one each time. Overall, a total of five **J**-values were evaluated, each used to construct fifteen models containing increasing numbers of LVs. These models were then evaluated based on R^2 and RMSEP by plotting these criteria in 3-dimensions as the number of LVs and value of **J** was changed.

Modified OPLEC (OPLECm) proposes a more robust and less laborious method of optimising the J value by the inclusion of a quadratic programming function, which enables the value of J to be inferred.¹³³ Both the modified and classical approaches to OPLEC optimisation were investigated and compared in this work.

4.4. Results and Discussion

4.4.1. Reaction Monitoring via Raman Spectroscopy

Progression from monomer to polymer can be followed by observing the Raman spectra collected over time, most notably when observing the decreasing intensity of the Raman scattering in the region between 1550 and 1650 cm^{-1} – the region corresponding to a C=C double bond – and the region immediately below 3000 cm^{-1} , where the formation of C-H bonds can be seen to cause Raman peaks to increase in intensity (Figure 4.3).

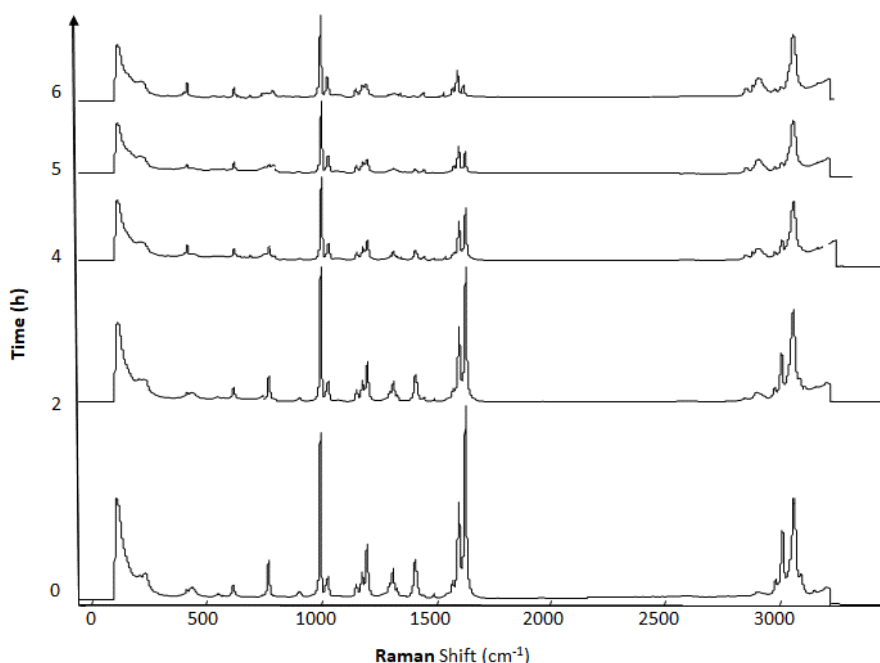


Figure 4.3 – Changing Raman spectrum as a reaction progresses from 0 – 6 hours. Spectra were collected using an IO probe head submerged in reaction media in a 1 L Radley’s reaction vessel. Each spectrum shown is an average of 10 acquisitions, 20 s per acquisition.

Figure 4.3 shows the changing Raman intensities of several peaks in the spectrum, most notably the band corresponding to the C=C stretch (See Table 4.2 for further Raman band assignments).

Table 4.2 - Raman band assignments for the suspension polymerisation reaction matrix.¹¹⁵

Peak Frequency (cm ⁻¹)	Assignment
594	Olefinic CH wag
771	Mono-substituted benzene CH wag
902, 987	Vinyl CH wag
1018, 1080, 1203, 1280	2, 4, 6 radial carbon in-phase aromatic stretch
1411	Unassigned
1450, 1496	Aromatic ring semi-circle stretch
1573, 1604	Aromatic ring quadrant stretch
1627	Olefinic C=C stretches
2900	Aliphatic CH vibrations
3050	Aromatic CH vibrations

The sharp, distinct bands generated in Raman spectroscopy allow reaction progression to be followed readily – particularly polymerisations reactions, as they often involve the breaking of Raman-active C=C double-bonds. By plotting the

changing height of the peak arising from this C=C interaction (Figure 4.4) the reaction trajectory can be followed.

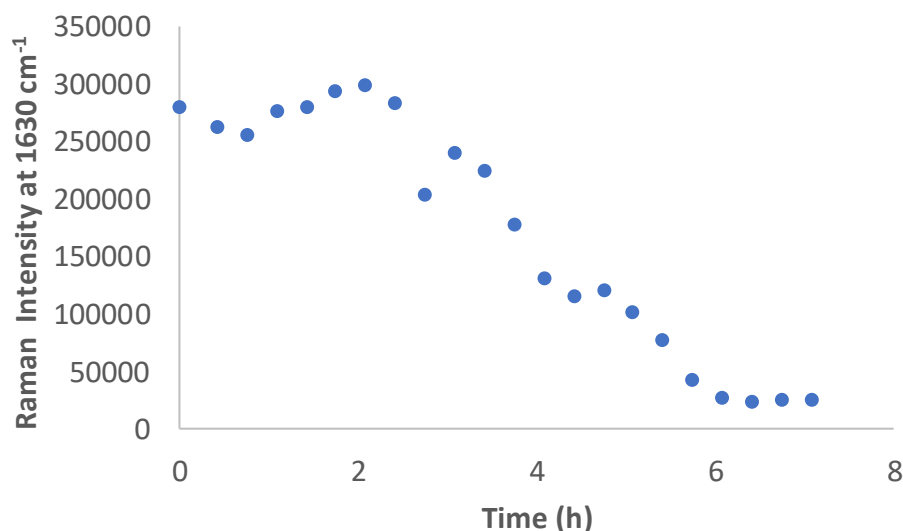


Figure 4.4 - Changing peak height at 1630 cm⁻¹ ('styrene peak') as a reaction progresses. Measurements were taken using an IO probe head over 7 hours at 15 minute intervals. Each measurement was an average of 10 acquisitions, 15 s per acquisition.

Though this method was successful in monitoring the reaction progress, the issue of probe fouling had to be overcome. Throughout the reaction, the probe was removed immediately after spectral acquisition and wiped clean with high quality tissue and acetone. It was then thoroughly dried before being placed back in the reaction vessel.

This univariate approach has been used to study polymerisation reactions on numerous occasions¹³⁴⁻¹³⁶ and it illustrates the suitability of Raman spectroscopy for the purposes of this study. This also highlights the inherent variability in taking a univariate approach in how the peak intensity reaches a maximum 2 hours into the reaction. As the reaction progresses, the number of C=C bonds decreases

continuously, meaning that the intensity of the associated Raman band should also decrease continuously. The intensity maximum seen around 2 hours into the reaction is likely caused by the addition of SDBS into the reaction matrix, which would cause a change in the PSD of the droplets formed, which would affect the Raman scattering properties of the sample. This can be mitigated by taking a multivariate approach.

Model building using multivariate analysis requires robust and reliable offline analysis to use as a bank of 'known' results to correlate to complex multivariate data. As previously shown, HPLC serves as an accurate and reliable offline analytical technique but is time-consuming and limited to samples taken from the final stages of the reaction when solid EPS beads are formed. The establishment of a suitable offline reference analytical technique is key to building multivariate models for predicting and controlling reaction progress.

4.4.2. Reaction Monitoring via HPLC

So far, only simple model systems have been analysed to establish the appropriate analytical methods for monitoring RM levels during suspension polymerisation reactions. Experiments with EPS bead products have shown RS to be a suitable candidate for online non-destructive monitoring of RM content – it shows good correlation with offline industry standard HPLC, and the employment of WAI probes has demonstrated the advantages of increased sampling volume on Raman data.

Samples were then taken directly from a suspension polymerisation reaction, analysed offline and compared to *in-situ* Raman measurements to provide a more realistic evaluation of the suitability of RS.

Figure 4.5 shows the changing styrene (C=C) peak intensity as a suspension reaction progresses. For clarity, this data has been treated with extended multiplicative

scatter correction (EMSC) – a common technique for eliminating variation in spectral data caused by physical variation in the sample (shown in Figure 4.4), as discussed later in this chapter.^{137, 138}

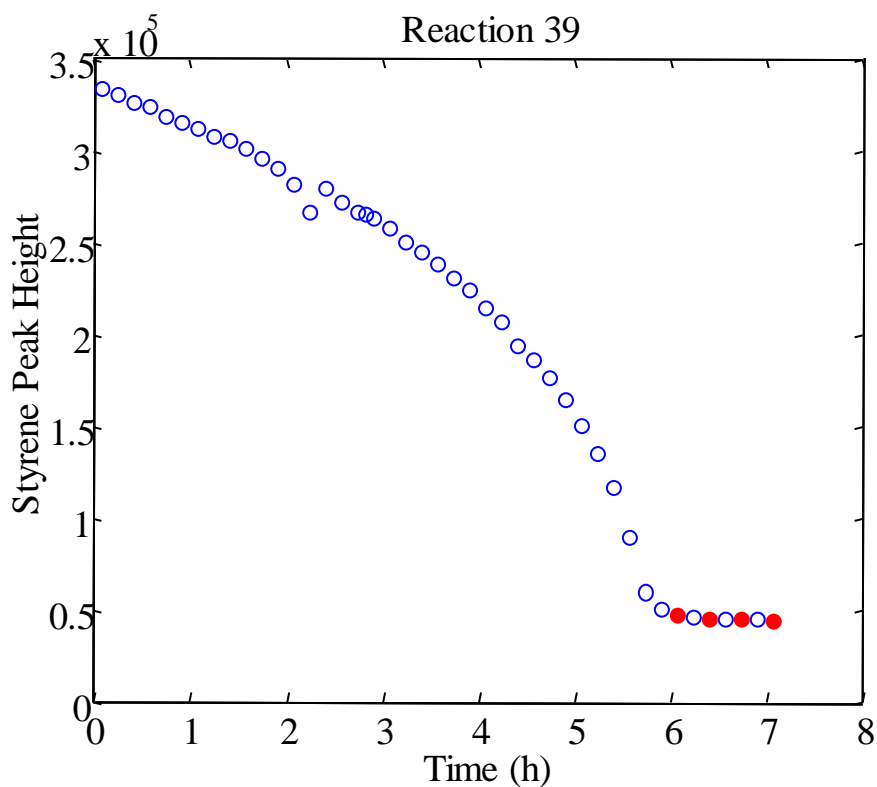


Figure 4.5 – EMSC treated Raman intensity of C=C peak height as the reaction progresses (blue points) using an IO probe head. Each spectrum was an average of 10 acquisitions, at 15 s exposure per acquisition. Red points indicate samples taken for HPLC analysis.

The peak intensities of several Raman scans taken towards the end of the reaction (red) were compared to the RM content of the same samples taken at the same time and analysed via HPLC (Figure 4.6):

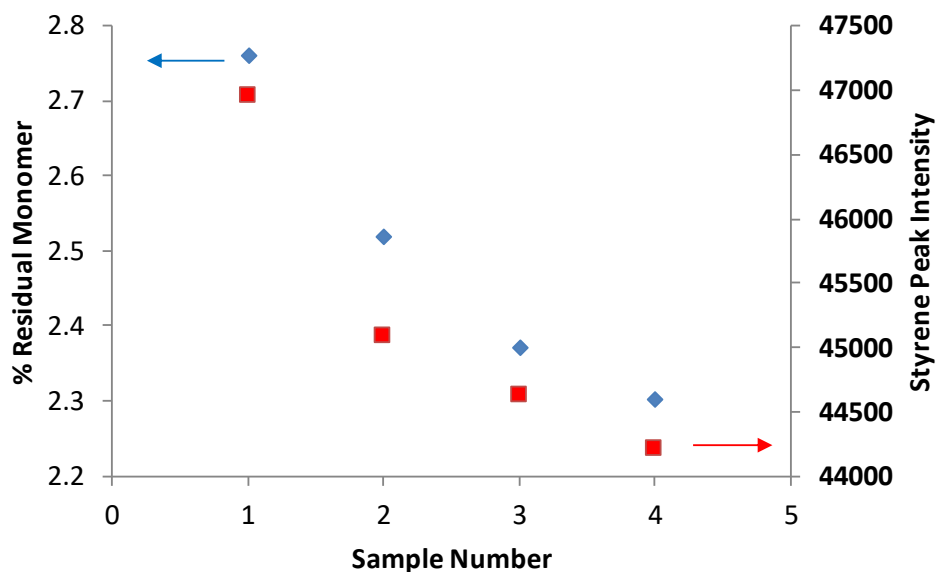


Figure 4.6 – Raman intensity of the C=C peak (red) vs. HPLC residual monomer content (blue) of samples taken towards the end of a suspension polymerisation reaction.

The correlation between the intensity of the Raman signal and the actual measured residual styrene concentration can be seen, highlighting the potential for RS in directly measuring this parameter during a reaction with an IO probe. The advantage of Raman over offline HPLC analysis in the study of polymers has been long known and implemented in a wide range of applications.¹³⁹⁻¹⁴¹ However, its application in the study of suspension polymerisation is – to the best of the author’s knowledge – largely unreported. In this case, the variability in HPLC measurements is around 3 times that of the offline Raman measurements (RSD = 8.2% and 2.7% respectively).

This was performed for two other reactions, and the high variability of the HPLC method compared to RS is highlighted along with the previously discussed results in Table 4.3:

Table 4.3 - %RSD from four samples taken in the final hour of three reactions and analysed via HPLC and *in-situ* Raman.

Reaction	%RSD HPLC	%RSD Raman
1	9.7	5.3
2	23.9	3.3
3	8.2	2.7

By adopting a multivariate approach to data handling, complex reactions like this can be deeper understood, building on the promising results from this univariate assessment.

This study shows that, despite the applicability of HPLC as an offline data source for monitoring reaction progression and the correlation to *in-situ* Raman measurements, the variability of HPLC measurements can be too high to consider this a reliable offline method for model building. Furthermore, the complexity of sample preparation at earlier stages in the reaction – when EPS beads are not fully formed and viscous – make this method unsuitable for collecting data throughout the entire reaction.

Another method must be assessed in order to find a suitable method for generating reliable reference data for model building. Offline gravimetric analysis is a common technique for this purpose, and various methods of this analysis were compared to establish the best method for achieving the goals of the project.

4.4.3. Reaction Monitoring via Gravimetric Analysis

It is generally accepted in industry that polymer bead formation occurs once the monomer is above 70% conversion, when there is sufficient polymer present to stop beads from sticking together.¹⁴² Repeat reactions using gravimetric Method A, however, show consistently lower maximum conversion estimates than this value despite the presence of solid polymer beads, suggesting that either the method of calculation contains errors, or the gravimetric method is unsuitable for this reaction. Given that no errors could be found in the calculation of conversion, it was clear that Method A was unsuitable for this study and simultaneous use of both methods should yield better and more reliable results with Method B. Figure 4.7 shows the difference in results obtained with each gravimetric method.

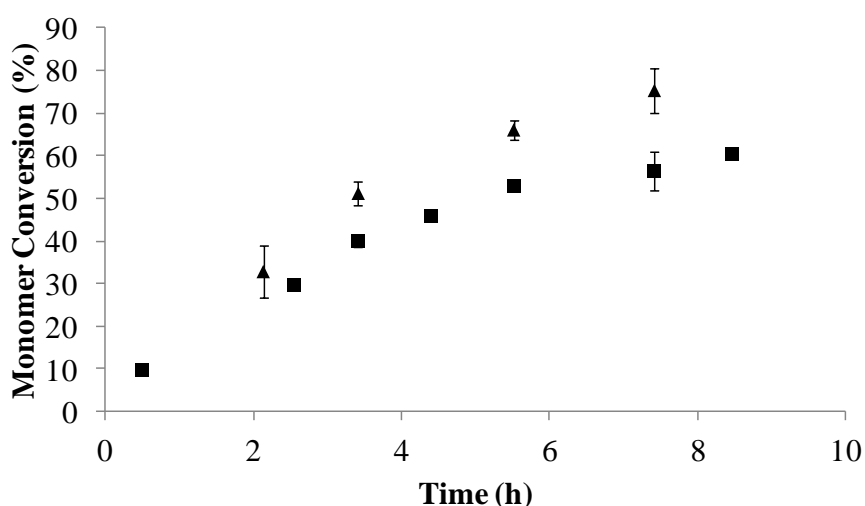


Figure 4.7 - Conversion estimates made by gravimetric analysis using Method A (squares) and Method B (triangles). Error bars represent the standard deviation of 3 replicate measurements.

Results produced by Method B are in closer agreement with those expected given the advice of industrial experts in the project, which is that reactions producing solid polymer beads should achieve >70% monomer conversion, whereas Method A results peak at around 60%. Whilst results from Method B are more subject to

variability throughout a reaction, both methods display similar levels of variability towards the end (4.6% and 5.2% RSD for Methods A and B respectively), where conversion estimates are most important. Therefore, Method B was used throughout all subsequent reactions – including all reactions used for PLS modelling.

Figure 4.8 shows the gravimetric conversion estimates for all 10 reactions using method B; each reaction displays a steady increase in monomer conversion until an endpoint is reached and the data begin to plateau when the polymerisation process ends.

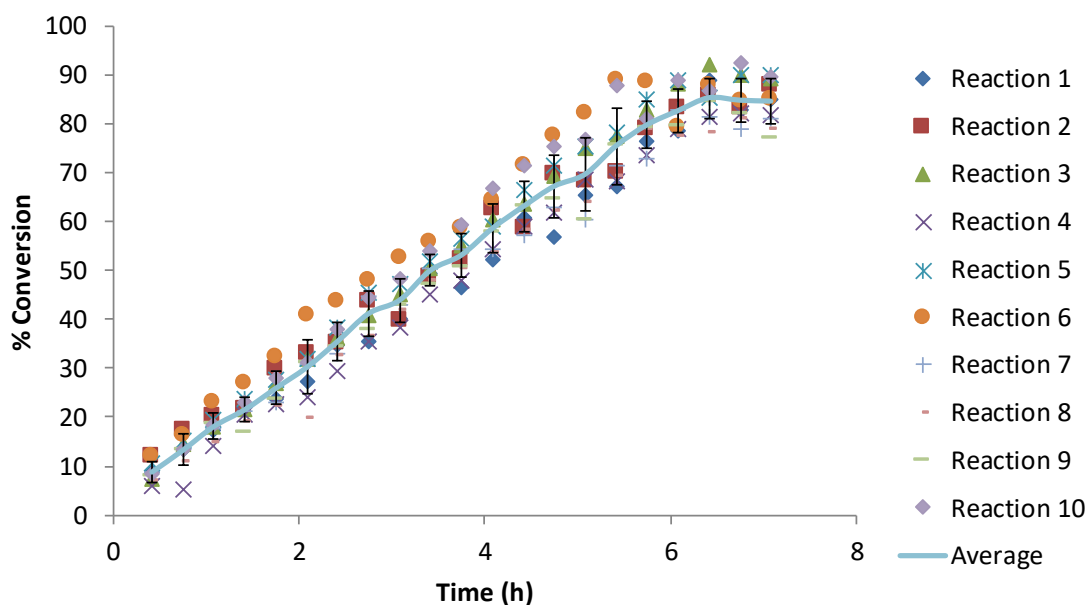


Figure 4.8 - Gravimetric analysis results from 10 different suspension polymerisation reactions and their standard deviation from the average conversion estimate at each timepoint using gravimetric method B.

This work highlights the ability of gravimetric analysis to produce data throughout the polymerisation. As each reaction progresses, the estimated conversion level increases until approximately 6 hours. At this point, which coincides with the point at which viscous polymer beads become solid, the gravimetric estimate of

conversion reaches a plateau. At this point, the residual monomer levels are potentially so low that the conversion increase in the last hour of the reaction cannot be detected by this simple offline method. Alternatively, the reaction may be finished at this time and no more conversion of monomer is possible.

Following the successful generation of reaction progress data by offline gravimetry, it was important to establish the correlation between the data and online Raman measurements to meet the project goals of monitoring the reaction in real time. Raman spectroscopy has already been shown to have the capability of measuring residual styrene in EPS bead reaction products to a desirable level offline, it now must be ascertained if it can perform in real time during a reaction.

4.4.4. Multivariate Analysis – PCA and PLS Modelling

Before building PLS models from the Raman and gravimetric data obtained, the appropriate data for use in calibration and validation datasets had to be established. Performing PCA allowed the determination of reaction trends and trajectories, and highlights reactions which progressed differently to the others.

Figure 4.9 illustrates that the reaction progression can be followed to its endpoint after approximately 6 hours. The otherwise smooth trajectory can be seen to undergo some disruption just after 1 hour had passed; this is due to a sudden change in the PSD caused by the addition of surfactant at 1 hour and 15 minutes.¹⁴³ After a further 2 hours, the variability in PSD appears to have subsided to allow the reaction to progress smoothly.

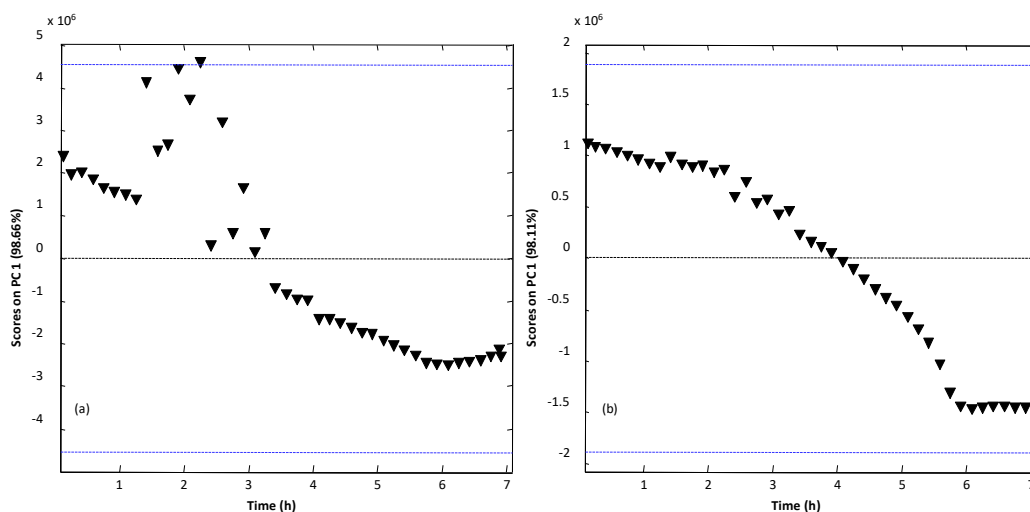


Figure 4.9 - Principal component 1 scores as a suspension polymerisation reaction progresses with (a) no preprocessing and (b) MSC preprocessing.

Applying a preprocessing technique such as MSC all but eliminates the variability caused by the changing PSD, as can be seen in Figure 4.9b. This deconvolutes the scores plot, allowing more reactions to be analysed at once more clearly. Figure 4.10 shows the results of performing PCA on all 10 sets of reaction data with MSC preprocessing, illustrating how an endpoint can clearly be seen for each reaction and the effect the reaction conditions can have on reaction progression. Scores plots of the reactions that used the highest amount of initiator – R4 and R10 – are represented by the two plots which show clear endpoints before all others (approximately 5.5 hours). Despite their differences in stirrer speed and stabiliser content, these reactions behave almost identically, implying that the amount of initiator present is the most influential factor in this experimental set-up. The initiator concentration has a direct influence on the initial polymerisation rate in suspension polymerisation reaction¹⁴² and has been shown to increase the overall reaction rate as well as PSD.¹⁴⁴

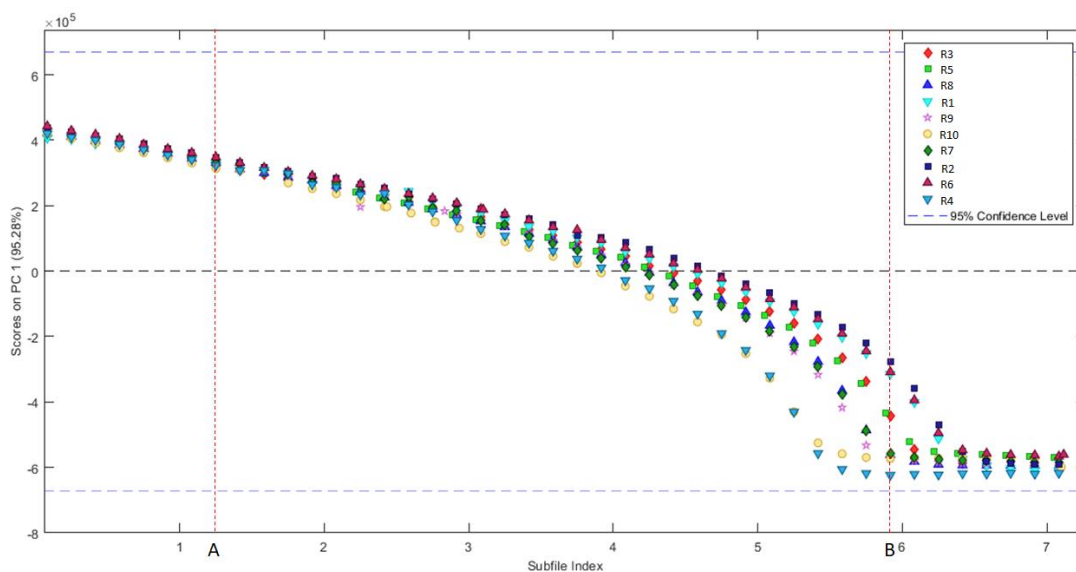


Figure 4.10 - Principal component 1 scores for all 10 suspension polymerisation reactions with MSC preprocessing. Points A and B indicate the point of surfactant addition and the average endpoint, respectively.

Evaluation of the loadings plot for a reaction (Figure 4.11) reveals that principal component 1 (PC1) contains most of the variance in the data (95.28%) and is most highly correlated with the C=C peak at 1630 cm^{-1} and anti-correlated with the peaks in the region just below 3000 cm^{-1} . This confirms that the consumption of monomer and formation of polymer are the two main sources of variation within the data. Therefore, the production of polymer ceases at the point where the scores plots in Figure 4.10 plateau, indicating that the reaction is complete, and all monomer units have either been converted to polymer or have become trapped inside polymer beads and are unable to react further.

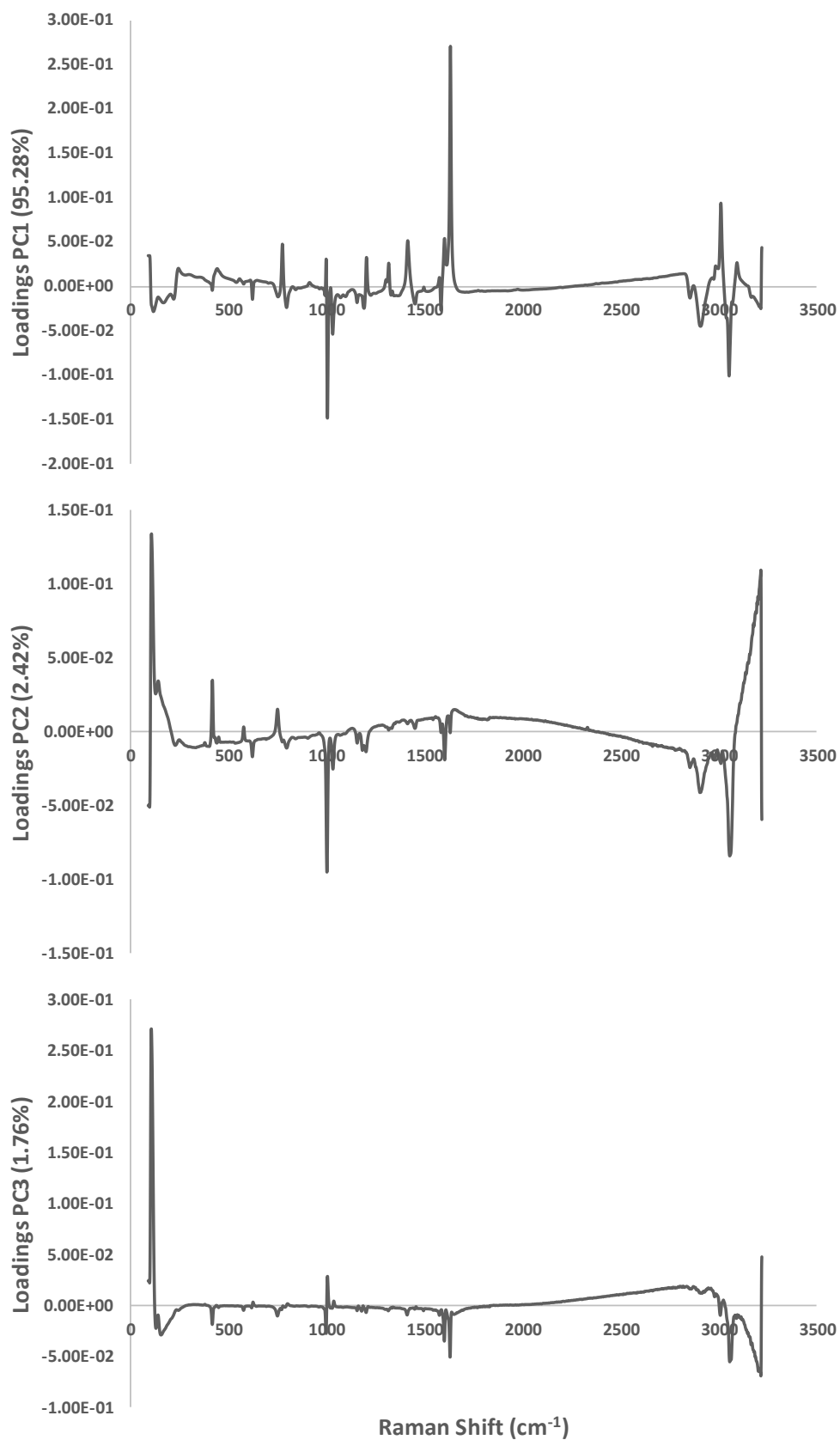


Figure 4.11 - Loadings plots for the first 3 PCs from PCA of all 10 sets of reaction data.

By examining the scores plots for the first three PCs in three dimensions (Figure 4.12), the identification of suitable validation batches can be made for building PLS models.

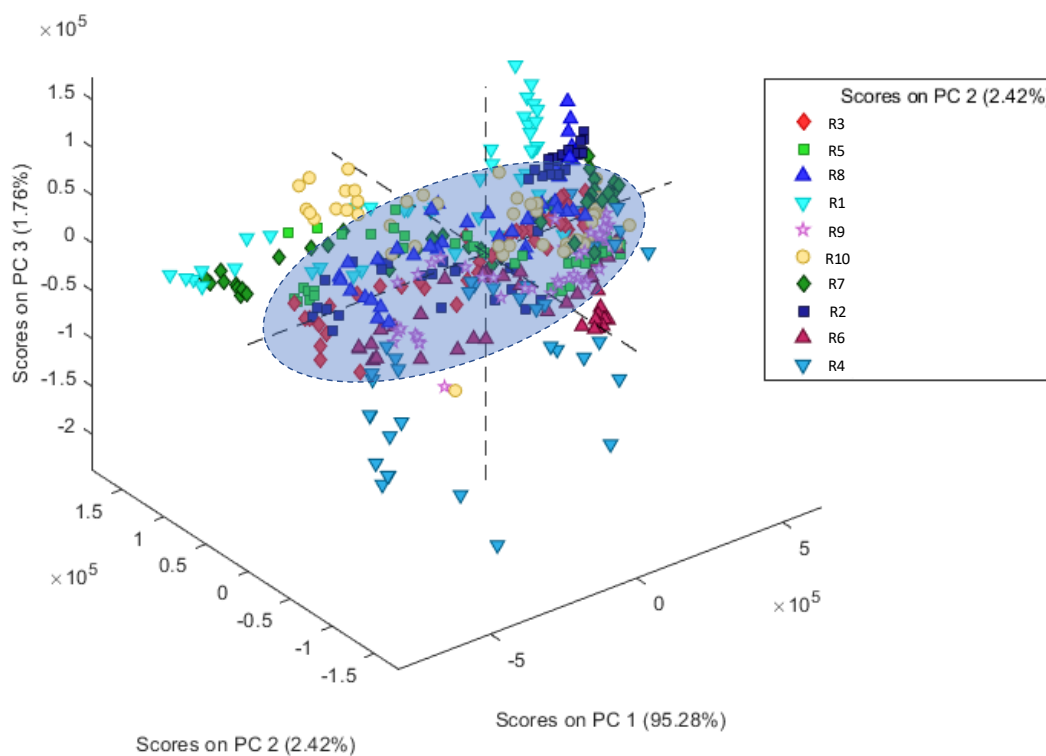


Figure 4.12 - Scores for the first three PCs for all 10 reactions. Blue shaded area indicates the experimental plane in which most of the data lies.

Most of the scores plots follow a similar trajectory, providing many options for suitably 'typical' reaction datasets for model validation, sets which lie in the shaded region of figure. Other datasets lie outside this typical region, showing deviation from the average reaction performance. To include as much variability in the data as possible, and to avoid overfitting, reactions 1 and 10 were chosen for model validation. This allowed for model validation using typical (R1) and atypical (R10) data.

Raman and gravimetric data for reactions 2 – 9 were therefore used as calibration data to create a PLS model, which was then validated using data from reactions 1 and 10. The results of these models are shown in Figure 4.13, which illustrates the effect of the different preprocessing methods as they were applied to the Raman data.

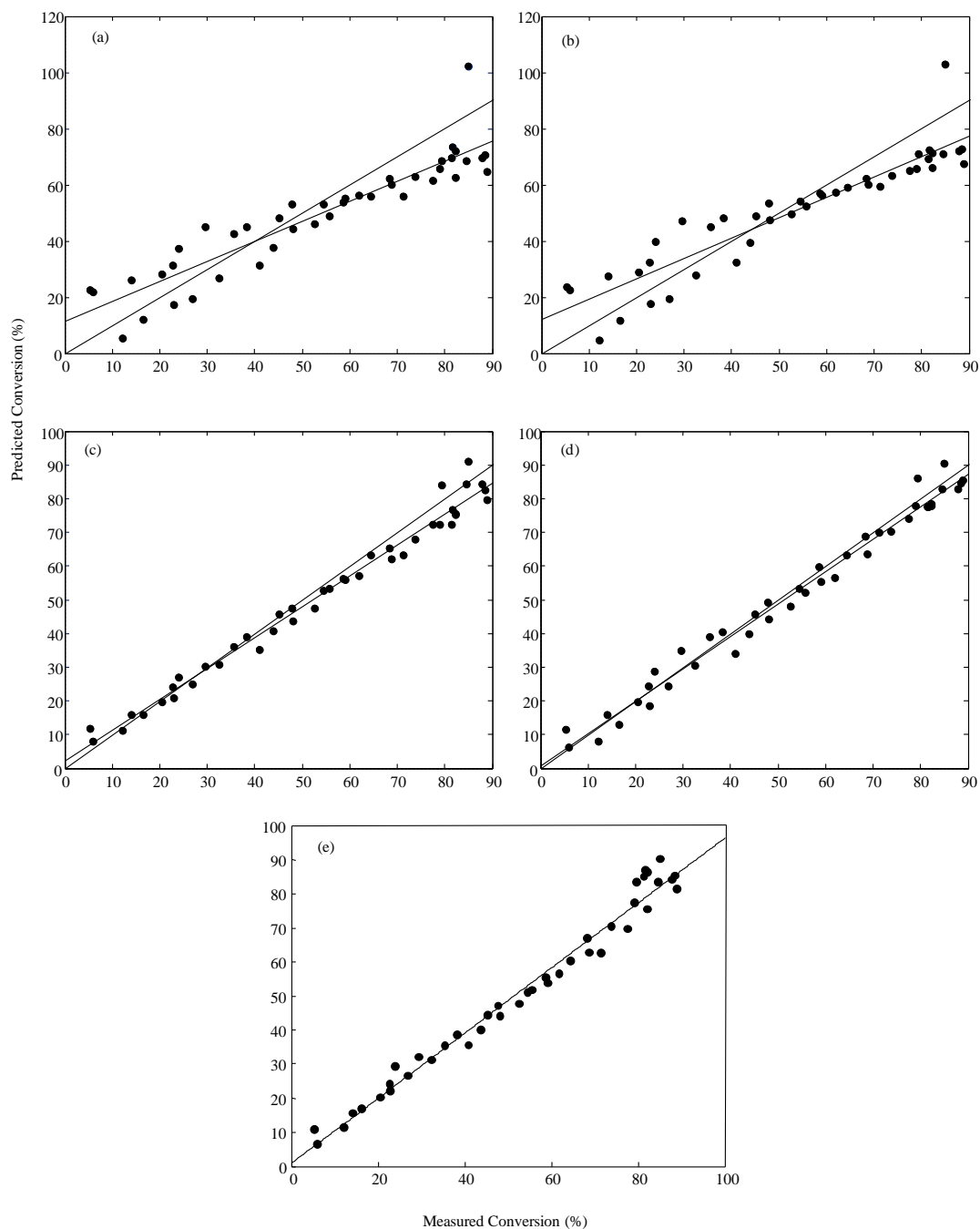


Figure 4.13 – PLS validation plots showing the conversion measured via Gravimetry vs. the conversion estimated from validation Raman treated with (a) no preprocessing; (b) SGFD; (c) SNV; (d) EMSC and (e) OPLEC.

Figure 4.13 illustrates the difference in predictive power between four PLS models and the improvements made when applying spectral pre-processing techniques – except SGFD, which makes little-to-no difference to the model’s abilities. The

difference in performance of these models can be quantitatively evaluated by inspecting the number of LVs, RMSEP and R^2 , shown in Table 4.4.

Table 4.4 – Predictive performance and number of latent variables used in PLS models built using different preprocessing methods. Predictive performance based on a concentration range of 6 – 85% conversion.

Preprocessing Method	LVs	R^2	RMSEP (%)
None	3	0.84	11.3
SGFD	3	0.84	11.4
SNV	6	0.98	4.1
EMSC	4	0.98	3.8
OPLEC	3	0.98	4.1

Each of the data pre-treatment techniques showed varying effect on the model's %RMSEP with SNV and OPLEC_m providing similarly improved results. Whilst the difference made to the model by SGFD pre-processing is negligible, models built using SNV, EMSC and OPLEC pre-processed data all have a correlation coefficient of 0.98 (c.f. 0.84 following SGFD or no pre-processing at all).

Applying SNV improves its predictive ability, achieving an RMSEP of 4.1%; however, this model required a far higher number of LVs and is therefore insufficiently robust. Upon applying EMSC and OPLEC, the predictive ability remains improved, giving similar RMSEP values of <5% while simultaneously achieving low numbers of required LVs. From this, advanced spectral pre-processing algorithms are shown to vastly improve PLS models, with OPLEC pre-processing and EMSC pre-processing

producing the best models with comparable predictive performance. The model resulting from OPLEC pre-processed data is more favourable as it requires fewer LVs than that built from EMSC pre-processed data, according to the parsimony principal outlined by Seasholtz and Kowalski¹⁴⁵ in order to ensure the model is robust with as few LVs as possible.¹⁴⁶ Furthermore, EMSC requires the spectra of all raw sample components, which is not always a viable option.¹⁴⁷ Of all methods investigated OPLEC provides the best predictions overall, consistent with similar studies published.¹⁴⁸

4.4.4. OPLEC Optimisation

The sensitivity of the OPLEC method with respect to the J value and the number of LVs used to build the model is highlighted in Figure 4.14:

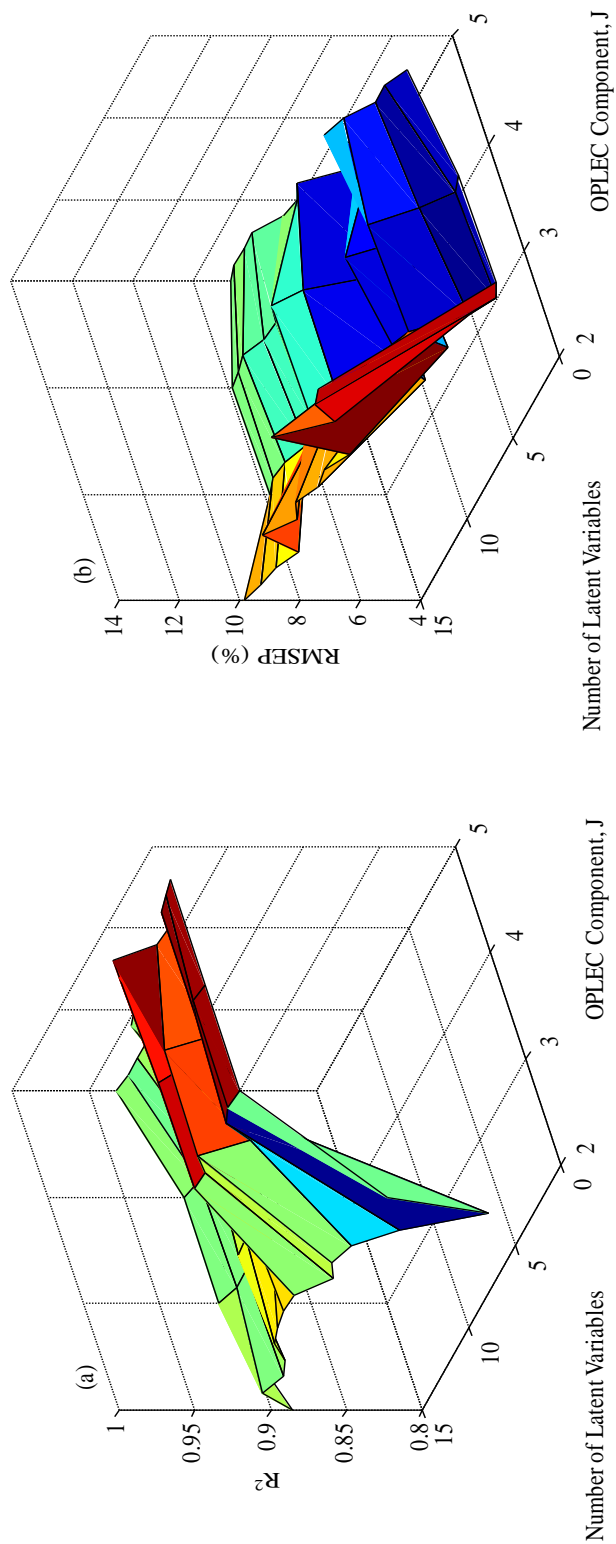


Figure 4.14 – (a) The correlation coefficient (R^2) and (b) RMSEP for predictive models built using different values of OPLEC Component, J, and different numbers of LVs used in the dual calibration step of OPLEC. High values (red) for R^2 and low values (blue) for RMSEP indicate optimum settings.

Figure 4.14a illustrates the sensitivity of the R^2 value in the models. Optimal performance – shown in the red area – is achieved with a J value of 3 and when 3 LVs are used. These same parameters produced the lowest RMSEP (Figure 4.14b, highlighted in red); therefore, these parameters were used when applying the OPLEC pre-processing method to data used for PLS modelling (Figure 4.13).

As discussed in the original literature, OPLECm provides a more convenient way of optimising these parameters. A simple plot of the number of columns in U_s , r , against $\min_p f(p)$ provides an estimated value of J in good agreement with the previous, more intensive method (Figure 4.15).

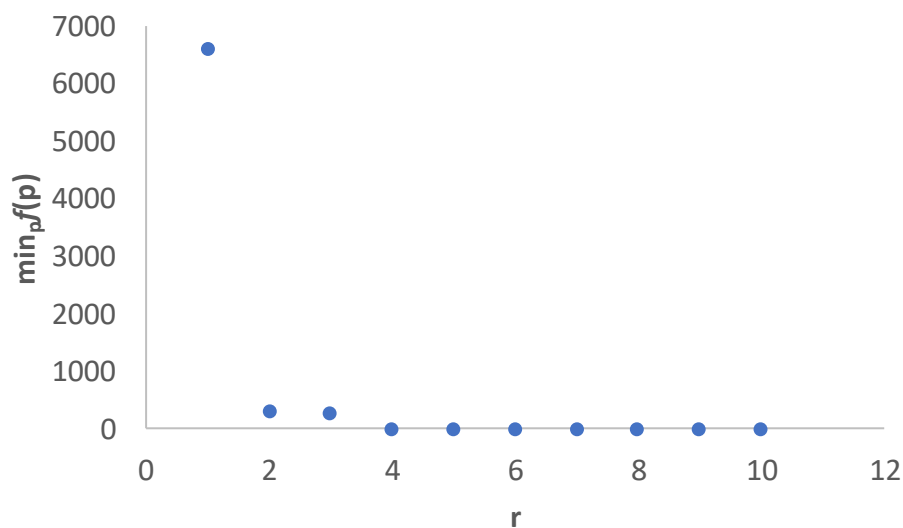


Figure 4.15 – Plot of r vs. $\min_p f(p)$ obtained from OPLECm.

Using this method, the minimum value of $\min_p f(p)$ is estimated at 4, in close agreement with the stepwise, more methodical approach discussed earlier. This highlights the improvements made to the OPLEC method and illustrates its potential as a preprocessing method for real-time process monitoring and provides a reliable way of optimising the model without expert knowledge or exhaustive reiteration required. Implementation of OPLEC(m) for the quantitative analysis of

heterogeneous systems has increased in recent years, with improvements to complex datasets from surface-enhanced Raman spectroscopy studies,¹⁴⁹ fluorescence¹⁵⁰ and liquid chromatography-mass spectrometry being shown.^{151, 152} However, the most complex system from which RS data has been deconvoluted using OPLECm involved relatively simplified model mixtures of turbid media;¹⁵³ other examples include powder mixtures¹⁵⁴ and crystallisation reactions,¹⁵⁵ which – whilst not trivial – are far simpler sample matrices than the suspension polymerisation reaction studied here.

This study has highlighted the importance of effective spectral pre-treatment when building PLS models for prediction of monomer conversion throughout suspension polymerisation. A series of reactions was to be carried out in the lab with simultaneous *in-situ* Raman analysis for the estimation of monomer conversion. To generate reliable models to achieve this, suitable offline methods of estimating monomer conversion had to be evaluated. As HPLC had been proven able to monitor the residual monomer level of EPS beads earlier in this work, it was assessed as a suitable offline method for this study. However, it was shown that this method was highly variable and only able to provide data at the end of the reaction. As an alternative, two variations of offline gravimetry were assessed and both were able to provide conversion profiles throughout the entire reaction. The method that provided data which aligned most with industrial data was chosen and the reactions were carried out under various controlled conditions.

Prior to model building, a series of spectral pre-treatment methods were applied to establish what, if any, benefits they provided. It was found that simple techniques like SGFD gave negligible improvement to the models, while more advanced and well-known methods (SNV and EMSC) improved the robustness with EMSC providing the best results. This technique, however, required knowledge of reaction component spectra beforehand to avoid using estimations that can decrease the reliability of the results. As a novel alternative, OPLEC and OPLECm were applied to

the data – the most complex dataset to which this technique has been applied to the best of the author’s knowledge. The improvements seen with this technique were comparable to EMSC.

4.5. Conclusions and Further Work

Once a suitable offline method for conversion estimation was established, datasets were then built using *in-situ* spectroscopy to collect data throughout the reactions. Using a series of MVA techniques to explore the data, correlations between the *in-situ* and offline measurements could be drawn and quantified using mathematical modelling methods. These models were markedly improved by the implementation of data pre-treatment techniques. The most novel of these preprocessing techniques (OPLEC and OPLECm) was then optimised in two different ways – one thorough and detailed method which established definitively optimal model parameters, and a more straightforward method which was simple to implement as it is part of the inherent mathematics of the modified OPLEC and showed good agreement with the first. These techniques are mostly well-established, but this study is one of the most complex examples of the implementation of OPLECm the author can find.

Advances in processing power and software currently in development will increase the applicability of more complex methodologies such as OPLECm, allowing their optimisation and implementation of the method in real-time. Utilisation of these developments as well as further investigation of a wider array of complex methodologies and their impact on models built from suspension polymerisation data would be beneficial to industry. These advancements would allow the study of suspension polymerisation in a controlled, industrial environment, meaning a wider range of reaction conditions could be studied including controlled batch failures to establish robust, real-time corrective action plans.

5. Monitoring of Suspension Polymerisation via Passive Acoustic Emission Spectroscopy

5.1. Introduction

As previously discussed, suspension polymerisation of EPS involves the formation of solid polymer beads from monomer droplets. This transition is likely to cause a significant change in the acoustic properties of the reaction matrix, which can be monitored non-invasively with acoustic emission spectroscopy (AES). Examples of non-invasive reaction monitoring with AES are numerous^{49, 51, 62, 156, 157} and it has proven useful in determining particle size information from simpler heterogeneous reaction matrices, but complex systems such as this have not been explored. Key to this project is the ability to monitor the evolving PSD of the sample matrix to allow greater control of the reaction products. To do this, passive AES was chosen as it provides a low-cost, reliable means of monitoring particle size.

In this study, the effect of particle size and concentration as well as vessel size and configuration on the collected spectra were investigated using simplified model systems. Following this, several suspension polymerisation reactions were carried out and monitored with AES. Various data analysis methods were employed and compared to more invasive and time-consuming methods to determine information on particle size. Offline particle sieving allows the determination of PSD and average particle size; however, it is time-consuming, potentially destructive and cannot be employed in real-time. NIR measurements have been successful in this application, but are either invasive¹⁵⁸⁻¹⁶² or require a transparent window capable of allowing non-invasive measurements.^{85, 163-166} Suspension polymerisation of polystyrene is therefore a challenge to monitor this way, as it is often performed in stainless steel reactors, making non-invasive measurements difficult. Furthermore, invasive probes are liable to probe fouling as a result of the multi-phase nature of the reaction, requiring continual probe maintenance.

5.2. Equipment and Materials

Model mixture experiments were performed in Radleys Reactor-Ready Core reaction vessels (250 and 1000 mL), Radleys, Essex, UK. Stirrer speed was controlled using a Radleys RS37 Digital Plus stirrer motor. Suspension polymerisation reactions were carried out as per section 5.3.2. EPS beads were provided by BASF, Ludwigshafen and separated using a Meinzer II sieve shaker, Jade Scientific, MI, USA. Acoustic signals were collected using a Nano30 piezoelectric transducer (Physical Acoustics Limited, Cambridge, UK), which was attached to a 2/4/6 series pre-amplifier (Physical Acoustics Limited). The pre-amplifier required a 28 V power supply (Physical Acoustics Limited) and the gain of the pre-amplifier was set to 60 dB. The output of the pre-amplifier was connected to an Agilent 54624A oscilloscope, (Agilent Technologies, UK), which was controlled using a laptop via a GPIB to USB interface (Agilent Technologies). Data collection was automated using a program written in C++ by Douglas McNab and Robert Robinson from the Centre for Ultrasonic Engineering (CUE) at the University of Strathclyde. Each acoustic emission signal comprised 4000 points and was acquired using a sampling rate of 2 MHz. Signals were collected every 2 s (limited by the GPIB-USB data transfer rate) and were saved as comma separated variable (csv) files. All signals were imported into Matlab for analysis. The complex Fourier transform of each signal was calculated, and then the power spectrum of each signal was computed. To improve the signal-to-noise ratio, spectra were co-added to give a composite spectrum.

5.3. Experimental Procedures

5.3.1. Model Mixtures

Several model systems were investigated with AES to better understand the different factors that might influence the signal in an industrial context. EPS beads were separated into different size ranges (500-630 μm ; 800-1000 μm ; 1000-1250 μm and 1250-1400 μm) and each range was then mixed in water at different %w/v ratios with continuous agitation. An acoustic transducer was fixed to the outer wall of the vessel using silicone-based vacuum grease and electrical tape, and the spectra collected as the bead concentration changed in increments of 5% w/v – this was

performed with beads from each size range and in vessels of different size and dimension. For each concentration, 450 spectra were collected and summed into three blocks of 150 when generating power spectra. Data was acquired at room temperature.

5.3.1.1. Effect of EPS Bead Concentration

The effect of particle concentration on the acoustic signal was investigated by increasing the % concentration of EPS beads in the vessel from 5% - 60% in 5% increments (Tables 5.1-5.2). At each concentration, the water/bead mixture was agitated at a rate of 250 rpm for 15 minutes whilst acquiring acoustic signals.

5.3.1.2. Effect of EPS Bead Size

The experimental conditions outlined in Section 5.3.3.1. were repeated for all bead size ranges. There was an insufficient number of largest bead size fraction (1250-1400 μm) to allow a greater than 55% w/v mixture in the 250 mL vessel. Furthermore, this meant that this fraction was not used at all in the 1000 mL vessel.

5.3.1.3. Effect of Vessel Size

The experiments in Sections 5.3.1.1. and 5.3.1.2. were carried out in a 250 mL vessel and a 1000 mL vessel (for reaction conditions, see Tables 5.1 and 5.2).

Table 5.1 – Conditions for model mixture experiments in a 250 mL vessel.

Bead Size Range (μm)	Volume of Water (mL)	Weight of EPS per increment (g)
500-630	150	7.5
800-1000	200	10
1000-1250	200	10
1250-1400	200	10

Table 5.2 – Conditions for model mixture experiments in a 1000 mL vessel

Bead Size Range (μm)	Volume of Water (mL)	Weight of EPS per increment (g)
500-630	800	40
800-1000	800	40
1000-1250	800	40

5.3.2. Suspension Polymerisation Reactions

Five suspension polymerisation reactions were carried out as outlined in Chapter 4 using the reaction conditions outlined in Table 5.3:

Table 5.3 - Initiator and stabiliser weights used in reactions monitored with AES. Stirrer speed was kept at 300 rpm for all reactions.

Reaction	TCP (g)	DBPO (g)
1	3	4
2	3	4
3	1.5	3.5
4	1.5	3.5
5	2.5	3
6	2.5	3

5.4. Results and Discussion

5.4.1. Effect of EPS Bead Concentration and Size in Model Mixtures

The effect of changing particle concentration can be seen in Figure 5.1. All peak areas increase gradually with increasing bead concentration, with peak A (Table 5.4) showing the greatest sensitivity. This was true for all bead size ranges and is a typical

response from the type of transducer used.⁵¹ At higher concentrations, however, the signals begin to plateau (Figure 5.2), as the large particle densities prevent further collisions with the vessel wall.

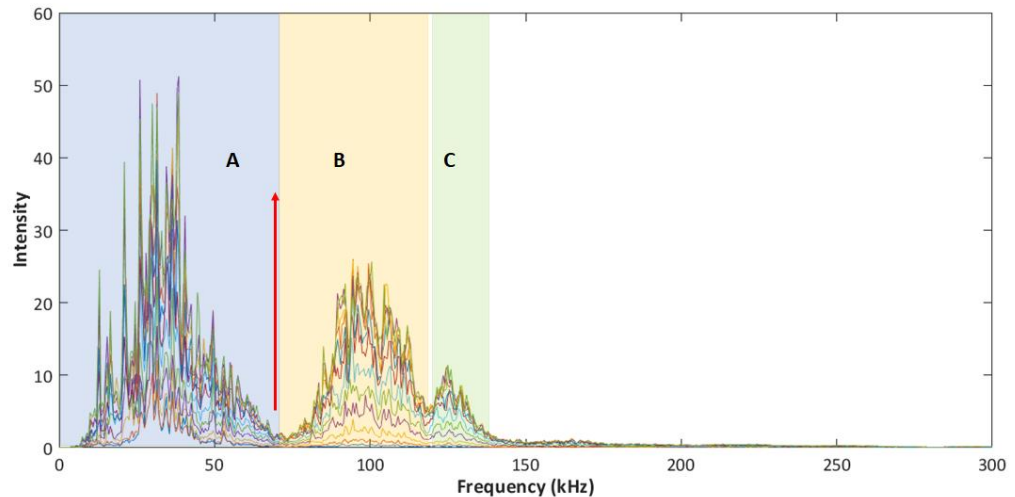


Figure 5.1 - Average AES power spectrum in the 0-300 kHz range for 800-1000 μm beads in a 250 mL vessel at concentrations from 5 - 60% w/v. Highlighted areas denote spectral frequency regions used to calculate the area of each peak – A (0-72 kHz), B (72-117 kHz) and C (119-138 kHz). Red arrow indicates the increasing acoustic signal corresponding to increasing bead concentration.

The calculated power spectra show three distinct peaks resulting from beads suspended in water under agitation (regions A, B and C). Region A includes the audible range (0.2 – 20 kHz). This is the most dominant region and should be the most sensitive to increasing the concentration of beads in any given size range, given that more beads mean more collisions, resulting in more audible sound generated.

The effect of bead concentration on the areas of peaks A-C are illustrated in Figure 5.2. The areas of each peak generally increase with increasing bead concentration, with peak A – which includes the audible region – being the most sensitive. This trend was seen across all bead sizes with a slight exception for the 500-630 μm beads

(Figure 5.3) – in this case, a slight decrease in peak area was seen at 55% before rising slightly at 60%. This was potentially caused by an inadvertent knock off the transducer, or the increase in bead density as the effect is seen across the entire spectrum.

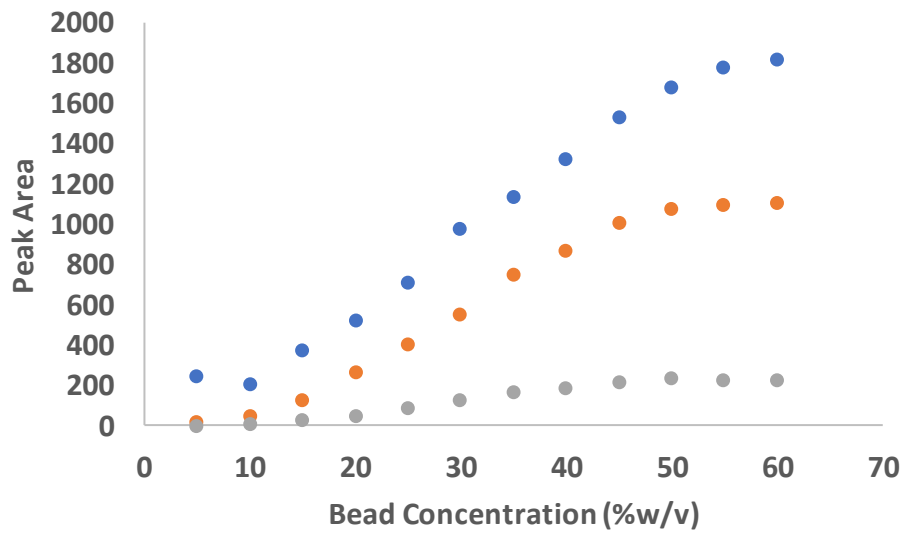


Figure 5.2 – Areas of three peaks in the acoustic emission spectrum (A blue, B orange, C grey) of 800-1000 um EPS beads in a 250 mL vessel as the bead concentration increases from 5 – 60 % w/v.

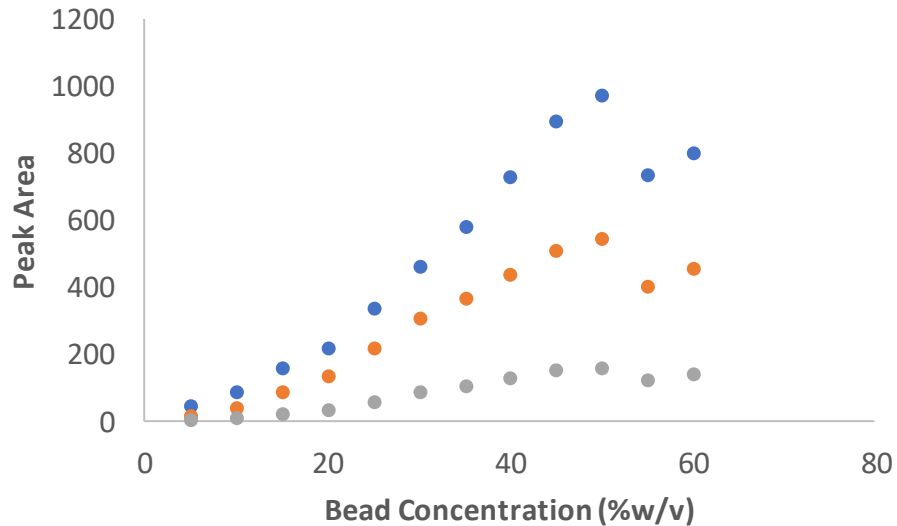


Figure 5.3 – Areas of three peaks in the acoustic emission spectrum (A blue, B orange, C grey) of 500-630 um EPS beads in a 250 mL vessel as the bead concentration increases from 5 – 60 % w/v. Slight loss of acoustic signal seen after 55% concentration.

As peak A includes the audible region of the acoustic spectrum (<20 kHz), it was expected that this peak would be the most sensitive to changes in the system with particles of this size. Across all concentrations, this spectral region showed the best discrimination of different particle concentrations. An examination of how this peak behaves across all available particle sizes (Figure 5.4) further emphasise this region’s sensitivity to changes in the system, but also shows the limitations in using discreet peak areas as a metric for analysis in complex systems.

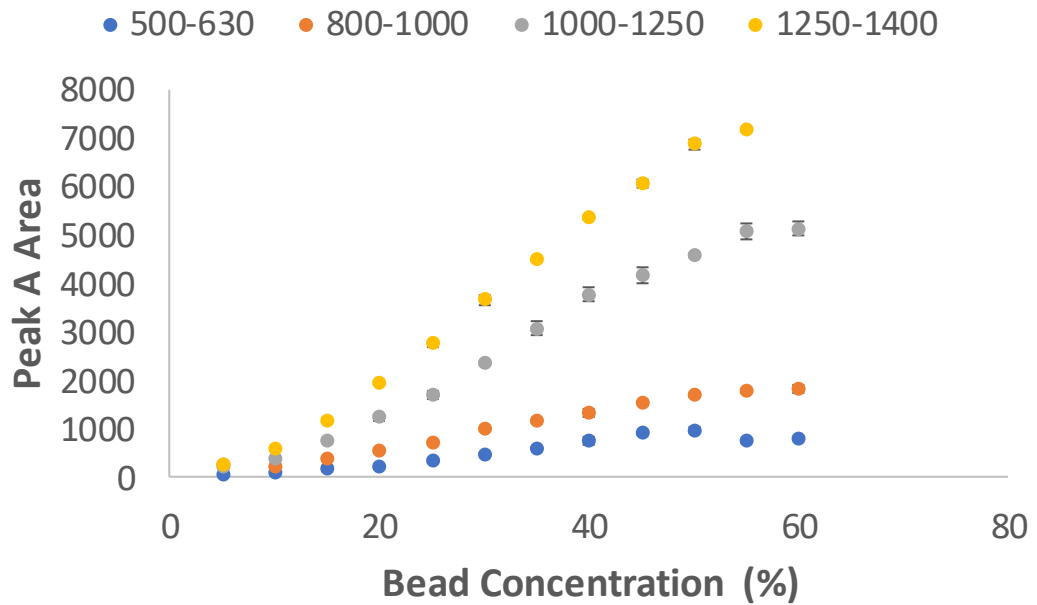


Figure 5.4 – The changing area of peak A - 0-72 kHz - as the bead concentration increases for 4 different bead size ranges. Error bars denote \pm one standard deviation (n=3).

Low frequencies are very sensitive to particle size and concentration in this system, with clear discrimination between signals from different sized particles at fixed concentrations above approximately 20% w/v. However, based on this peak area alone, it would be impossible to distinguish a high concentration of small beads from a low concentration of larger beads. For example, peak areas of 974 and 982 for 50% w/v 500-630 μm beads and 30% w/v 800-1000 μm beads respectively.

Previous works have had success in solving this problem by examining the change in spectral features at a fixed concentration, and calculating area of the more sensitive peaks as a percentage of a larger spectral region.⁶² For example, at a constant bead concentration of 30% (Figure 5.5) the 0-72 kHz region shows good sensitivity to changes in particle size, while the 72-117 and 119-139 kHz regions do not appear as sensitive. This is true across the entire concentration range from at 15% w/v and above. At lower concentrations, large beads' signals become indistinguishable from

one another, likely due to the relatively low number of beads required – leading to a low number of collisions – for a low concentration solution of larger beads.

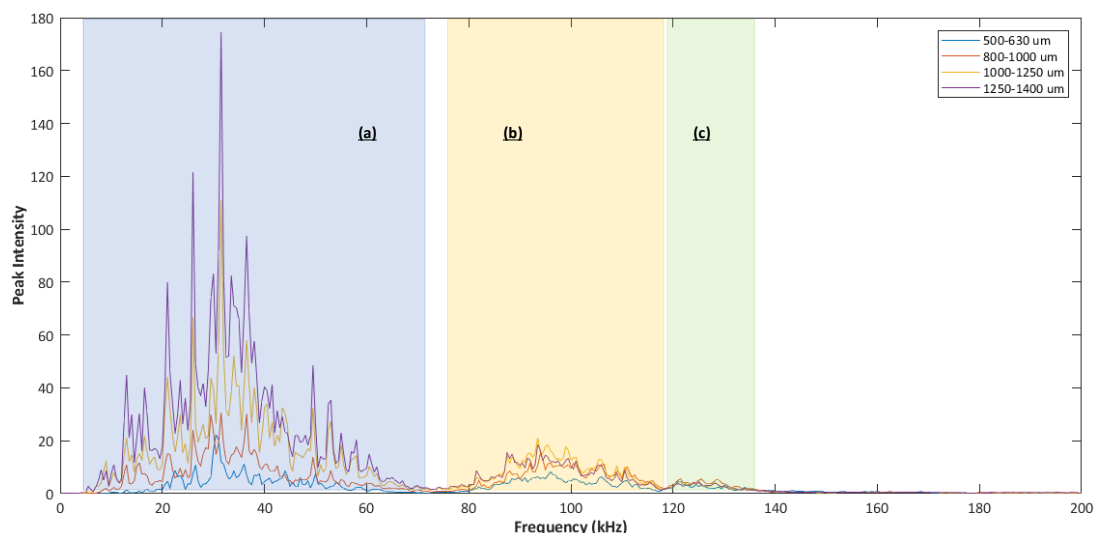


Figure 5.5 – Changing acoustic frequency in the 0-200 kHz region at a fixed bead concentration of 30% w/v with different bead size fractions in a 250 mL vessel.

When the particle concentration is kept constant, peak A shows clear discrimination between particle sizes. The discrimination between bead size and concentration shown so far highlights the potential for this technique to be used for particle size determination in a complex system. However, as stated previously, peak area alone is not enough to determine bead size when mixtures of bead sizes are present – as would be during a reaction.

5.4.2. Effects of Vessel Size and Dimensions

The size and dimensions of the reactor vessel could also affect the acoustic signal, as can be seen from Figures 5.6 and 5.7. The magnitude of the acoustic signal increases substantially, which is expected as the number of beads required to achieve each concentration has increased by a factor of 4 – therefore increasing the number of

collisions. Furthermore, signals will be subject to different filtering effects that are dependent on the vessel size and shape. The sensitivity of the peaks is also affected by vessel size; in the 1000 mL vessel, signal trends obtained from 500-630 μm and 800-1000 μm beads deviate significantly from those seen in the smaller vessel.

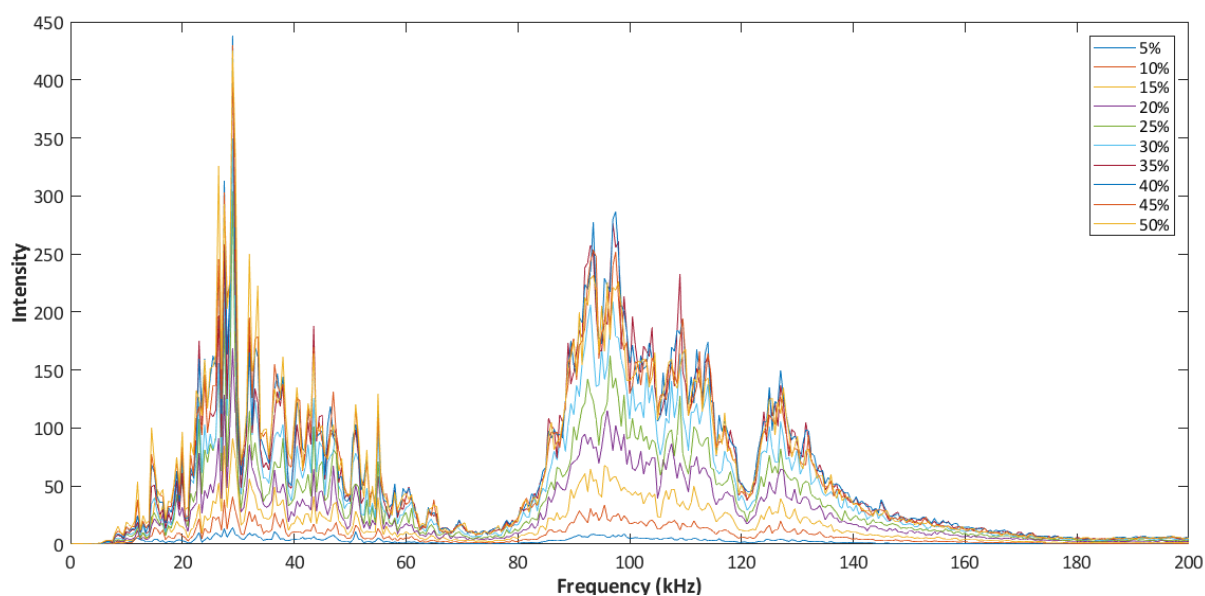


Figure 5.6 – Average AES in the 0-200 kHz range for 800-1000 μm beads in a 1 L vessel at concentrations from 5 - 50% w/v.

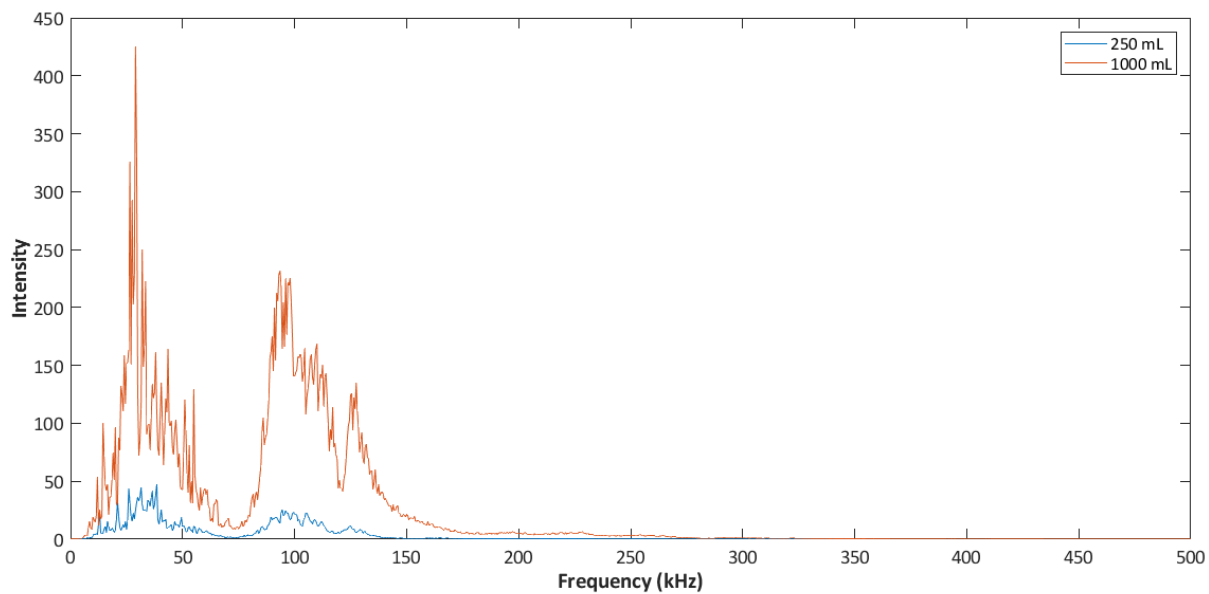


Figure 5.7 – Average AES signals obtained from 800-1000 μm EPS beads at a concentration of 50% w/v in a 250 mL vessel (blue) and a 1000 mL vessel (red).

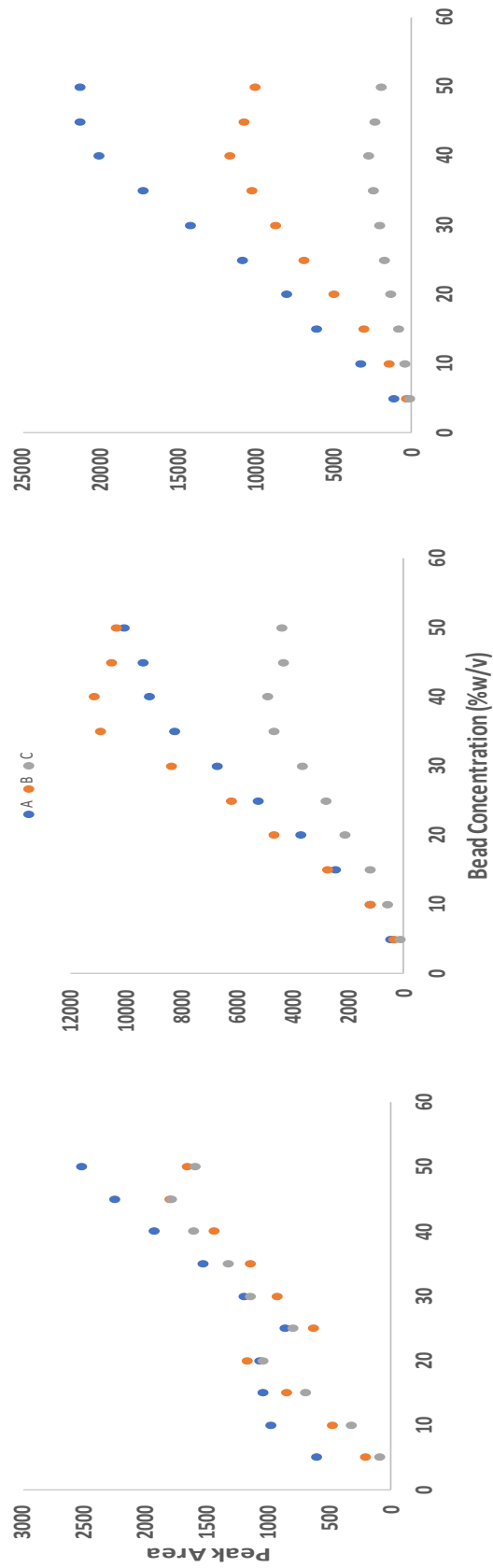


Figure 5.8 – Changing peak height for peaks A - C with increasing concentration for small (left), medium (middle) and large (right) bead ranges in a 1 L vessel.

The impact of changing vessel size is shown in Figure 5.8. Compared to the 250 mL vessel, the peaks show decreased sensitivity to changes in bead concentration. Peak areas for smallest 500 – 630 μm beads show almost no difference in sensitivity to changes in bead concentration; 800 – 1000 μm beads show little difference in sensitivity of peaks A and B, but they appear more sensitive than peak C; and 1000 – 1250 μm beads show a clear sensitivity of all peaks to bead size and concentration. Overall, peak A is most sensitive in this case, which is again expected as this includes the audible region of the spectrum. The differences observed between the peak sensitivities in the small and large vessels are likely caused by several factors, such as the filtering effects of each vessel, particle velocities and the number density of particles contributing to the signal.

Overall, signals obtained show sensitivity to particle size and concentration. However, peak area measurements cannot distinguish between an increase in size and an increase in concentration. Therefore, some data manipulation methods were used to determine the applicability of AES to particle size and concentration determination.

5.4.3. Relative Peak Area

Relative peak areas and %area values provide better discrimination of particle size over a wider concentration range. Several iterations of peak area ratios were calculated, the best of which is shown in Figure 5.9:

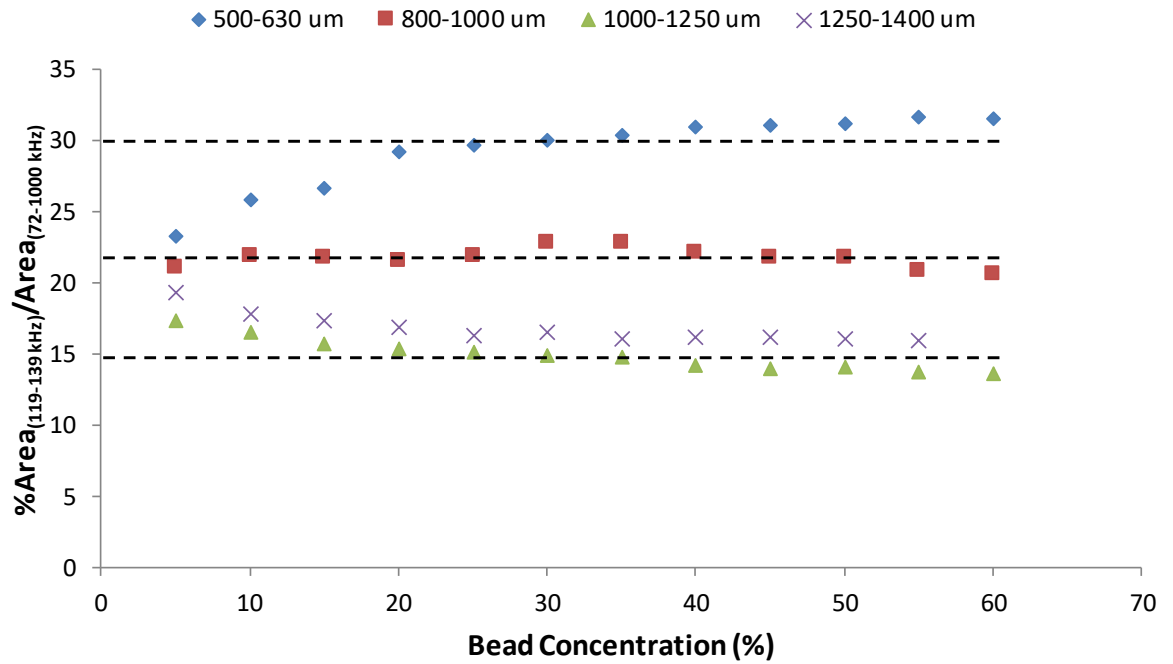


Figure 5.9 – The area of peak C as a percentage of the entire spectrum excluding the audible region, as the bead concentration changed from 0-60% w/v in a 250 mL vessel with agitation.

In all cases, signals from the two largest bead size fractions were not clearly separated from one another by calculating peak ratios or percentages. Figure 5.9 highlights the best peak ratio, capable of distinguishing between beads of three different size ranges – 500-630 μm ; 800-1000 μm ; and >1000 μm beads. These size ranges can be determined at concentrations of 20% and above, below this concentration the data become non-linear and potentially ambiguous. Despite these limitations, this method significantly improves on the use of peak area alone and serves as a quick and convenient way of estimating the bulk bead size throughout a complex reaction such as suspension polymerisation.

This approach was also applied to the data from the 1000 mL vessel as shown in Figure 5.10:

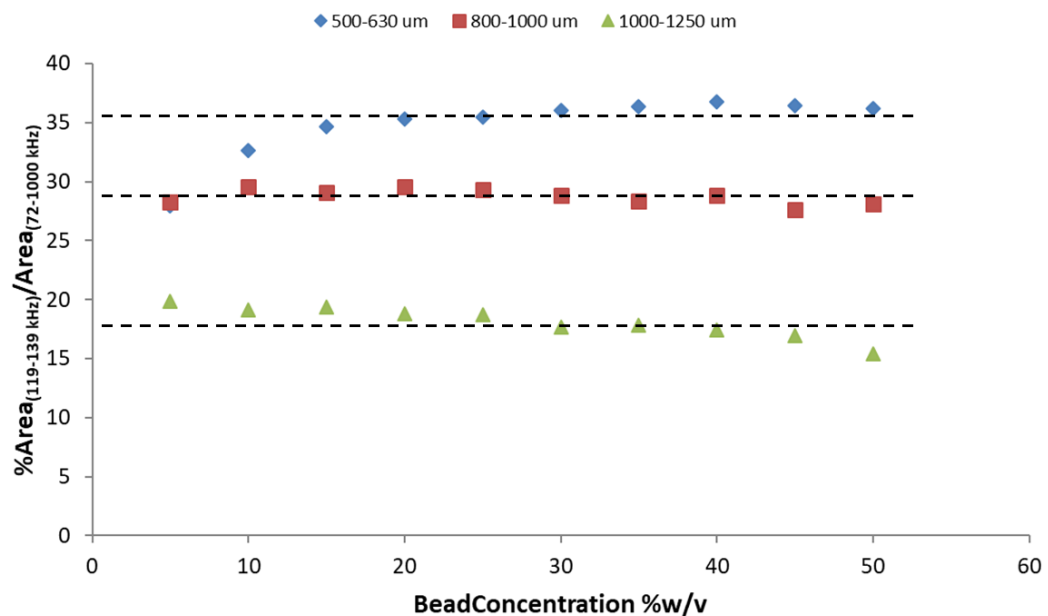


Figure 5.10 – The area of peak C as a percentage of the entire spectrum excluding the audible region, as the bead concentration changed from 0-50% w/v in a 1000 mL vessel with agitation.

This peak area ratio again shows good discrimination between particle sizes from a concentration of 15% onwards, highlighting the effectiveness of this method. Differences in % peak areas for each size range seen in different vessels further highlights the influence of scale on AES measurements. However, further work should be done to ascertain the reproducibility of these results, as only one experiment in each instance. Further work would also include mixtures of different PSD samples at known concentrations, to assess the efficiency with which this method works.

5.4.4. Determination of Size and Concentration by PCA

An examination of the loadings and scores plots from the PCA of data acquired from the small vessel highlights the changing influence that different spectral regions have on the data (Figure 5.11):

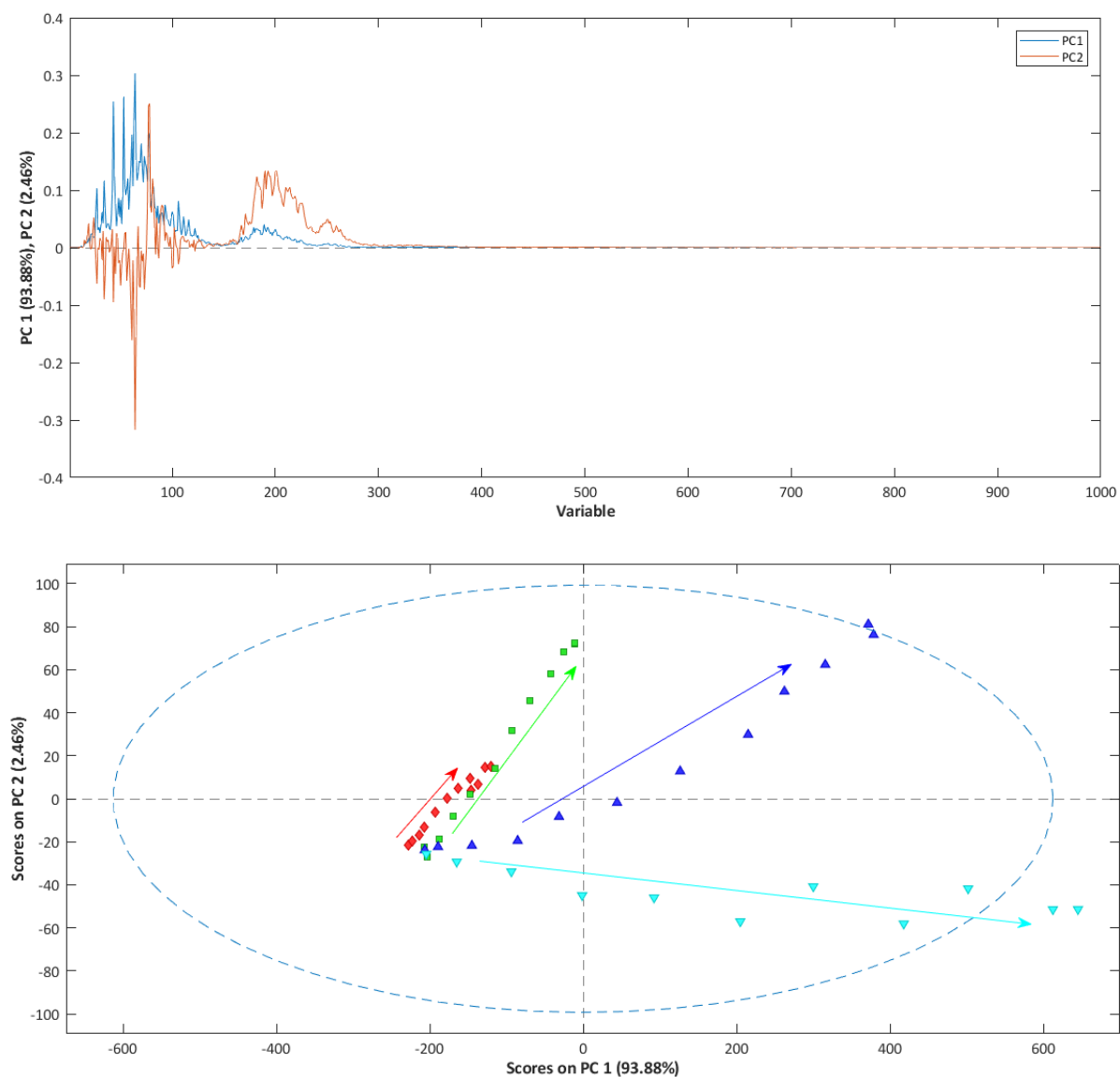


Figure 5.11 – Loadings (top) and scores (bottom) plots from PCA of model mixture data in a 250 mL vessel. Arrows in the scores plot indicate the order of each data cluster (red = 500-630 μm , green = 800-1000 μm , blue = 1000-1250 μm and cyan = 1250-1400 μm) with increasing bead concentration.

The loadings plot shown in Figure 5.11 indicates that PC1 – containing 93.88% of the variance in the data – is positively correlated across all regions of the spectrum, while PC2 shows some anticorrelation with lower frequencies (<72 kHz). The corresponding scores plot further illustrates the different ways in which size and concentration affect the data. The data from each bead size range is clearly separated into distinct clusters, the data within each being ordered according to concentration. In all cases, increasing concentration results in a more positive PC1 score – increased particle concentration results in an increased number of collisions with the vessel wall, increasing the intensity of the signal across all frequencies. Furthermore, increasing the size of the particles results in an even bigger increase in PC1 score – larger particles also increase the signal intensity across all frequencies.

An examination of the loadings and scores plots from the PCA of data from the larger vessel shows that particle size and concentration affect the data in very similar ways as they did in the smaller vessel (Figure 5.12). One key difference, however, is the point at which the loadings of PC2 go from anticorrelated to correlated. In the smaller vessel, this occurred around 72 kHz; whereas in the 1 L vessel, it occurs at around 145 kHz. This clearly illustrates the filtering effects that vessel size and dimensions can have on the signals obtained.

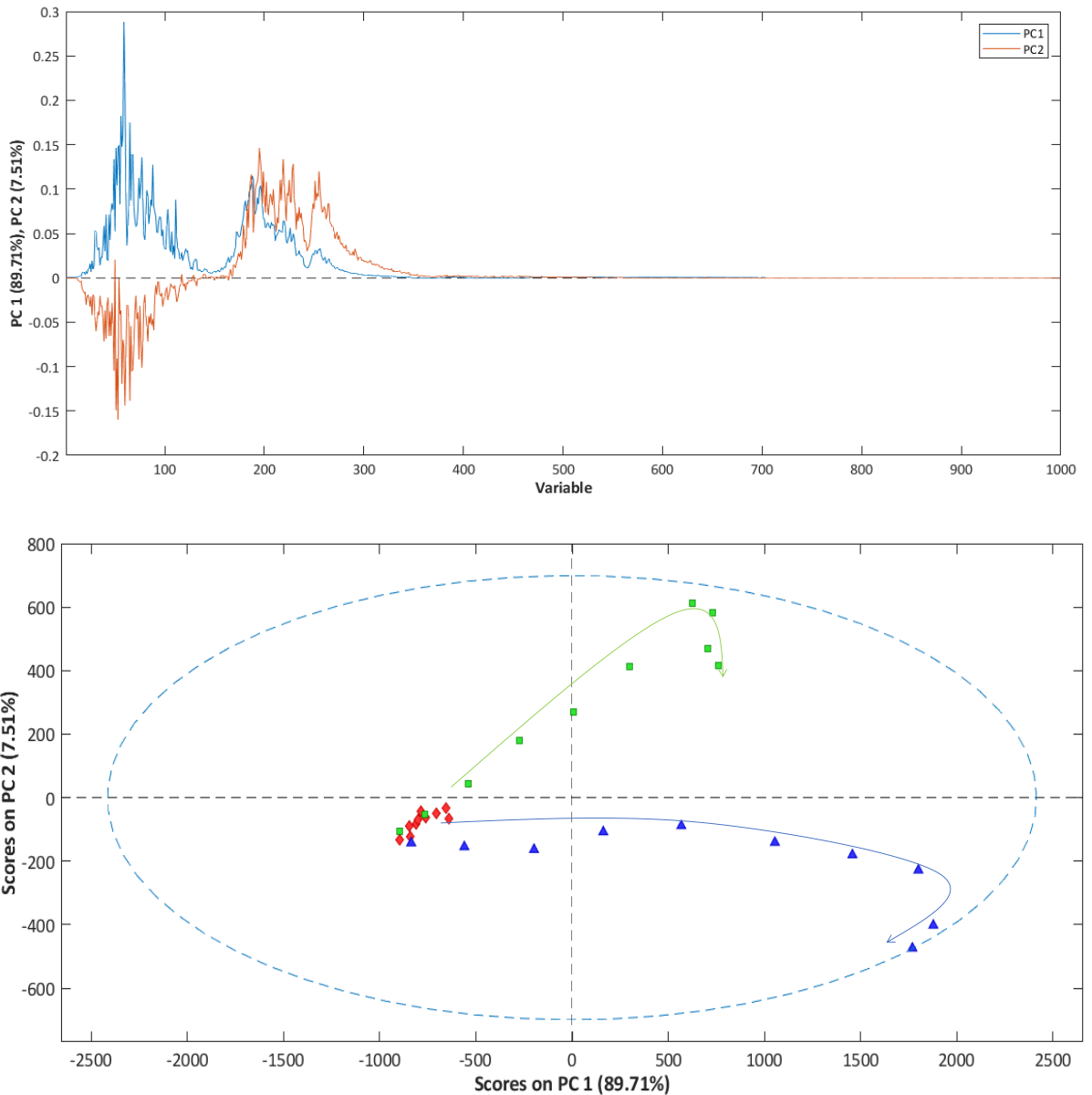


Figure 5.12 – Loadings (top) and scores (bottom) plots from PCA of model mixture data in a 1000 mL vessel. Arrows in the scores plot indicate the order of each data cluster (red = 500-630 μm , green = 800-1000 μm and blue = 1000-1250 μm) with increasing bead concentration.

In the larger vessel, the scores plot shows the data from the smallest beads clustered together, not changing significantly in either direction with changing concentration. As seen in Figure 5.8, there were no spectral regions that were especially sensitive to changing concentration.

PCA and relative peak area calculations show clearly that the AES signals generated in these model experiments can be used to determine EPS bead size and concentration effectively. These approaches could then be applied to data acquired during a suspension polymerisation reaction.

5.4.5. Suspension Polymerisation Reactions

AES measurements were taken throughout several EPS suspension polymerisation reactions, the data from which were then analysed to determine information on particle size and concentration

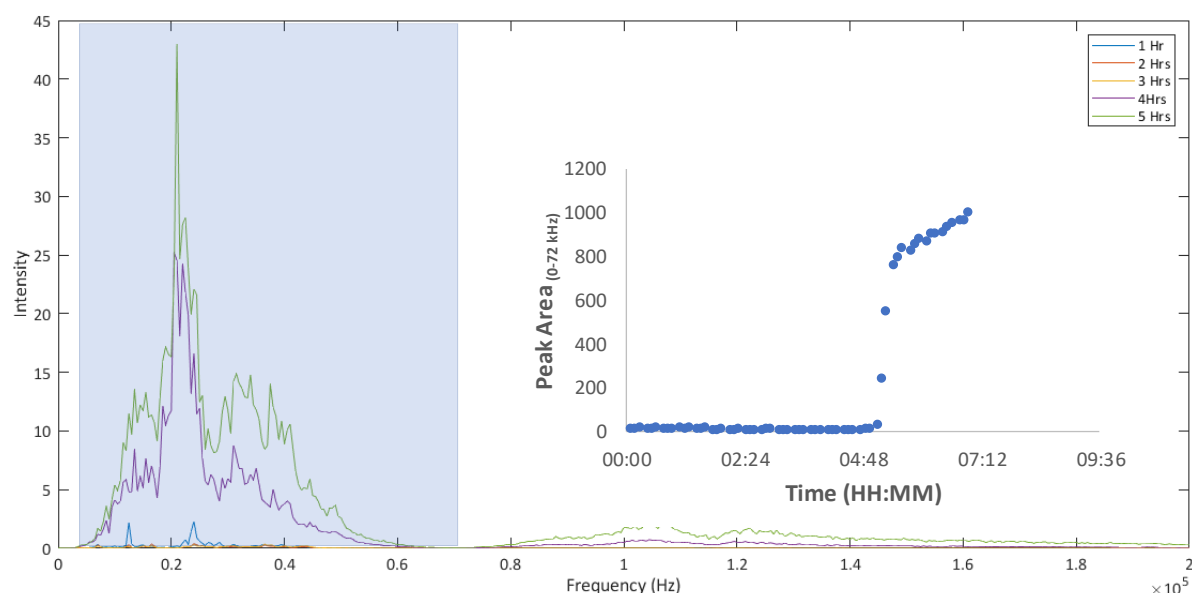


Figure 5.13 – Selected AES data collected throughout suspension polymerisation reaction 1. The 0-72 kHz region is highlighted and its area plotted against time (inset). This was performed in a 1 L Radleys reaction vessel with a stirrer rate of 300 rpm.

Acoustic data acquired throughout the reaction (Figure 5.13) showed no change across the entire spectrum until approximately 5 hours after the reaction had started – the point at which the droplets became hardened beads. At this point, a sharp

increase in signal is seen, followed by a slow increase as the reaction proceeds to completion. Following the successful implementation of peak area ratios in model mixtures of beads in water for determining particle size information, the same was applied to this data. To eliminate interference from the stirrer motor and ambient sounds, the audible region was eliminated from the calculation.

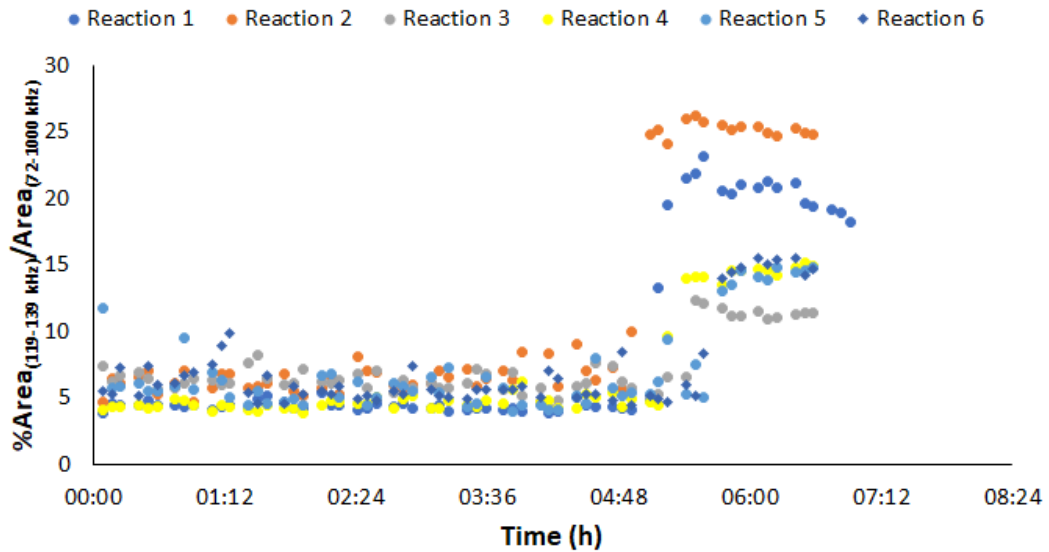


Figure 5.14 – The area of peak C as a percentage of the entire spectrum excluding the audible region, throughout each suspension polymerisation reaction.

By taking the same peak ratio as was used on the model mixture data (Figure 5.14), the data for all reactions behave very similarly up until approximately 5 hours after the reaction had started, coinciding with the appearance of hardened beads in the samples removed for gravimetric analysis. Closer examination of this event is shown in Figure 5.15:

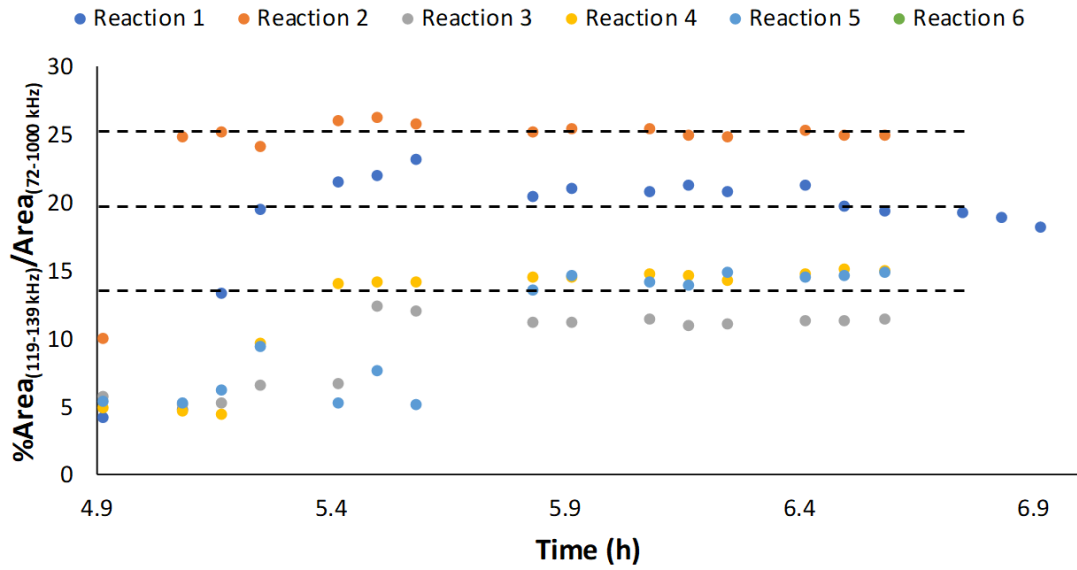


Figure 5.15 – The area of peak C as a percentage of the entire spectrum excluding the audible region, from 5 hours after each reaction had started until completion.

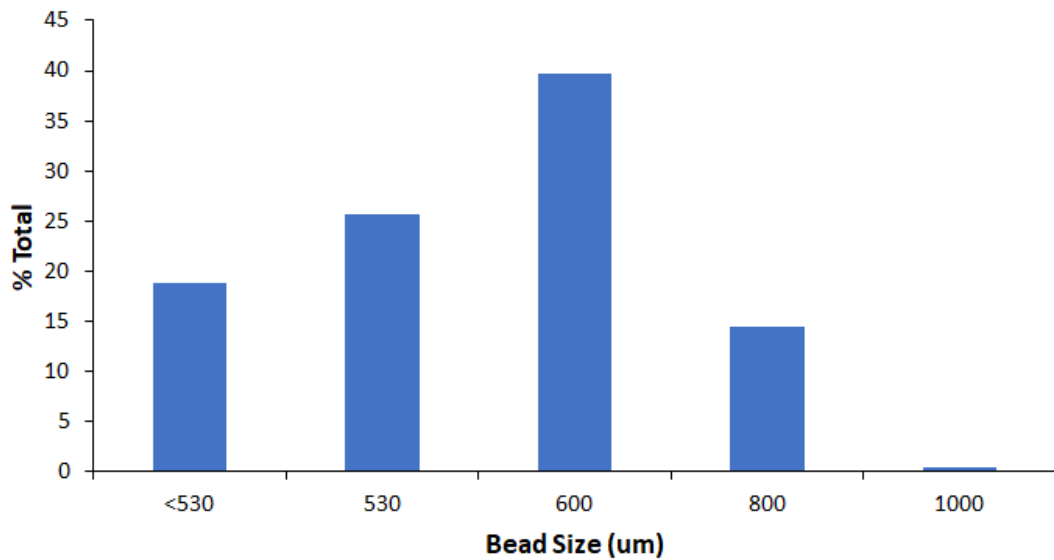


Figure 5.16 - Bead sieving analysis of the beads produced by reaction 1. Each fraction is shown as a percentage of the total weight of beads produced.

Figure 5.14 shows that reactions 1 and 2 – identical reactions with the highest amounts of initiator and stabiliser – stand out from the other reactions performed. Based on the peak ratio values, these reactions should have produced smaller beads than reactions 3-6, which is consistent with the known effects of the reaction conditions. This is emphasised in Figure 5.15, with most of the beads produced by reaction 1 being 600 μm and smaller in diameter and further confirmed by particle sieving analysis results from this same reaction (Figure 5.16).

The peak area ratio for reaction 1 shown in Figure 5.15 differs slightly from the value obtained from the model mixture in the larger vessel, which could be attributed to filtering effects caused by the differences in the vessels dimensions – while both the model mixture vessel and the process vessel have a 1 L capacity, the process vessel is shorter and wider than the one used in the model experiments – or potential temperature effects, as the model mixtures were measured at room temperature and the reactions at 80°C.

The discrepancy between the % peak area expected from the model mixtures of 600 μm beads and those measured during a reaction is lessened when model mixture experiments were repeated in the process vessel (Figure 5.17):

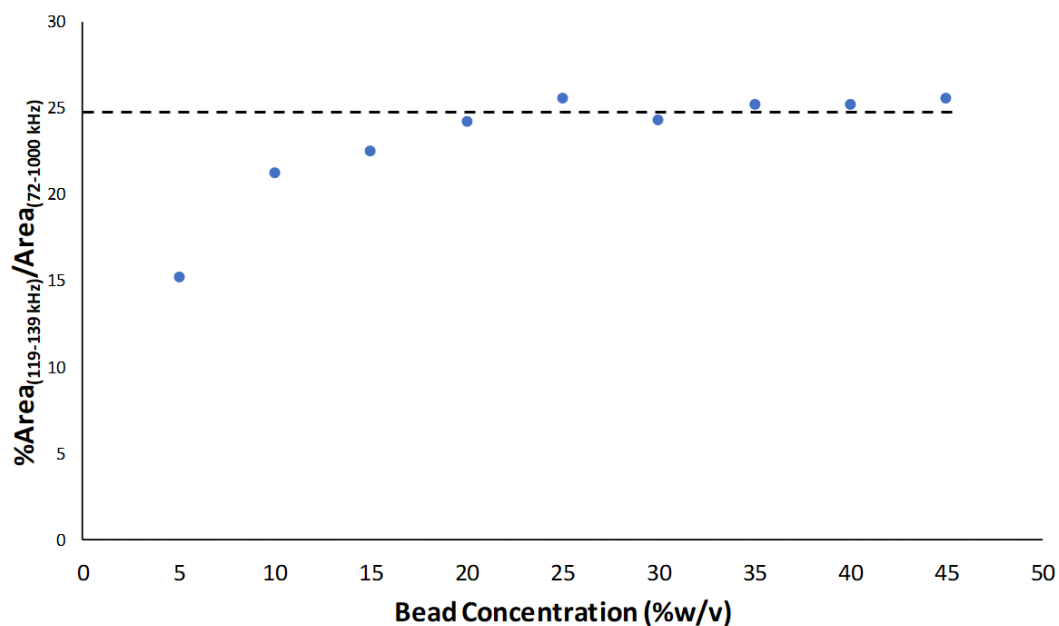


Figure 5.17 - The area of peak C as a percentage of the entire spectrum excluding the audible region, as the concentration of 500-630 μm beads increased in a 1000 mL reactor vessel with agitation at 300 rpm.

Here, the peak area ratio used in previous analyses gives results in closer agreement with data collected throughout a reaction – showing a peak area ratio of ~ 25 . Reactions performed in the same vessel which produced mostly beads in this same size range gave a peak area ratio of approximately 20-25 (Figure 5.15). This further highlights the influence of vessel dimensions on the acoustic data collected, showing that vessels of the same size but different dimensions can produce significantly different acoustic data.

5.5. Conclusions and Further Work

In this study, the potential importance of AES in the monitoring of complex industrial reactions is illustrated. Simple model experiments allowed the determination of factors affecting the acoustic signal – particle size, particle concentration and vessel dimensions – which could be subsequently solved using ratios of peak areas

throughout the reaction and PCA. Several reactions were then carried out and successfully monitored using AES

This approach showed some correlation to time-consuming offline sieving analysis, indicating the potential of this technique as an in-situ, cheap and real-time method for the determination of particle size information from a multi-phase reaction matrix. While particle size measurements have shown promise, further investigation into the PSD of beads produced for the other reactions is needed to assess the applicability of this promising method for such a challenging and complex reaction.

Building on these results, it would be of benefit to determine the PSD of the bead products from all reactions monitored with AES. Furthermore, a wider variety of reaction conditions and controlled batch failures would allow more robust datasets for AES analysis. Model mixtures of a range of known PSDs could also help in the building of robust predictive models which could then be applied to these reactions. The ease of implementation of AES technologies means that these experiments could readily be performed in an industrial setting, providing more realistic datasets for modelling.

6. Project Conclusions and Further Work

The key goals of this project were to detect the presence of unreacted styrene within polystyrene beads produced by a radical suspension polymerization below 0.1% w/w and to gain particle size information in real time throughout the reaction. A comprehensive evaluation of commonly used techniques for monitoring these reactions identified Raman and infrared spectroscopies as being suitable methods for *in-situ* monitoring, capable of providing detailed chemical information in real time. Furthermore, gravimetry and HPLC were shown to be capable of providing accurate and reliable offline data for monitoring the reaction progress and determining residual monomer content of the EPS bead products for comparison with the spectroscopic data.

Due to the highly aqueous nature of the reaction media, MIR spectra were dominated by strong water bands and this technique was pursued no further. Raman spectroscopy, however, is unaffected by water and was therefore more successful in discerning key reaction components in the complex matrix. The sharp Raman C=C stretching band at 1630 cm^{-1} was shown to be unique to styrene in the reaction media and could be followed throughout the reaction as the bonds were broken and the peak intensity declined. This band was also present in the polymer bead products of the reaction, but the intensity was too low to measure directly. Therefore, derivatisation and smoothing techniques were applied to the spectra to minimize baseline drifting and noise contributions, making the peak easier to measure. Due to limitations of the available EPS samples, artificial 'standards' were produced to create a range of EPS samples with a range of residual monomer content to establish a calibration curve with offline HPLC. This allowed the residual monomer content of the beads to be accurately determined and compared to the height of the unique Raman band at 1630 cm^{-1} . Using offline Raman measurements, this method provided residual monomer measurement down to 0.4% w/w without derivatisation, which was improved to 0.05% w/w when using second order derivatisation. This showed Raman spectroscopy to be capable of meeting one of the project's key aims.

The effect of changing the particle size and concentration on the Raman data collected was also assessed and highlighted the issue with using probes with a small laser diameter. Sampling depth studies showed that the majority of Raman signal is obtained from the top 2-3 mm of the sample and gave an overall sampling volume of 54.9 nL using the 100 μm MR probe head. The use of a WAI ('PhAT') probe was then investigated and showed that increasing the spot diameter to 6 mm, this sampling volume was increased to 424.12×10^3 nL with beads of the same size range. Overall, through experiments with beads of different sizes ranges, the use of a WAI probe increased the sampling volume by 6000-7000 times using half the exposure time than the 100 μm MR probe, indicating the potential benefits of including a WAI probe in monitoring this reaction. A final comparison of an array of probe head configurations and sampling environments showed that the WAI probes provided much more sensitivity. However, further investigations using an immersion PhAT probe are required as the glass wall of the reaction vessel hindered the in-line use of this technique.

Raman measurements with some spectral data treatment and increasing sample volume have proven to meet the challenges of this project. The remaining challenge was to then apply the successes of this work in a way that would be meaningful to industrial partners by monitoring reactions using *in-situ* methods. To do this, a series of suspension polymerization reactions was carried out under different conditions and monitored using an IO Raman probe with simultaneous offline measurements, providing a profile of the changing reaction matrix as the reaction progressed. Analysis of the reaction media showed the C=C Raman band to decrease over time and served as an ideal marker for monitoring reaction progress. To relate this to residual monomer levels, a suitable offline method had to be established for comparison. HPLC showed good agreement with online Raman measurements made using the intensity of the C=C peak at 1630 cm^{-1} as a marker. However, this technique was only applicable towards the end of the reaction when beads had hardened and is time-consuming and labour intensive. A suitable alternative had to be identified.

Having already identified gravimetry as a potential technique, two different methods were compared to ascertain which would provide the most accurate and reliable reaction profile.

- **Method A** involved removing a hot sample from the reactor before quenching with hydroquinone solution. The weight of this mixture was then recorded before rapidly cooling the sample in a freezer and weighing once more. This sample was then dried in an oven for several days until a consistent weight was achieved. Gravimetric calculations then allowed the % conversion of monomer to polymer to be estimated. The use of hydroquinone in this method meant that the quenching agent was more soluble in the aqueous phase of the sample and thus would not quench the reaction in the organic phase quickly. Furthermore, estimated conversion maxima failed to exceed 70%, which contradicts the advice from industry experts who say that solid polymer beads would not be formed below 70% conversion. As the samples collected and analysed via this method were solid polymer beads, this method was seen to be unreliable.
- **Method B** involved a very similar process with a few key differences, primarily in the quenching agent used. The use of para-benzoquinone meant that the quenching agent was able to diffuse more readily into the organic phase of the samples taken, thus quenching the reaction faster. Furthermore, the sample is weighed before the addition of quenching agent and there is no cooling of the sample. After adding quenching agent, it was placed directly in the oven to dry for several days until a consistent weight was obtained. This method showed more variation than Method A at the beginning of the reaction, but both showed comparable results towards the end when the conversion estimation is most critical. Furthermore, Method B gave more reliable results, showing final conversion estimates of > 70%.

Once suitable online and offline methods were established, the reactions were carried out and monitored to build a dataset for reaction modelling. The complexity of the heterogeneous reaction matrix and the formation of solid polymer particles make spectroscopic analysis difficult when relying on a univariate approach. Multivariate methods allowed the entirety of the Raman spectrum to be used and related to offline measurements by PLS regression, allowing the correlation of Raman data and offline gravimetry to be quantified. Prior to this, PCA was used to identify key spectral regions and individual reaction datasets that could be used to validate models, leaving the rest for calibration. Using the calibration datasets to build models and the validation datasets to assess their robustness allowed an investigation into spectral pre-treatment methods. Several standard and advanced pre-treatment techniques were applied to the data before building models – SGFD, SNV, EMSC and OPLEC/OPLECm. The models were then assessed by correlation coefficient, r^2 , RMSEP and the number of LVs required to build the model. The data showed SGFD to give no improvements, while SNV, EMSC and OPLEC improving the r^2 of the data from 0.84 to 0.98 in all cases. Furthermore, SNV and EMSC improved the RMSEP from 11.3% to 4.1 and 3.8%, respectively. EMSC was the better of the two techniques, as the number of LVs required to build the model (4) was lower than the number required following SNV pre-treatment (6). EMSC, however, requires the spectra of all individual components contributing to the sample matrix, which is not always viable. OPLEC pre-treatment provided the best overall improvement to models, giving increased correlation, low RMSEP (4.1%) and only 3 LVs to build a robust model.

This method requires some optimization, which can hinder its applicability to real-time process monitoring, despite the improvements it brings to modelling. Modifications to the original OPLEC method have allowed the estimation of the optimization parameters, making the technique more applicable to this work. The original OPLEC method was optimized via a laborious iterative process to establish the optimum parameter settings for robust modelling, which was then compared to the parameter estimation via OPLECm. This comparison gave good agreement ($J = 3$

and $J = 4$ from OPLEC and OPLECm, respectively), indicating OPLECm as a good candidate for spectral pre-treatment for increasing the robustness of modelling data collected throughout this reaction. The project would benefit greatly from utilising spectral pre-treatment methods, including advanced techniques like OPLECm. Other pre-treatment methods should be investigated with this data, and a wider range of reaction conditions should be investigated in a working industrial environment to increase the reliability of modelling and make optimal use of the data provided by spectroscopic methods.

Finally, the implementation of AES for the determination of PSD was investigated as this was a key goal of the project. The ability to monitor the PSD throughout the reaction would allow manufacturers to control the final product size and is of great interest to industry. Firstly, model mixtures of beads in water were used (using beads of varying size ranges) to ascertain the effect of bead size on the acoustic signals collected by attaching a piezoelectric broadband acoustic transducer to the outer vessel wall. The effect of bead size and concentration was assessed, showing the area of peaks in the collected power spectra to increase with increasing size and concentration. Using the data collected from the model systems, a relationship between particle size and peak area ratio was found following an iterative process of calculating multiple peak area ratios. Once established, this ratio was evaluated in model bead/water mixtures in vessels of different size and dimension, again showing clear discrimination between different particle sizes. A series of suspension polymerization reactions were then performed with simultaneous AES measurements being taken. The peak area ratio established before could then be calculated, which was then compared to the PSD determined by offline particle sieving analysis of the final polymer product. This showed some good correlation, although further work should be done to investigate the effect of a wider range of PSD model mixtures and vessel dimension effects to allow this method to be applied in an industrial setting.

The work presented in this thesis shown the applicability of Raman spectroscopy to the challenges faced by industry today. Offline measurements have shown Raman spectroscopy to be capable of surpassing the detection limits required, and the implementation of WAI probes has shown the benefits of increasing sample volume. This work suggests that immersion WAI probes and their applicability to polymerization monitoring should be investigated, as they could provide highly sensitive, real-time data for process monitoring control. Furthermore, multivariate modelling has been shown to be improved by advanced spectral preprocessing techniques. A fuller range of reaction conditions as well as implementation of novel OPLECm preprocessing in real-time monitoring software could be greatly advantageous in industrial monitoring.

7. References

1. Wünsch, J. R., *Polystyrene: Synthesis, production and applications*. iSmithers Rapra Publishing: 2000; Vol. 112.
2. http://www.thermalps.com.au/imagesDB/wysiwyg/TDS_Expanded_Polystyrene.pdf. (accessed 30/08/2018).
3. <http://www.ceresana.com/en/market-studies/plastics/expandable-polystyrene/expandable-polystyrene-market-share-capacity-demand-supply-forecast-innovation-application-growth-production-size-industry1323.html>. (accessed 07/01/2014).
4. Frontmatter. In *Handbook of Radical Polymerization*, John Wiley & Sons, Inc.: 2003; pp i-xii.
5. Jung, J.; Park, C.; Yun, G. J., Free radical polymerization simulation and molecular entanglement effect on large deformation behavior. *European Polymer Journal* **2019**, *114*, 223-233.
6. Ying, Z.; Su, C.; Yongshen, X.; Caideng, Y., Suspension Polymerization of Styrene without Extra-Surfactant. *Chemical Industry and Engineering* **2015**, (4), 7.
7. Guan, D.; Li, J.; Sun, G.; Zhai, X. In *Some Reflections On Styrene Suspension Polymerization Experiment Teaching*, 2019; IOP Publishing: p 012026.
8. On-line Identification and Optimization of Feed Rate Profiles for Fed-batch Culture of Hybridoma Cells. In *Modelling and Optimization of Biotechnological Processes*, Springer Berlin Heidelberg: 2006; Vol. 15, pp 29-40.
9. Kessler, R.; Hergeth, W.-D.; Maiwald, M.; Steinmuller, D. http://presse.achema.de/achema_presse/en/ACHEMA+Press+Releases/Trend+Reports/tb_8_en+Process+analytical+technology.html. (accessed 10/01/2014).
10. Daynes, H. A., *Gas Analysis by Measurement of Thermal Conductivity*. University Press: 1933.
11. **Guidance for Industry PAT — A Framework for Innovative Pharmaceutical Development, Manufacturing, and Quality Assurance.** <http://www.fda.gov/downloads/Drugs/GuidanceComplianceRegulatoryInformation/Guidances/UCM070305.pdf> (accessed 06/01/2013).

12. Fonseca, G. E.; Dube, M. A.; Penlidis, A., A Critical Overview of Sensors for Monitoring Polymerizations. *Macromolecular Reaction Engineering* **2009**, 3 (7).
13. Weeks, N.
http://www.flowresearch.com/Press_Releases/Flow_Research_Release-Temp_Sensors.pdf.
http://www.flowresearch.com/Press_Releases/Flow_Research_Release-Temp_Sensors.pdf (accessed 10/01/2013).
14. Bendada, A.; Cole, K.; Lamontagne, M.; Simard, Y., Infrared radiometry using a dielectric-silver-coated hollow glass waveguide for polymer processing. *Infrared Physics & Technology* **2004**, 45 (1), 59-68.
15. Lin, P.; Falk, B.; Jang, M.; Crivello, J. V., Study of laser-induced photopolymerizations by optical pyrometry. *Macromolecular Chemistry and Physics* **2004**, 205 (15).
16. Frauendorfer, E.; Wolf, A.; Hergeth, W.-D., Polymerization Online Monitoring. *Chemical Engineering & Technology* **2010**, 33 (11).
17. Jobling, A., An introduction to rheology H. A. Barnes, J. F. Hutton and K. Walters, Elsevier Science Publishers, Amsterdam, 1989. *Polymer International* **1991**, 25 (1), 61-61.
18. Yoder, J., New-technology flowmeters offer performance breakthroughs. *Control Solutions* **2002**, 75 (4), 30-33.
19. Dominauskas, A.; Heider, D.; Gillespie Jr, J. W., Electric time-domain reflectometry sensor for online flow sensing in liquid composite molding processing. *Composites Part A: Applied Science and Manufacturing* **2003**, 34 (1), 67-74.
20. Dominauskas, A.; Heider, D.; Gillespie Jr, J. W., Electric time-domain reflectometry distributed flow sensor. *Composites Part A: Applied Science and Manufacturing* **2007**, 38 (1), 138-146.
21. Dyakowski, T.; Jeanmeure, L. F. C.; Jaworski, A. J., Applications of electrical tomography for gas-solids and liquid-solids flows - a review. *Powder Technology* **2000**, 112 (3).
22. Dyakowski, T.; Jaworski, A. J., Non-invasive process imaging - Principles and applications of industrial process tomography. *Chemical Engineering & Technology* **2003**, 26 (6).

23. Fyrippi, I.; Owen, I.; Escudier, M. P., Flowmetering of non-Newtonian liquids. *Flow Measurement and Instrumentation* **2004**, *15* (3).
24. Sheem, S. K. Low Cost Fibre-Optic Pressure Sensor. 2003.
25. Ceysens, F.; Driesen, M.; Wouters, K.; Puers, R.; Leuven, K. U., A low-cost and highly integrated fiber optical pressure sensor system. *Sensors and Actuators A: Physical* **2008**, *145–146* (0), 81-86.
26. Bhat, S. A.; Saraf, D. N.; Gupta, S.; Gupta, S. K., Use of agitator power as a soft sensor for bulk free-radical polymerization of methyl methacrylate in batch reactors. *Industrial & Engineering Chemistry Research* **2006**, *45* (12), 7530-7539.
27. Santos, G. P.; Martins, C.; Fortuny, M.; Santos, A. F.; Turmine, M.; Graillat, C.; McKenna, T. F. L., In-line and in situ monitoring of ionic surfactant dynamics in latex reactors using conductivity measurements and ion-selective electrodes. *Industrial & Engineering Chemistry Research* **2007**, *46* (5).
28. Hua, H.; Dubé, M. A., Off-line monitoring of butyl acrylate, methyl methacrylate and vinyl acetate homo- and copolymerizations in toluene using ATR-FTIR spectroscopy. *Polymer* **2001**, *42* (14), 6009-6018.
29. Vautz, W.; Mauntz, W.; Engell, S.; Baumbach, J. I., Monitoring of Emulsion Polymerisation Processes using Ion Mobility Spectrometry—A Pilot Study. *Macromolecular Reaction Engineering* **2009**, *3* (2-3), 85-90.
30. Kroner, H.; Klostermann, R.; Birk, J.; Hauff, T. 2002.
31. Taylor, M.; Antonucci, J.; Racz, R. Method and apparatus for predicting polymer latex properties in an emulsion polymerization process to improve the quality and productivity of the polymer latex. 2003.
32. Elizalde, O.; Azpeitia, M.; Reis, M. M.; Asua, J. M.; Leiza, J. R., Monitoring emulsion polymerization reactors: Calorimetry versus Raman spectroscopy. *Industrial & Engineering Chemistry Research* **2005**, *44* (18).
33. Gossen, P. D.; MacGregor, J. F., On-Line Particle Diameter for Poly(Vinyl Acetate) Latex Using Specific Turbidity Method. *Journal of Colloid and Interface Science* **1993**, *160* (1), 24-38.
34. Celis, M.-T.; Garcia-Rubio, L. H., Continuous Spectroscopy Characterization of Emulsions. *Journal of Dispersion Science and Technology* **2002**, *23* (1-3), 293-299.

35. Reed, Wayne F. (New Orleans, LA) 2000 Miniature, submersible, versatile, light scattering probe for absolute equilibrium and non-equilibrium characterization of macromolecular and colloidal solutions United States The, Administrators Of The Tulane Educational Fund (New Orleans, LA) 6052184.
36. Reed, W. F., (New Orleans, LA) 2003 Automatic mixing and dilution methods for online characterization of equilibrium and non-equilibrium properties of solutions containing polymers and/or colloids United States The, Administrators Of The Tulane Educational Fund (New Orleans, LA) 6653150.
37. Chai, X. S.; Schork, F. J.; Oliver, E. M., ATR-UV monitoring of methyl methacrylate miniemulsion polymerization for determination of monomer conversion. *Journal of Applied Polymer Science* **2006**, *99* (4), 1471-1475.
38. Kim, Y. S.; Sung, C. S. P., UV and fluorescence characterization of styrene and methyl methacrylate polymerization. *Journal of Applied Polymer Science* **1995**, *57* (3), 363-370.
39. Santos, J. C.; Reis, M. M.; Machado, R. A. F.; Bolzan, A.; Sayer, C.; Giudici, R.; Araujo, P. H. H., Online monitoring of suspension polymerization reactions using Raman spectroscopy. *Industrial & Engineering Chemistry Research* **2004**, *43* (23).
40. Jiang, Y.; Garland, M.; Carpenter, K. J.; Suresh, P. S.; Widjaja, E., Kinetic study of the solution polymerization of methacrylamide initiated with potassium persulfate using In Situ Raman Spectroscopy and band-target entropy minimization. *Journal of Polymer Science Part a-Polymer Chemistry* **2007**, *45* (23).
41. Stuart, B. H., *Infrared Spectroscopy: Fundamentals and Applications*. Wiley: 2004.
42. Roberge, S.; Dube, M. A., Inline monitoring of styrene/butyl acrylate miniemulsion polymerization with attenuated total reflectance/Fourier transform infrared spectroscopy. *Journal of Applied Polymer Science* **2007**, *103* (1).
43. Cherfi, A.; Fevotte, G.; Novat, C., Robust on-line measurement of conversion and molecular weight using NIR spectroscopy during solution polymerization. *Journal of Applied Polymer Science* **2002**, *85* (12), 2510-2520.

44. Reis, M. M.; Araújo, P. H. H.; Sayer, C.; Giudici, R., Correlation between Polymer Particle Size and in-situ NIR Spectra. *Macromolecular Rapid Communications* **2003**, *24* (10), 620-624.
45. Fontoura, J. M. R.; Santos, A. F.; Silva, F. M.; Lenzi, M. K.; Lima, E. L.; Pinto, J. C., Monitoring and control of styrene solution polymerization using NIR spectroscopy. *Journal of Applied Polymer Science* **2003**, *90* (5).
46. Xalter, R.; Mülhaupt, R., Online monitoring of polyolefin particle growth in catalytic olefin slurry polymerization by means of lasentec focused beam reflectance measurement (FBRM) and video microscopy (PVM) probes. *Macromolecular Reaction Engineering* **2010**, *4* (1), 25-39.
47. Poblete, I. B.; Castor, C. A.; Nele, M.; Pinto, J. C., On-line monitoring of chord distributions in liquid–liquid dispersions and suspension polymerizations by using the focused beam reflectance measurement technique. *Polymer Engineering & Science* **2016**, *56* (3), 309-318.
48. Boxall, J. A.; Koh, C. A.; Sloan, E. D.; Sum, A. K.; Wu, D. T., Measurement and calibration of droplet size distributions in water-in-oil emulsions by particle video microscope and a focused beam reflectance method. *Industrial & Engineering Chemistry Research* **2009**, *49* (3), 1412-1418.
49. Nordon, A.; Waddell, R. J.; Bellamy, L. J.; Gachagan, A.; McNab, D.; Littlejohn, D.; Hayward, G., Monitoring of a heterogeneous reaction by acoustic emission. *Analyst* **2004**, *129* (5), 463-467.
50. Storti, G.; Hipp, A. K.; Morbidelli, M., Monitoring latex reactors by ultrasonics. *Polymer Reaction Engineering* **2000**, *8* (1), 77-94.
51. Allan, P.; Bellamy, L. J.; Nordon, A.; Littlejohn, D., Non-invasive monitoring of the mixing of pharmaceutical powders by broadband acoustic emission. *Analyst* **2010**, *135* (3), 518-524.
52. Gherras, N.; Serris, E.; Févotte, G., Monitoring industrial pharmaceutical crystallization processes using acoustic emission in pure and impure media. *International journal of pharmaceutics* **2012**, *439* (1), 109-119.
53. Wang, X.; Huang, Y., An investigation of the acoustic emission generated during crystallization process of salicylic acid. *Powder technology* **2017**, *311*, 350-355.

54. Mukhopadhyay, C. K.; Haneef, T. K.; Jayakumar, T.; Devaraj, R.; Bar, H. N.; Metya, A. K.; Murthy, G. V. S.; Parida, N., Acoustic emission monitoring during hydrotesting of a mounded LPG storage vessel of petrochemical industry. *Strength, Fracture and Complexity* **2015**, *9* (4), 251-264.
55. Prakash, M.; Kanthababu, M.; Rajurkar, K. P., Investigations on the effects of tool wear on chip formation mechanism and chip morphology using acoustic emission signal in the microendmilling of aluminum alloy. *The International Journal of Advanced Manufacturing Technology* **2015**, *77* (5-8), 1499-1511.
56. Grammatikos, S.; Aggelis, D. G.; Paipetis, A. S., Continuous monitoring of setting and hardening of epoxy resin. In *Nondestructive Testing of Materials and Structures*, Springer: 2013; pp 491-496.
57. Haiyan, W.; Zhe, W.; Weiguo, L.; Jing, W.; Dongdong, L. In *Agglomeration detection in gas-phase ethylene polymerization based on the Gaussian of acoustic signal*, 2016; IEEE: pp 6924-6928.
58. Pawelzyk, P.; Toledo, M. L.; Willenbacher, N., Ultrasonic in-line monitoring of styrene miniemulsion polymerization. *Chemical engineering journal* **2013**, *219*, 303-310.
59. Quinebeche, S.; Navarro, C.; Gnanou, Y.; Fontanille, M., In situ mid-IR and UV-visible spectroscopies applied to the determination of kinetic parameters in the anionic copolymerization of styrene and isoprene. *Polymer* **2009**, *50* (6).
60. Carson, G.; Mulhollandt, A.; Nordon, A.; Tramontana, M.; Gachagan, A.; Hayward, G. In *P1H-2 Particle Sizing in the Process Industry using Hertz-Zener Impact Theory and Acoustic Emission Spectra*, Ultrasonics Symposium, 2006. IEEE, IEEE: 2006; pp 1406-1409.
61. Carson, G.; Mulholland, A. J.; Nordon, A.; Tramontana, M.; Gachagan, A.; Hayward, G., Particle sizing using passive ultrasonic measurement of particle-wall impact vibrations. *Journal of Sound and Vibration* **2008**, *317* (1), 142-157.
62. Nordon, A.; Carella, Y.; Gachagan, A.; Littlejohn, D.; Hayward, G., Factors affecting broadband acoustic emission measurements of a heterogeneous reaction. *Analyst* **2006**, *131* (2), 323-330.
63. Herrmann, F.; (Westbrook, ME) 2009 Hahn, D.; Flik, G., Sensor array and method for determining the density and viscosity of a liquid. 7552619

64. Eggen, S.; Esbensen, K.; Halstensen, M., Viscosity measurement. Google Patents: 2005.
65. Smith, E.; Dent, G., *Modern Raman spectroscopy: a practical approach*. J. Wiley: 2005.
66. <https://www.toyo-chem.com/en/products/electronics/column/emishield.html>. (accessed 29/09/2019).
67. <https://www.quora.com/What-are-the-categories-of-the-Electromagnetic-Spectrum>. (accessed 29/09/2019).
68. Brun, N.; Youssef, I.; Chevrel, M. C.; Chapron, D.; Schrauwen, C.; Hoppe, S.; Bourson, P.; Durand, A., In situ monitoring of styrene polymerization using Raman spectroscopy. Multi-scale approach of homogeneous and heterogeneous polymerization processes. *Journal of Raman Spectroscopy* **2013**, *44* (6), 909-915.
69. Santos, J. C.; Lopes, C. N.; Reis, M. M.; Giudici, R.; Sayer, C.; Machado, R. A. F.; Araujo, P. H. H., Comparison of techniques for the determination of conversion during suspension polymerization reactions. *Brazilian Journal of Chemical Engineering* **2008**, *25* (2).
70. Schlenoff, J. B.; Fong, Y.; Wang, C.; Vickers, T. J.; Mann, C. K., In-situ monitoring of emulsion and bulk-polymerization by fibre optic Raman-spectroscopy. *Abstracts of Papers of the American Chemical Society* **1995**, *209*.
71. Raman, C. V.; Krishnan, K. S., A new type of secondary radiation. *Nature* **1928**, *121*, 501-502.
72. Stokes, R. J.; McKenzie, F.; McFarlane, E.; Ricketts, A.; Tetley, L.; Faulds, K.; Alexander, J.; Graham, D., Rapid cell mapping using nanoparticles and SERRS. *Analyst* **2009**, *134* (1), 170-175.
73. Smith, W. E., Practical understanding and use of surface enhanced Raman scattering/surface enhanced resonance Raman scattering in chemical and biological analysis. *Chemical Society Reviews* **2008**, *37* (5), 955-964.
74. Kaiser Optical Systems MR Probe Operations Manual, 2007975 R4.
75. Wikstrom, H.; Lewis, I. R.; Taylor, L. S., Comparison of sampling techniques for in-line monitoring using Raman spectroscopy. *Applied Spectroscopy* **2005**, *59* (7), 934-941.

76. Kinsler, L. E.; Frey, A. R.; Coppens, A. B.; Sanders, J. V., Fundamentals of acoustics. *Fundamentals of Acoustics, 4th Edition, by Lawrence E. Kinsler, Austin R. Frey, Alan B. Coppens, James V. Sanders, pp. 560. ISBN 0-471-84789-5. Wiley-VCH, December 1999. 1999, 1.*
77. Amoodeh, M.; Khoshtaghaza, M.; Minaei, S., Acoustic on-line grain moisture meter. *Computers and Electronics in Agriculture* **2006**, *52* (1), 71-78.
78. Hakanen, A.; Laine, E., Acoustic characterization of a microcrystalline cellulose powder during and after its compression. *Drug development and industrial pharmacy* **1995**, *21* (13), 1573-1582.
79. Folkestad, T.; Mylvaganam, K., Acoustic measurements detect sand in North Sea flow lines. *Oil and Gas Journal;(USA)* **1990**, *88* (35).
80. McClements, D. J.; Gunasekaran, S., Ultrasonic characterization of foods and drinks: principles, methods, and applications. *Critical Reviews in Food Science & Nutrition* **1997**, *37* (1), 1-46.
81. Asher, R., Ultrasonics in chemical analysis. *Ultrasonics* **1987**, *25* (1), 17-19.
82. Asher, R., Ultrasonic sensors in the chemical and process industries. *Journal of Physics E: Scientific Instruments* **1983**, *16* (10), 959.
83. Asher, R. C., *Ultrasonic Sensors for chemical and process plant*. Taylor & Francis: 1997.
84. Alexander, R.; Clements, L.; Guest, R.; Hailey, P.; Leiper, K.; Moffat, A.; Pugh, K.; Wicks, S., Acoustics-are we listening? *European Pharmaceutical Review* **1999**, *4* (4), 39-45.
85. Bellamy, L. J. Application of non-invasive process analytical technologies to characterise the factors influencing mixing and measurement of powders. University of Strathclyde, 2006.
86. Boyd, J. W.; Varley, J., The uses of passive measurement of acoustic emissions from chemical engineering processes. *Chemical Engineering Science* **2001**, *56* (5), 1749-1767.
87. Fowler, T., Chemical industry applications of acoustic emission. *Materials Evaluation* **1992**, *50* (7), 875-882.
88. Huebler, J. E.; Ziolkowski, C. J., Enhanced acoustic detection of gas leaks in underground gas pipelines. Google Patents: 2004.

89. Vervloet, D.; Nijenhuis, J.; Van Ommen, J., Monitoring a lab-scale fluidized bed dryer: A comparison between pressure transducers, passive acoustic emissions and vibration measurements. *Powder Technology* **2010**, *197* (1), 36-48.
90. Jaffe, B., *Piezoelectric ceramics*. Elsevier: 2012; Vol. 3.
91. Priya, S., Criterion for material selection in design of bulk piezoelectric energy harvesters. *IEEE transactions on ultrasonics, ferroelectrics, and frequency control* **2010**, *57* (12), 2610-2612.
92. Tramontana, M.; Gachagan, A.; Nordon, A.; Littlejohn, D.; O'Leary, R.; Mulholland, A. J., System modelling and device development for passive acoustic monitoring of a particulate-liquid process. *Sensors and Actuators A: Physical* **2015**, *228*, 159-169.
93. Dong, M. W., *Modern HPLC for practicing scientists*. John Wiley & Sons: 2006.
94. Kazakevich, Y.; LoBrutto, R., *HPLC for pharmaceutical scientists*. Wiley Online Library: 2007; Vol. 43.
95. Millerand, J. N.; Miller, J. C., *Statistics and chemometrics for analytical chemistry*. Pearson Education: 2005.
96. Brereton, R. G., *Chemometrics: data analysis for the laboratory and chemical plant*. John Wiley & Sons: 2003.
97. Kong, K.; Kendall, C.; Stone, N.; Notingher, I., Raman spectroscopy for medical diagnostics—From in-vitro biofluid assays to in-vivo cancer detection. *Advanced drug delivery reviews* **2015**, *89*, 121-134.
98. Mojtabai, R.; Olfson, M., Proportion of antidepressants prescribed without a psychiatric diagnosis is growing. *Health Affairs* **2011**, *30* (8), 1434-1442.
99. Washburn, K. E.; Birdwell, J. E., Multivariate analysis of ATR-FTIR spectra for assessment of oil shale organic geochemical properties. *Organic geochemistry* **2013**, *63*, 1-7.
100. Melendez, L. V.; Lache, A.; Orrego-Ruiz, J. A.; Pachon, Z.; Mejía-Ospino, E., Prediction of the SARA analysis of Colombian crude oils using ATR-FTIR spectroscopy and chemometric methods. *Journal of Petroleum Science and Engineering* **2012**, *90*, 56-60.

101. Riley, B. J.; Lennard, C.; Fuller, S.; Spikmans, V., An FTIR method for the analysis of crude and heavy fuel oil asphaltenes to assist in oil fingerprinting. *Forensic science international* **2016**, *266*, 555-564.
102. Ferreira, A. P.; Menezes, J. C.; Tobyn, M., *Multivariate Analysis in the Pharmaceutical Industry*. Academic Press: 2018.
103. Hukkanen, E. J.; Braatz, R. D., Measurement of particle size distribution in suspension polymerization using in situ laser backscattering. *Sensors and Actuators B-Chemical* **2003**, *96* (1-2).
104. Frauendorfer, E.; Hergeth, W.-D., Industrial Polymerization Monitoring. *Polymer Reaction Engineering - 10th International Workshop* **2011**, 302.
105. Frauendorfer, E.; Hergeth, W.-D., Industrial application of Raman spectroscopy for control and optimization of vinyl acetate resin polymerization. *Analytical and Bioanalytical Chemistry* **2017**, *409* (3), 631-636.
106. Moros, J.; Garrigues, S.; de la Guardia, M., Vibrational spectroscopy provides a green tool for multi-component analysis. *TrAC Trends in Analytical Chemistry* **2010**, *29* (7), 578-591.
107. Ly, C.; Tom, K.; Byington, C. S.; Patrick, R.; Vachtsevanos, G. J. In *Fault diagnosis and failure prognosis for engineering systems: A global perspective*, 2009; IEEE: pp 108-115.
108. Gemperline, P., *Practical Guide To Chemometrics, Second Edition*. Taylor & Francis: 2006.
109. Martens, H.; Stark, E., Extended multiplicative signal correction and spectral interference subtraction: New preprocessing methods for near infrared spectroscopy. *Journal of Pharmaceutical and Biomedical Analysis* **1991**, *9* (8), 625-635.
110. Chen, Z. P.; Xiong, S.; Zuo, Q.; Shi, C. X., Quantitative analysis based on spectral shape deformation: A review of the theory and its applications. *Journal of Chemometrics* **2017**, e2913.
111. Kim, M.; Chung, H.; Woo, Y.; Kemper, M., New reliable Raman collection system using the wide area illumination (WAI) scheme combined with the synchronous intensity correction standard for the analysis of pharmaceutical tablets. *Analytica Chimica Acta* **2006**, *579* (2), 209-216.

112. <http://www.speciation.net/Database/Instruments/Waters-Corporation/2690-Alliance-i411>. (accessed 09/07/2018).
113. <http://elsichrom.se/details.asp> (accessed 09/07/2018).
114. M. Reis, M.; Hermes de Araujo, P. H.; Sayer, C.; Giudici, R., *Evidences of Correlation Between Polymer Particle Size and Raman Scattering*. 2003; Vol. 44, 20, p 6123-6128.
115. Larkin, P., *Infrared and Raman Spectroscopy; Principles and Spectral Interpretation*. Elsevier Science, 2, 3, 2011.
116. Ahmed, E. M., Hydrogel: Preparation, characterization, and applications: A review. *Journal of Advanced Research* **2015**, 6 (2), 105-121.
117. Wang, H. L.; Mann, C. K.; Vickers, T. J., Effect of powder properties on the intensity of Raman scattering by crystalline solids. *Applied Spectroscopy* **2002**, 56 (12), 1538-1544.
118. Hu, Y.; Wikstrom, H.; Byrn, S. R.; Taylor, L. S., Analysis of the effect of particle size on polymorphic quantitation by Raman spectroscopy. *Applied Spectroscopy* **2006**, 60 (9), 977-984.
119. Hamilton, P.; Littlejohn, D.; Nordon, A.; Sefcik, J.; Slavin, P.; Dallin, P.; Andrews, J., Studies of particle drying using non-invasive Raman spectrometry and particle size analysis. *Analyst* **2011**, 136 (10), 2168-2174.
120. Meyer-Kirschner, J.; Mitsos, A.; Viell, J., Polymer particle sizing from Raman spectra by regression of hard model parameters. *Journal of Raman Spectroscopy* **2018**.
121. Johansson, J.; Pettersson, S.; Folestad, S., Characterization of different laser irradiation methods for quantitative Raman tablet assessment. *Journal of pharmaceutical and biomedical analysis* **2005**, 39 (3-4), 510-516.
122. Downes, A., Wide area Raman spectroscopy. *Applied Spectroscopy Reviews* **2019**, 1-12.
123. Allan, P.; Bellamy, L. J.; Nordon, A.; Littlejohn, D.; Andrews, J.; Dallin, P., In situ monitoring of powder blending by non-invasive Raman spectrometry with wide area illumination. *Journal of Pharmaceutical and Biomedical Analysis* **2013**, 76, 28-35.

124. Overall, N.; Hahn, T.; Matousek, P.; Parker, A. W.; Towrie, M., Photon migration in Raman spectroscopy. *Applied Spectroscopy* **2004**, *58* (5), 591-597.
125. Schrader, B.; Hoffmann, A.; Keller, S., Near-infrared Fourier-Transform Raman-spectroscopy - Facing absorption and background. *Spectrochimica Acta Part a-Molecular and Biomolecular Spectroscopy* **1991**, *47* (9-10), 1135-1148.
126. Zhang, B.; Feng, S., Advances in the modelling and simulation of emulsion polymerisation. *International Journal of Modelling, Identification and Control* **2010**, *11* (3-4), 262-273.
127. Bogomolov, A., Multivariate process trajectories: capture, resolution and analysis. *Chemometrics and Intelligent Laboratory Systems* **2011**, *108* (1), 49-63.
128. Altarawneh, I. S.; Gomes, V. G.; Srour, M. H., Online polymer molecular weight and conversion monitoring via calorimetric measurements in RAFT emulsion polymerization. *Polymer International* **2009**, *58* (12), 1427-1434.
129. Srour, M. H.; Gomes, V. G.; Altarawneh, I. S.; Romagnoli, J. A., Online model-based control of an emulsion terpolymerisation process. *Chemical Engineering Science* **2009**, *64* (9), 2076-2087.
130. Esposito, M.; Sayer, C.; de Araújo, P. H. H., In-Line Monitoring of Emulsion Polymerization Reactions Combining Heat Flow and Heat Balance Calorimetry. *Macromolecular Reaction Engineering* **2010**, *4* (11-12), 682-690.
131. Dehanov, N. F.; Thennadil, S. N., Monitoring of conversion during emulsion polymerisation using near infrared spectroscopy. *NIR news* **2014**, *25* (3), 9-16.
132. Chen, Z.-P.; Morris, J.; Martin, E., Extracting Chemical Information from Spectral Data with Multiplicative Light Scattering Effects by Optical Path-Length Estimation and Correction. *Analytical Chemistry* **2006**, *78* (22), 7674-7681.
133. Jin, J.-W.; Chen, Z.-P.; Li, L.-M.; Steponavicius, R.; Thennadil, S. N.; Yang, J.; Yu, R.-Q., Quantitative spectroscopic analysis of heterogeneous mixtures: the correction of multiplicative effects caused by variations in physical properties of samples. *Analytical chemistry* **2011**, *84* (1), 320-326.
134. Al-Khanbashi, A.; Dhamdhere, M.; Hansen, M., Application of in-line fiber-optic Raman spectroscopy to monitoring emulsion polymerization reactions. *Applied Spectroscopy Reviews* **1998**, *33* (1-2), 115-131.

135. McCaffery, T. R.; Durant, Y. G., Monitoring of Seeded Batch, Semi-batch, and Second Stage Emulsion Polymerization by Low Resolution Raman Spectroscopy. *Polymer Reaction Engineering* **2003**, *11* (3), 507-518.
136. Santos, J. G. F., Jr.; Way, D. V.; Melo, P. A.; Nele, M.; Pinto, J. C., Analysis of Near Infrared Spectra during Methyl methacrylate (MMA) Suspension Polymerizations. In *Brazilian Polymer Congress*, Pinto, J. C., Ed. 2011; Vol. 299-300.
137. Poon, K. W. C.; Lyng, F. M.; Knief, P.; Howe, O.; Meade, A. D.; Curtin, J. F.; Byrne, H. J.; Vaughan, J., Quantitative reagent-free detection of fibrinogen levels in human blood plasma using Raman spectroscopy. *Analyst* **2012**, *137* (8), 1807-1814.
138. Santos, A. F.; Silva, F. M.; Lenzi, M. K.; Pinto*, J. C., Monitoring and Control of Polymerization Reactors Using NIR Spectroscopy. *Polymer-Plastics Technology and Engineering* **2005**, *44* (1), 1-61.
139. Wancheck, P. L.; Wolfram, L. E., Quantitative Analysis of Styrene Monomer in Styrene/Butadiene Latexes Using Raman Spectroscopy. *Applied Spectroscopy* **1976**, *30* (5), 542-544.
140. Lempel, E.; Czibulya, Z.; Kunsági-Máté, S.; Szalma, J.; Sümegi, B.; Böddi, K., Quantification of Conversion Degree and Monomer Elution from Dental Composite Using HPLC and Micro-Raman Spectroscopy. *Chromatographia* **2014**, *77* (17), 1137-1144.
141. Lorber, N.; Pavageau, B.; Mignard, E., Droplet-based millifluidics as a new miniaturized tool to investigate polymerization reactions. *Macromolecules* **2010**, *43* (13), 5524-5529.
142. Yuan, H. G.; Kalfas, G.; Ray, W. H., SUSPENSION POLYMERIZATION. *Journal of Macromolecular Science, Part C* **1991**, *31* (2-3), 215-299.
143. Shaghghi, S.; Mahdavian, A. R., The Effect of Sodium Dodecyl Benzene Sulfonate on Particle Size in Suspension Polymerization of Styrene: A New Investigation. *Polymer-Plastics Technology and Engineering* **2006**, *45* (1), 109-115.
144. Jahanzad, F.; Sajjadi, S.; Brooks, B. W., Characteristic intervals in suspension polymerisation reactors: An experimental and modelling study. *Chemical Engineering Science* **2005**, *60* (20), 5574-5589.
145. Seasholtz, M. B.; Kowalski, B., The parsimony principle applied to multivariate calibration. *Analytica Chimica Acta* **1993**, *277* (2), 165-177.

146. Gromski, P. S.; Xu, Y.; Correa, E.; Ellis, D. I.; Turner, M. L.; Goodacre, R., A comparative investigation of modern feature selection and classification approaches for the analysis of mass spectrometry data. *Analytica Chimica Acta* **2014**, *829* (0), 1-8.
147. Bi, Y.; Tang, L.; Shan, P.; Xie, Q.; Hu, Y.; Peng, S.; Tan, J.; Li, C., Interference correction by extracting the information of interference dominant regions: Application to near-infrared spectra. *Spectrochimica Acta Part A: Molecular and Biomolecular Spectroscopy* **2014**, *129*, 542-550.
148. Chen, Z.-P.; Zhong, L.-J.; Nordon, A.; Littlejohn, D.; Holden, M.; Fazenda, M.; Harvey, L.; McNeil, B.; Faulkner, J.; Morris, J., Calibration of multiplexed fiber-optic spectroscopy. *Analytical chemistry* **2011**, *83* (7), 2655-2659.
149. Song, J.; Chen, Z.-P.; Jin, J.-W.; Chen, Y.; Yu, R.-Q., Quantitative surface-enhanced Raman spectroscopy based on the combination of magnetic nanoparticles with an advanced chemometric model. *Chemometrics and Intelligent Laboratory Systems* **2014**, *135*, 31-36.
150. Chen, Y.; Chen, Z.-P.; Yang, J.; Jin, J.-W.; Zhang, J.; Yu, R.-Q., Quantitative fluorescence spectroscopy in turbid media: a practical solution to the problem of scattering and absorption. *Analytical chemistry* **2013**, *85* (4), 2015-2020.
151. Du, H.-L.; Chen, Z.-P.; Song, M.; Chen, Y.; Yu, R.-Q., Novel calibration model maintenance strategy for solving the signal instability in quantitative liquid chromatography–mass spectrometry. *Journal of Chromatography A* **2014**, *1338*, 44-50.
152. Shi, C.-X.; Chen, Z.-P.; Chen, Y.; Yu, R.-Q., Quantitative analysis of hormones in cosmetics by LC-MS/MS combined with an advanced calibration model. *Analytical Methods* **2015**, *7* (16), 6804-6809.
153. Yang, J.; Chen, Z.-P.; Zhang, J.; Jin, J.-W.; Chen, Y., Quantitative Raman spectrometry: The accurate determination of analytes in solution phase of turbid media. *Chemometrics and Intelligent Laboratory Systems* **2013**, *126*, 6-10.
154. Chen, Z.-P.; Li, L.-M.; Jin, J.-W.; Nordon, A.; Littlejohn, D.; Yang, J.; Zhang, J.; Yu, R.-Q., Quantitative analysis of powder mixtures by Raman spectrometry: the influence of particle size and its correction. *Analytical chemistry* **2012**, *84* (9), 4088-4094.

155. Chen, Z.-P.; Fevotte, G.; Caillet, A.; Littlejohn, D.; Morris, J., Advanced calibration strategy for in situ quantitative monitoring of phase transition processes in suspensions using FT-Raman spectroscopy. *Analytical chemistry* **2008**, *80* (17), 6658-6665.
156. Allan, P. Studies in Raman, infrared and acoustic emission spectrometries and reaction calorimetry for process analysis. The University of Strathclyde, 2009.
157. Palmer, L. Investigation of batch and continuous crystallisation processes using non-invasive Raman and acoustic emission spectrometries. University of Strathclyde, 2013.
158. Hailey, P. A.; Doherty, P.; Tapsell, P.; Oliver, T.; Aldridge, P. K., Automated system for the on-line monitoring of powder blending processes using near-infrared spectroscopy part I. System development and control. *Journal of Pharmaceutical and Biomedical Analysis* **1996**, *14* (5), 551-559.
159. Sekulic, S. S.; Wakeman, J.; Doherty, P.; Hailey, P. A., Automated system for the on-line monitoring of powder blending processes using near-infrared spectroscopy: Part II. Qualitative approaches to blend evaluation. *Journal of pharmaceutical and biomedical analysis* **1998**, *17* (8), 1285-1309.
160. Sekulic, S. S.; Ward, H. W.; Brannegan, D. R.; Stanley, E. D.; Evans, C. L.; Sciavolino, S. T.; Hailey, P. A.; Aldridge, P. K., On-line monitoring of powder blend homogeneity by near-infrared spectroscopy. *Analytical Chemistry* **1996**, *68* (3), 509-513.
161. Berntsson, O.; Danielsson, L. G.; Lagerholm, B.; Folestad, S., Quantitative in-line monitoring of powder blending by near infrared reflection spectroscopy. *Powder Technology* **2002**, *123* (2-3), 185-193.
162. Bodson, C.; Dewé, W.; Hubert, P.; Delattre, L., Comparison of FT-NIR transmission and UV-vis spectrophotometry to follow the mixing kinetics and to assay low-dose tablets containing riboflavin. *Journal of pharmaceutical and biomedical analysis* **2006**, *41* (3), 783-790.
163. Bellamy, L. J.; Nordon, A.; Littlejohn, D., Effects of particle size and cohesive properties on mixing studied by non-contact NIR. *International journal of pharmaceuticals* **2008**, *361* (1-2), 87-91.

164. Ely, D.; Chamrathy, S.; Carvajal, M. T., An investigation into low dose blend uniformity and segregation determination using NIR spectroscopy. *Colloids and Surfaces A: Physicochemical and Engineering Aspects* **2006**, *288* (1-3), 71-76.
165. Shi, Z.; Cogdill, R. P.; Short, S. M.; Anderson, C. A., Process characterization of powder blending by near-infrared spectroscopy: blend end-points and beyond. *Journal of pharmaceutical and biomedical analysis* **2008**, *47* (4-5), 738-745.
166. Moes, J. J.; Ruijken, M. M.; Gout, E.; Frijlink, H. W.; Ugwoke, M. I., Application of process analytical technology in tablet process development using NIR spectroscopy: Blend uniformity, content uniformity and coating thickness measurements. *International journal of pharmaceutics* **2008**, *357* (1-2), 108-118.